NON-EQUILIBRIUM PLASMA IN OIL

A Dissertation

by

ROBERT PAUL GEIGER

Submitted to the Office of Graduate and Professional Studies of
Texas A&M University
in partial fulfillment of the requirement for the degree of

DOCTOR OF PHILOSOPHY

Chair of Committee,	David Staack
Committee Members,	Jonathan Felts
	Berna Hascakir
	Waruna Kulatilaka
Head of Department,	Andreas A. Polycarpou

May 2017

Major Subject: Mechanical Engineering

ABSTRACT

A non-equilibrium plasma can be generated in a liquid when the energy density is controlled. The process of initiating a plasma starting with a liquid phase can be initiated by applying a sufficiently large electric potential between a pair of electrodes submerged in the liquid. An electric field propagates between the electrodes at a rate that is only limited by the speed of light. Energy is subsequently transferred from the electric field to the liquid medium in various ways. Currently, the exact physical processes that occur after an electric field is present, and just prior to electrical breakdown, are not completely understood. During this prebreakdown process, charge multiplication is occurring, reactive species are being generated, and non-equilibrium plasma is being initiated. Once breakdown occurs, charge generation and reactive species production are further accelerated, thermal energy is rapidly dissipated in the dense medium and the plasma tends toward equilibrium. This plasma initiation process will proceed as far as it can, depending on the amount of energy being provided by the external circuit. Limiting the supply of energy will therefore determine the extent to which the plasma will achieve an equilibrium state.

Non-equilibrium and non-thermal plasmas can provide some rather unique chemistry. This dissertation explores, both theoretically and experimentally, the chemistry that occurs when non-equilibrium plasma is generated in oils. To generate consistent non-equilibrium plasma, a new technique, called the Electrodynamic Ball Discharge (EBD), is devised and analyzed. This technique allows for very small energy

inputs to ensure non-equilibrium plasma generation. By controlling the chemistry in this way, the oil can be cracked and upgraded rather than go through pyrolysis as would occur with the application of a thermal arc.

ACKNOWLEDGEMENTS

The work presented in this dissertation would have never been initiated without the help, support, and guidance of Prof. David Staack. His interest in exploring the boundaries of non-thermal, non-equilibrium plasma generation, specifically in high-density media, is what led him to many of the ideas explored herein. While exploring the electrodynamic behaviors of conductive particles in dielectric media, and the plasmas they create, it became apparent that this topic should be explored further. Upon sharing his ideas with me I was able to explore the idea of low-energy plasma generation in liquids in greater detail. The results of that exploration are presented within this dissertation.

CONTRIBUTORS AND FUNDING SOURCES

Much of the work contained in this dissertation was carried out with the assistance of several other students and I wish to recognize them here. Sixto Almazan assisted with early tests where the effect of ball radius was studied. He also helped to analyze the process of scaling single Electrodynamic Ball Discharges (EBDs) to Electrodynamic Ball Reactors (EBRs) by exploring experimentally using columns of balls. Upon discovering some of the scaling issues, Kimberly Hogge led the effort of utilizing a single ball per column. She proceeded to design a new reactor that would be able to operate at much larger total power densities while maintaining low energy plasma discharges. Finally, Master's student Stephen Slavens carried out numerous experiments using the EBRs for various liquids. He characterized viscosity changes due to dilution and due to plasma treatment, analyzed off gases, and studied the current-voltage characteristics. More of his work can be found in his thesis (1). All their work contributed to the work presented here in and I am very grateful for all their efforts.

This work was partially support by NSF grant 1057175 and by Chevron TEES contract C12-00654.

TABLE OF CONTENTS

Page

LIST OF TABLES

Page

LIST OF FIGURES

Page

INTRODUCTION

Background

The following sections provide some background to assist in describing the thesis and the subsequent implications of the thesis. The plasma phase of matter will be described in some detail. The physical process of transitioning from a non-plasma phase to the plasma phase is of utmost importance for the thesis. The fundamental mechanisms of transitioning from a gas phase to a plasma phase are generally considered well understood and will be briefly reviewed where it is relevant. The physical mechanisms of transitioning from a liquid phase to a plasma phase are not completely understood and the current understanding of these mechanisms will be briefly reviewed and further explored with particular focus on the energy of the process.

Non-equilibrium plasma, specifically generated from liquids, is the focus of this thesis therefore some of the concepts of non-equilibrium processes will be reviewed. To determine how non-equilibrium plasma phases can be produced in a liquid understanding of the physical mechanisms are important but exact details are not required. Non-equilibrium plasma phases, generated within liquids, can be identified experimentally several ways as will be shown throughout this dissertation.
There are various motivations for generating non-equilibrium plasma in liquids as will be discussed. Experimental work carried out to support the thesis involves the chemistry of heavy oil upgrade. Generating non-equilibrium plasma in heavy oils can provide

beneficial chemistry for upgrading such oils and was a key motivation in line with the thesis. This work will be described throughout the dissertation and reviewed briefly in this section.

The plasma phase of matter

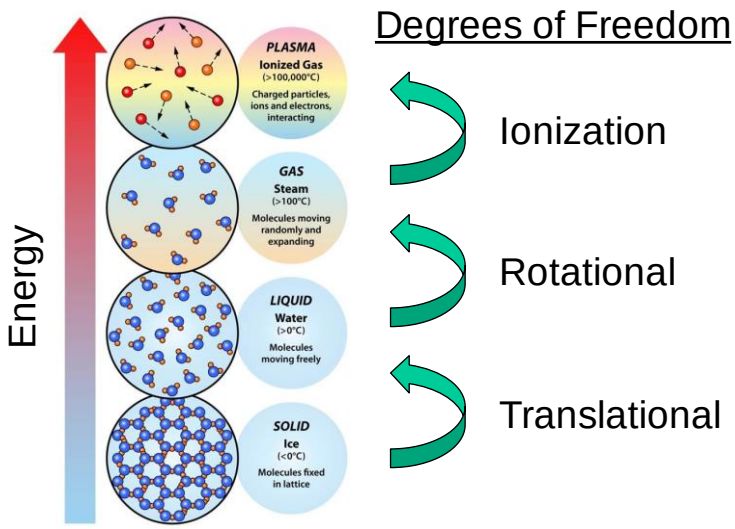

Figure 1 An illustration of phase changes as they relate to additional degrees of freedom (2)

Plasma is often referred to as the fourth state of matter. This can be illustrated by initially considering matter that is in a solid phase, Figure 1. If energy is added to the solid by heating, it will soon reach its melting point and transition to a liquid phase. On a purely physical level, this transition occurs because the molecules have gained enough energy to overcome the intermolecular bonding forces that once held them in place; thus, the atoms have obtained a new degree of freedom, namely a translational degree of freedom. If more energy is added the translational energy of the molecules will increase

further until a new phase is achieved, the gas phase. This transition too is accompanied by the addition of a new degree of freedom, free rotation. When the translational energy is large enough the average density of the molecules decrease and the intermolecular forces become entirely negligible; this allows the molecules to gain rotational degrees of freedom becoming a gas. Once again if more energy is added another transition occurs, this time from the gas phase to a plasma phase. The transition to a plasma phase occurs when the translational energy becomes so high that collisions can lead to ionization, producing free electrons and ions. This thermal ionization process occurs only at very high temperatures, when radiative losses become significant, therefore a large source of energy is required to sustain the state; for example, thermonuclear fusion can sustain stars such as our sun in a plasma phase, Figure 2.

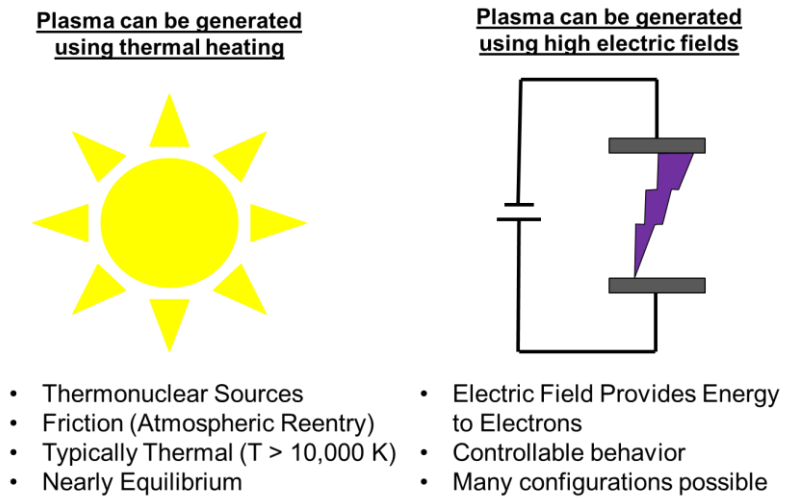

Figure 2 Thermally generated plasmas versus electromagnetically generated plasmas

The usefulness of describing plasma as the fourth state of matter is arguably only applicable when the plasma phase that is generated occurs through a thermal mechanism. Thermally ionized plasmas are not easily created within the laboratory. There is however another method for generating a plasma phase that does not require excessive translational energy of molecules producing thermal ionization; this method uses electromagnetic mechanisms instead of heating.

It is also common to describe the plasma phase as an ionized gas, consisting of neutral molecules, ions, and free electrons. This is useful because the description encompasses plasmas that are formed both by thermal ionization mechanisms and electromagnetic mechanisms, Figure 2. Either a photon with sufficient energy or a free charged particle, such as an electron, with sufficient energy can interact with a neutral molecule and ionize it. The various electromagnetic ionization mechanisms do not depend on the translational energy of the neutral molecules; therefore, a plasma phase can be generated at much lower gas temperatures then thermally generated plasmas. Furthermore, these plasmas often exist in highly nonequilibrium states, also referred to as local thermodynamic equilibrium, where the various degrees of freedoms can be described as having different temperatures. When the translational, rotational, vibrational, electronic excitation, and electron temperatures (T_{trans}, T_{rot}, T_{vib}, T_{el}, T_e) are all equal the plasma is said to be in equilibrium; when they are different the plasma is said to be non-equilibrium. Plasmas are also considered to be thermal plasmas when the gas temperatures are several thousands of degrees or higher and non-thermal when the gas temperature is closer to room temperature or colder. Lastly, another classification for

plasmas is whether they are transient or steady state which describes whether the properties of the plasma are changing with time. An example of a plasma that can be considered as steady state, thermal, and equilibrium is the arc, such as those used for welding; although an arc is not actually in equilibrium it is often modeled as though it is. Typically for the steady state, non-thermal, non-equilibrium plasmas that are generated in a laboratory using electric fields, the relative temperatures are: $(T_{trans} \approx T_{rot}) < (T_{vib} \approx T_{el}) < T_e$. Plasmas that fall into the classification of non-equilibrium will be the focus of this thesis. Non-equilibrium plasmas are commonly initiated within a gas by generating a high electric field between two electrodes; this process will be considered first, then initiating the same plasma from a high-density medium will be considered.

Plasma initiation mechanism from the gaseous phase

In the early 1900's John S. Townsend successfully identified and described the mechanism by which a gas becomes conductive due to the application of a high electric field (3; 4); his analysis led to what is now called the Townsend Avalanching model. The Townsend Avalanche model considers some initial concentration of electrons, so called seed electrons, which are naturally created by cosmic radiation or radioactivity on earth. Upon application of a potential to the electrodes, seed electrons are accelerated and can gain enough energy to cause ionization. When an ionization event occurs, an additional electron is produced. These two electrons will both proceed to have another

ionization event therefore creating a total of four electrons. This process continues and leads to an avalanche of electrons between the electrodes.

The success of the Townsend Avalanching model was not just in describing the avalanching model but lies in its ability to accurately predict breakdown voltages, the critical voltage at which the gas becomes highly conductive. What Townsend discovered was that the seed electrons were not sufficient to explain how a highly conductive channel is created between the electrodes; therefore, another source of electrons is required. Townsend noted that the ions which are produced in the avalanching process will naturally accelerate towards the cathode, where they can be neutralized by pulling an electron out of the electrode. For the ion to accomplish this feat the ionization potential must be equal to or greater than the work function of an electron in the electrode material; furthermore, any excess energy can be dissipated into the electrode. Sometimes the excess energy is enough to cause secondary electrons to be emitted into the gap. When secondary electrons are being emitted into the gap they too, along with the seed electrons, can cause electron avalanching.

Townsend realized that the seed electrons can avalanche creating ions, these ions can proceed to the cathode where some of the ions will generate secondary electrons, but one last condition must be satisfied for breakdown to be achieved. The critical condition occurs when the number of ions that are generating secondary electrons is equal to the number ions beings created by the electrons. When this condition is met the ionization, process becomes self- sustaining; in other words, the seed electrons are no longer the main producer of ions, but the secondary electrons become the main source of ion

production and the discharge becomes self-sustaining. As soon as this self-sustaining condition is crossed ion, and electron, production in the gap grows exponentially and that is what is called breakdown. This transition to the self-sustaining mode is very important because it is the moment when the current in the gap solely depends on what can be provided by the external circuit.

Many researchers continued to successfully extrapolate the results of the theory to determine breakdown voltages for longer gap distances between electrodes, *d*, and to higher pressures, *p*. However eventually a boundary to the theory was discovered and a new theory was required to explain the breakdown mechanism for much higher pressures and larger gaps.

From the early 1900's to 1940 several researchers were investigating electrical breakdown in gases at much larger electrode gap lengths and much higher pressures. It soon became apparent that the Townsend mechanism was no longer valid for these conditions. This conclusion was arrived at when researchers began measuring the time lag, the time difference between the application of a potential and breakdown. When the measured time lags were compared with the theoretical values provided by Townsends theory they were only accurate for values of *pd* below 200 mmHg*cm. The measured time could be off by as much as an order of magnitude (0.1 μs compared to 1 μs as predicted by Townsend theory for a 1 cm gap at atmospheric pressure); in fact, the breakdown process appeared to be occurring faster than the time required for ions to move to the cathode. Furthermore, Townsend theory has a very clear dependence on the cathode material, more specifically the work function and surface conditions; however,

for high values of *pd* this dependency becomes unimportant. Do to the discrepancies for both the time lag and cathode material dependencies between experimental observations and Townsend theory predictions a new theory was required.

A solution to this problem was presented in an article by J. M. Meek wherein he proposed a possible explanation for the short-comings of the Townsend theory at these larger values *p* and *d* (5). He stated that for *pd* values larger than 200 mmHg*cm in air the Townsend mechanism is no longer applicable predominately because the space charge that exists in the gap becomes significant and must be considered. Furthermore, Meek noted the importance of photoelectrons. It was well known at that time that photons were generated near the head of the avalanche and these photons head enough energy to ionize nearby gas. Therefore, Meek combined the ideas of photoelectron generation, and field distortion near the avalanche head to define a new critical transition in the breakdown mechanism.

Considering a large electrode gap, Townsend Avalanching can occur as usual when an appropriate potential is applied, however due to the longer distance between the electrodes the avalanches will produce a larger volume of ions near the head of the avalanche before reaching the anode. The electric field created by these ions, near the head of the avalanche, can no longer be ignored. The field due to these ions distorts the field produced by the external circuit. The distortion of the external field has two important effects on the flow of electrons through the gap: 1) It can slow the free electrons down in the axial direction; 2) It can pull photoelectrons generated near the avalanche head radially inward generating secondary avalanches towards the head of the

primary avalanche. The first effect makes it more difficult for the electrons to cross the gap. The second effect results in accelerated production of ions near the head of the primary avalanche resulting in an ionization wave that propagates towards both the cathode and the anode. These ionization waves are known as streamers.

The importance of streamer formation was noted by Meek and he proposed a method for quantifying their formation. Meek provided a condition, what is now known as the Meek criterion, that must occur for a streamer to be produced. The criterion states that when the radial electric field strength due to the ions produced in a primary avalanche is equal to the field strength of the external electric field a stream can form. This criterion provided by Meek is like the Townsend criterion for secondary electron emission in that it defines a critical transition point; the Townsend criterion defined a transition to a self-sustaining mode due to secondary electron emission whereas the Meek criterion defines an Avalanche to Streamer transition.

The Townsend avalanching model and the Meek sparking model are two important initiations mechanisms. It was said by Y. P. Raizer that "An individual avalanche is a primary and inescapable element of any breakdown mechanism." (6) This is a very important statement especially when considering high density mediums. Furthermore, the Meek criterion becomes important when *pd* is large which also can correspond to high density mediums. Currently the plasma initiation process in liquids is still under debate and there has been no decisive experimental evidence of a well-defined initiation process.

Plasma initiation in liquids

The difficulty of applying the Townsend model for liquid plasma generation is apparent when considering that the mean free path for molecules in a liquid is on the order of about 2.5 Angstroms. Due to the proximity of molecules, conduction bands are created which are difficult to define due to the constant motion of the molecules; therefore, the idea of mean free path becomes ill-defined. If, however, it is assumed that very short mean free paths could exist as in polar crystals (7), and that electrons can remain 'free electrons' then Townsend theory can be applied to estimate the required field strengths to initiate avalanching. To accelerate a free electron up to the ionization energy of a molecule the required electric field strength in the range of 1e4→1e5 kV/cm is expected. This is peculiar since experimentally it is possible to generate a plasma from a liquid phase with electric field strengths in the range of 10→100 kV/cm; these electric field strengths are the like those required to cause breakdown in the gas phase. Therefore, there is an inconsistency between experimental evidence for plasma generation in liquids and the basic idea of Townsend Avalanching theory as applied to such dense media.

Keeping in mind that a fundamental requirement for any plasma initiation mechanism is electron avalanching, the scientific community has become split into two schools of thought: 1) Plasma generation in the liquid phase begins in a low density region within the liquid, either by some preexisting bubble or by a low density region generated somehow by the application of the electric field, 2) Electron avalanche does

actually occur in the high density liquid phase which can be explained by either high energy electrons emitted from the electrode or perhaps the mean free paths are sufficiently large for electrons at liquid densities (8). These two ideas will be explored further in the literature review sections.

Since there is not yet sufficient evidence to confirm the high-density initiation mechanism it can be challenging to characterize plasmas generated from the liquid phase, especially for the case of short duration pulsed electric fields, on the order of nanoseconds. For these short duration pulses, the electric field might prevent the initiation process from achieving a breakdown criterion, in which case it is likely that the plasma can be classified as non-equilibrium plasma. Alternatively, if the pulse duration is long enough to allow the plasma to meet a breakdown criterion then the plasma will run away and become self-sustaining consuming as much current as is available from the external circuit. If there is sufficient current available the plasma can rapidly thermalize and will tend to approach equilibrium. This rapid thermalization process has a characteristic time associated with it which will depend on the density of the medium; this will be explored further in later sections. Therefore, non-equilibrium plasma should be expected for short duration, on the order of the initiation time, pulsed electric fields that are current limited; this should be valid regardless of the density of the initiating medium; however, the rate at which equilibrium can be achieved will be faster in denser mediums simply due to the more collisional nature of the medium. Therefore, to ensure the generation of non-equilibrium plasma in dense mediums controlling the available current in the external circuit is of the utmost importance.

Time scales and non-equilibrium plasma

A crucial aspect of plasma initiation mechanisms is the characteristic times at which they occur. The sparking mechanism was developed when it was observed that the breakdown process was occurring as rates much faster than the time required for an ion to cross the electrode gap. Since the Townsend breakdown mechanism requires ion bombardment at the cathode to produce secondary electrons it became apparent that another mechanism had to be responsible for the very fast breakdowns that occur at larger *pd* values. Having a grasp of these timescales can greatly assist in the understanding of the physical mechanisms at play when transitioning to a plasma phase, as well as the time required for achieving steady state.

Non-equilibrium plasmas can exist as either transient or steady state processes. All plasmas that are generated by electromagnetic mechanisms are initially in a state of non-equilibrium and are driven towards equilibrium while attempting to maximize entropy; this is according to Boltzmann's H-Theorem (9). This previous statement must be valid when it is considered that the electromagnetic mechanisms all begin by accelerating free electrons through free space. Since energy from the external electric field is recovered initially by free electrons, the free electron temperature will necessarily become larger than the surrounding temperature and therefore a non-equilibrium state exists. There are three fundamental processes that are occurring initially during the action of transferring external electric field energy to the free electrons: 1) Charge accumulation occurs at the electrodes setting up an electric field, 2)

The electric field propagates from the electrode through free space, 3) Free electrons gain energy from the electric field, potentially leading to an ionization event. The time constant of each of these processes will be considered.

The fastest process is naturally the propagation of the electric field through free space, as this is only limited by the permittivity of free space, and therefore occurs at the speed of light. If a 1 cm gap is considered, then the characteristic time for electric field propagation is about 33 picoseconds. Next, the charge accumulation in the electrodes will depend on the configuration of the external circuit and the geometry and materials of the electrodes, however for a rough approximation the drift velocity of an electron in a wire will be considered as a characteristic time. Drift velocities tend to be on the order of hundreds of meters per second for the kilovolt range in standard copper wires. With these conditions, the time it would take an electron to move between atoms in the wire is on the order of picoseconds. Lastly the time it takes for free electrons to gain enough energy to ionize a molecule depends on the mean free path and the drift velocity. For a gas at atmospheric conditions the mean free path is on the order 40e-6 cm and typical drift velocities are about 2e6 cm/s which gives a characteristic time of about 20 picoseconds. These initial three processes are very fast, occurring at the picosecond time scale. Therefore, as soon as the electrons accumulate at the electrode, the electric field will propagate and the electrons will react.

It can also be noted that the electron energy distribution function (EEDF) can obtain equilibrium after about 20-200 collisions which can be on the order of 10^{-8} to 10^{-9} seconds (10). The electric field and electron related time constants are very fast, while

the time constants associated with heavy molecules are several orders of magnitude slower and therefore allow for highly non-equilibrium states to exist between electrons and molecules. Furthermore, the time constants between molecular exchanges also allow for non-equilibrium states to exist between the other degrees of freedom.

Characteristic times for the translational relaxation of molecules, rotational relaxation of molecules, vibrational relaxation of molecules, and electron relaxation of molecules can provide some insight into why non-equilibrium states can exist in weakly ionized plasmas. Typically, the characteristic relaxation times for each of these processes have the following relationship (10):

$$\tau_{TT} < \tau_{RT} < \tau_e < \tau_{VT},,_{\mathrm{h}}$$

Here the subscripts represent relaxation characteristic times for Translational-Translation, Rotational- Translations, Free Electron, Vibrational-Translation, Electronic-Translational, and Chemical Conversion respectively. From this hierarchy, it is apparent that Translational-Translational and Rotational-Translational relaxation times happen as fast as or faster than the already determined Free Electron relaxation times (~ 10^{-9} seconds); subsequently it is usually the case that the translational and rotational temperatures are nearly equal. Some of the most interesting behavior of non-equilibrium plasma comes from the fact that the relaxation times for Vibrational-Translational and Electronic-Translation are relatively long and therefore can have temperatures that are much different than the other temperatures.

These relaxation time constants are very useful in understanding the evolution of the plasma from a non-equilibrium state to an equilibrium state. A small perturbation to

the translational degrees of free of a gas, such as a sudden heat source, will not tend to disrupt the energy distribution for very long and the rotational degrees of freedom will adjust just as quick. Free electrons tend to respond quickly as well, on the order of picoseconds to nanoseconds. Vibrational and Electronic timescales can be much longer. Therefore, if a plasma has a very short lifetime, from initiation to full relaxation, then it is unlikely that equilibrium was obtained. The lifetime of the plasma depends, in general, depends on two main factors: 1) Is the plasma in a self-sustaining mode, 2) How much energy is supplied or available from the external circuit.

Thesis statement

This dissertation describes the theory and application of non-equilibrium plasmas in dense mediums. The thesis states, "Non-equilibrium plasma can be generated in a high density medium when the energy density is controlled." The ability to obtain and utilize non-equilibrium plasma in a dense medium is described both theoretically and experimentally. While there are several possible methods of experimentally controlling the energy density of a plasma discharge in a dense medium and the present study describes a new method referred to as an Electrodynamic Ball Reactor (EBR). The EBR provides a unique opportunity to controlling energy density allowing very low energy densities to be explored.

This dissertation is segmented into three main sections: the first section describes the initial theory of generating non-equilibrium plasmas in high density mediums based

on current theoretical consensus of the scientific community as well as promising theoretical speculations of yet unexplained phenomena; the second section describes the theory and modeling of the electrodynamic ball reactor; the third and last section describes experimental findings for non-equilibrium plasma in high density mediums.

Motivation

Non-thermal and non-equilibrium plasma can provide unique chemical reactions that can be exploited for various applications. Such plasmas produce reactive radicals, excited molecules, charged species, and photons that often lead to unique chemical pathways. Historically, these plasmas have been exploited for gas phase chemistry such as ozone production (11), fuel reforming (12; 13), pollution control (14; 15), ammonia production (16), carbon dioxide dissociation (17; 9), production of novel compounds such as carbon nanotubes (18) and carbon suboxide (19; 20), assisted combustion (21), and as light sources (22). More recently however, the focus is shifting to applications of non-thermal, non-equilibrium plasma in liquid phases.

The experimental research presented in this dissertation focuses on the desire to upgrade heavy oils using electrically generated plasma within the liquid; however there exist numerous other important applications of liquid phase generated plasma (23). Direct chemical processing of liquids by using non-equilibrium plasma has potential of destroying harmful chemicals (24), reforming heavy oil (25), as well as many new synthesis reactions for producing nanoparticles, carbon nanotubes, and thin films to

name a few. Non-equilibrium plasma has been applied to new and exciting applications in the biomedical field for wound treatment (26), water treatment (27) and sterilization (28; 29).

The following sections will introduce the specific application of non-equilibrium plasma for heavy oil upgrading.

Heavy oil upgrading

Within the oil industry the most desirable type of oil are those oils which require the least amount of processing to get the desired products. The types of oil that fall into this category are typically called sweet, light oils. The term sweet refers to a low amount of sulfur content while the term light is a reference to the API gravity of the oil. Since light, sweet oil is such a desired resource it has been vastly depleted over the years and the oil supply the remains is less desirable heavy and extra heavy oil. The heavier oil is more difficult to transport and process, as a result many oil companies would like a better solution to work with these oils then the currently available options (30).

The oil industry already has some well-developed processes that can convert heavy oil into lighter more desirable oil (31); these technologies were developed mainly to work with the bottoms product from distillation towers but also are used with heavy crude direct from the ground. Some of the more common processes include delayed coking, fluid catalytic cracking, and hydrocracking. These processes can be split into two main categories: carbon rejection and hydrogen addition.

Delayed coking is a thermal cracking method. This process heats the heavy oil up to very high temperatures to initiate a thermal cracking mechanism which can be considered as a carbon rejection process; this is because it produces coke. Carbon rejection is an undesirable process because coke is a much lower valued product. Furthermore, this is a very energy intensive process. Delayed coking is widely utilized mainly due to the lower capital investment that is required. Due to the many undesirable attributes associated with thermal cracking technologies alternative methods have been developed such as catalytic cracking. If a source of hydrogen is available then yet another technology can be used which is a hydrogen addition processes such as hydrocracking.

Even with several well developed technologies available to the industry, there is a desire to improve them. To improve on existing technologies plasma may be able to assist in several ways. Beneficial plasma chemistry might act to pretreat heavy oil to breakdown some of the heavier components such as asphaltenes which can help prevent fouling issues, reduce viscosity, help remove impurities, and increase catalyst lifetimes (32). Plasma chemistry can also direct crack oil and potentially do so in a more efficient way compared to thermal processes. Some of these ideas will be explored throughout the research presented within this thesis. One key idea to keep in mind is that while thermal plasma methods will produce cracking chemistry, the equilibrium nature of thermal plasmas will push the hydrocarbons to produce solid carbon, hydrogen, and waste heat; this is to be avoided. The main objective of non-equilibrium plasma is to control the

chemistry so that cracking can occur without allowing excessive heat and carbon production.

Non-equilibrium plasma processing of oil

Non-equilibrium plasma chemistry has some unique properties that make them attractive for many applications. In some cases, the chemistry that is created by non-equilibrium plasmas are simply not accessible by normal means. A popular example of some unique non-equilibrium plasma chemistry is ozone generation. Non-thermal, non-equilibrium oxygen plasma can produce relatively large amounts of plasma (33). This method of ozone generation from oxygen is better than other standard known thermal methods and therefore plasma generation of ozone has become an important process. Similarly, ozone can be generated simply using UV radiation which has a similar mechanism and still utilizes the concept of non-equilibrium chemistry.

Another example of interesting non-equilibrium chemistry is from a carbon monoxide plasma (19). From a non-equilibrium carbon monoxide, a unique film composed entirely of carbon and oxygen can be formed; this film is postulated to be a carbon suboxide polymer. Any attempts to create this film from carbon monoxide using only standard thermal chemistry is yet unknown and seemingly unlikely due to the unfavorable equilibrium thermodynamics. However, it was also demonstrated that when carbon monoxide is taken to extremely high pressures (~ 1-10 GPa) that a similar film

can be created. The non-equilibrium chemistry that occurs at atmospheric conditions is mimicking the chemistry that occurs at extremely pressures (34).

A lot of the interesting chemistry associated with non-equilibrium plasma can be attributed to the long lifetimes of vibrationally excited molecules and their interaction with molecules having low translational energies. Vibrational excitation of molecules can occur within plasma by several methods such as direct electron impact or photon absorption. These excited states will then last quite long due to adiabatic collision considerations (9) (10). This can lead to a somewhat selective relaxation process for the vibrationally excited states and subsequently the interesting chemistry mentioned previously.

With the understanding that non-equilibrium plasma chemistry can offer some unique chemical reactions it becomes desirable to extend this chemistry to other areas such as liquid processing. It has been known for more than a century that plasma can be generated directly in a liquid however the process is very complicated and difficult to study. The exploration of non-equilibrium plasma processing of oil should help shed more light on the underlying physics taking place.

Dissertation overview

This section presented the thesis topic, the motivation behind the research, and the approach used to explore the thesis statement experimentally. The next section entitled “Background and Literature Review” reviews the current literature and explains

in detail the state of knowledge for high density non-equilibrium plasma. To effectively describe high density non-equilibrium plasma, both equilibrium and non-equilibrium low density plasmas are also reviewed. The third section is entitled “Theory and Modeling” and it begins the theoretical exploration of high density plasma generation. Attention is given to a new method of generating non-equilibrium plasma in liquids referred to as an Electrodynamic Ball Discharge (EBD). Important parameters are defined that are required for characterizing the plasma state and the operating conditions of an EBD; of utmost importance is the definition of the energy density along with the energy balance terms the define it. Also presented are detailed timescale analyses which characterize the transience associated with non-equilibrium states. The fourth section is entitled, “Experimental Results” where the various experimental techniques for characterizing the non-equilibrium plasma will be presented. This includes direct measurements of the electrical characteristics of the discharge, the optical emission spectrum of the plasma, and the chemical changes of the oil. Finally, the Summary and Conclusions are presented in the last section.

BACKGROUND AND LITERATURE REVIEW

A plasma state can be achieved not only by natural thermal mechanisms, such as those produced during fusion processes occurring in stars, but also from relatively high electric field. Electric fields control the movement of charged particles and can stimulate ionization processes; the production of charged species within an electric field can lead critical breakdown events. Due to their high mobility and small mass, electrons are the first species to gain energy from an externally applied electric field (9); therefore, they are the most important species when considering plasma initiation. To begin the process of electrical breakdown leading to the formation of a plasma state one or more free electrons must first be present. These primary electrons are often referred to as seed electrons, and they can be produced in several ways.

There are a limited number of ways to produce free electrons. When considering plasma formation in gases, electron production can be conceptually split into two categories, homogeneous and heterogeneous, Table 1. Homogeneous electron production occurs within the electrode gap while heterogeneous electron production occurs at an interface, typically the electrode/gas interface. From an energy perspective, it is easier to extract electrons from a solid surface; the energy required to do so is referred to as the work function and typical values are around 2-5 eV (9). Ionization potentials for gaseous molecules are typically around 10 eV, more than twice as much as work functions. This interfacial surface effect is quite significant and arises from the breaking of the crystal symmetry of the solid at the surface. This results in a rearrangement of the electron

distribution creating a dipole layer across which the electrical potential rises from the Fermi level inside the metal to the vacuum level outside, the difference being the electron work function (35). Since a smaller energy is required to produce electrons from an interface, there are more mechanisms available to do so. However, under normal atmospheric conditions in air, homogeneous mechanisms are typically responsible to produce primary electrons. To understand this, consider that under these conditions in air background conduction currents on the order of 1e-16 → 1e-17 A/cm^2 exist naturally; this current is caused by free electron production due to cosmic radiation and radioactive substances present in the earth and the atmosphere (36). There is therefore always a small concentration of free electrons available from these high-energy photon sources; assuming atmospheric pressure, a near ground earth electric field of 150 V/m and an electron mobility of about 600 cm^2/V*s means there is approximately 1 free electron per cubic centimeter. If care is taken to avoid these naturally occurring free electrons then high electric fields can be achieved before a breakdown happens; in which case electrons will be emitted from the electrode before any homogeneous reactions can occur.

Table 1 Generalized mechanisms of electron production (A, B are Molecules, S is a surface)

		Homogeneous Electron Production	Heterogeneous Electron Production	Ionization Energy Source
1	Photoionization	$h\nu + A \rightarrow^{+} + e^-$	$h\nu + S \rightarrow S^+ + e^-$	*Photons*
2	Electron Impact	$e^- + A \rightarrow A^+ + e^-$	$e^- + S \rightarrow S^+ + 2e^-$	*Thermal Electrons*
3	Ion Impact	N/A	$A^+ + S \rightarrow A + S^{2+} + e^-$	*Ionization Energy*
4	Penning	$A^* + B \rightarrow A + B^+ + e^-$	$A^* + S \rightarrow A + S^+ + e^-$	*Excitation Energy*
5	Field Emission	$A + E \rightarrow A^+ + E + e^-$	$S + E \rightarrow S^+ + e^-$	*Electric Field*
6	Thermal Emission	$A \rightarrow A^+ + e^-$	$S \rightarrow S^+ + e^-$	*Thermal Heating*

All the electron production mechanisms can occur simultaneously but typically one mechanism will dominate. Figure 3 illustrates a generalized view of the breakdown process. A breakdown event typically occurs when a secondary ionization process provides feedback to the primary process and/or becomes the main driver of electron avalanching; this process is also referred to as self-sustaining. If the breakdown process occurs due to secondary electron emission from ion bombardment, then the characteristic time of the breakdown will depend on the mobility of the ions; which may be on the order of microseconds. Secondary emission due to photoemission, from photons generated by electrons entering the anode, can lead to much faster breakdowns since they depend on the mobility of the electrons. Perhaps the quickest mechanism is the streamer breakdown, which occurs when the space charge generated from avalanching becomes so large that the local electric field initiates homogeneous ionization mechanisms.

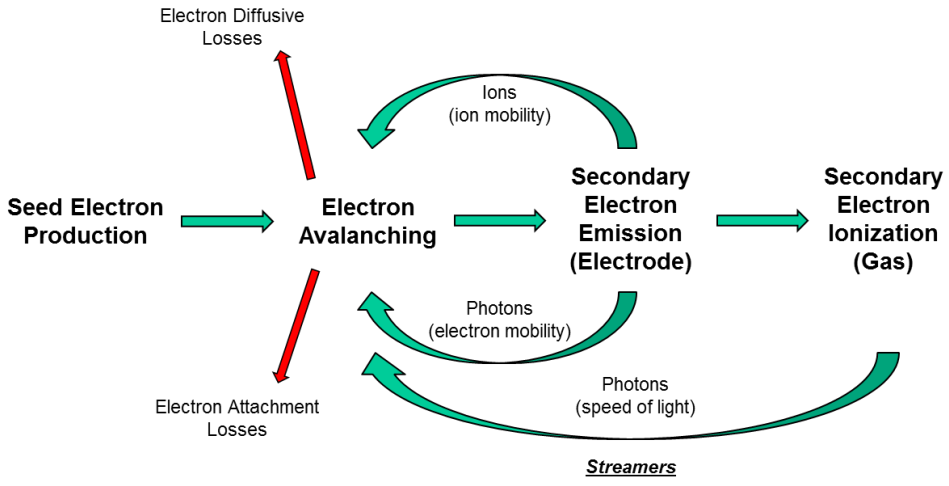

Figure 3 Generalized view of electron production mechanisms and breakdown processes for plasma generation

The electrical breakdown process in liquid is a complicated topic of discussion for both theoretical and experimental reasons. Experimentally there are many challenges to overcome to get accurate and consistent measurements. Theoretically it is also challenging due largely to the high density and amorphous organization of the molecules; this means that intermolecular forces play a critical role in defining ‘free’, or perhaps more accurate ‘quasi-free’, electron transport through the medium. To obtain a better grasp on liquid breakdown this chapter will approach liquid breakdown from two different directions, gaseous breakdown tending toward higher densities and solid breakdown. Gaseous breakdowns have been studied for more than 100 years and are considered understood; furthermore, the study of gaseous breakdowns provides a method of studying the effect of increasing density. In fact, a key parameter in gaseous breakdowns is the similarity parameter, *pd*, which is the product of the pressure and the electrode gap. Since pressure is directly proportional to the density, *n*, the *pd* parameter essentially describes how many molecules are between the electrode; for this reason, some people prefer, *nd*, as the similarity parameter. It seems logical that as the density is increased, approaching densities like liquid densities, that the breakdown mechanisms should be like liquid breakdown. Solid breakdown is perhaps more like liquid breakdown since the densities are much closer. The current state of understanding for solid breakdowns are better than liquids, however there are still many questions and speculations regarding mechanisms for solid breakdown.

Once a breakdown process is initiated it will naturally drive towards an equilibrium state, however the type of discharge that will occur after a breakdown event

is dependent upon many parameters such as the number density of the medium, the gap length and shape, the waveform of the applied voltage and the characteristics of the external circuit (37). Each one of these factors essentially can provide a way of controlling the rate at which electrical energy from the external circuit is converted to plasma energy, consisting of chemical energy and heat. A core concept of the thesis is that dynamic and transient processes of the plasma discharge are much different than the steady state characteristics. This can be conceptualized in a rather general way.

Consider a simplified circuit whereby a capacitor is discharged across a gap creating a plasma, Figure 4.

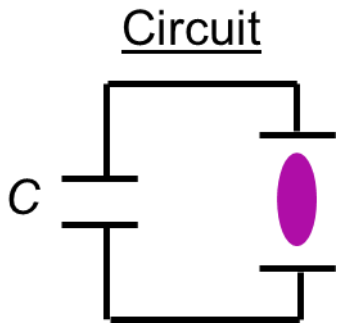

Figure 4 Simplified circuit, consisting of only a charged capacitor and a gap, for generalized transient analysis

The voltage will initially be at the breakdown voltage and as the current flows through the plasma the voltage will decrease according to a time constant associated with the resistance of the plasma, **Equation** 1.

$$V(t) = V_o e^{-\left(\frac{t}{R_p C}\right)} \qquad 1$$

Here the initial voltage, V_o, is the charge on a capacitor with a value of C and the plasma has a resistance R_p which is also a function of time but will be assumed constant over the range of interest for simplicity. At the beginning of the breakdown process the avalanching process will produce an exponential growth in current, Equation 2.

$$I_a = I_o e^{\left(\frac{\alpha \mu_e V}{d}\right)t} \qquad 2$$

As the voltage drops and the electric field decreases the free electrons in the gap will gain a reduced amount of kinetic energy therefore the electron production from the avalanching will slow down; furthermore, the available current from the capacitor will continually decrease, Equation 3.

$$I = I_a e^{-\left(\frac{t}{R_p C}\right)} \qquad 3$$

As a resulting of the competing growth and decay of the current the plasma will only be allowed to progress for a duration of about five time constants. Since the resistance of the plasma is a fundamental property of the medium in which the plasma is being generated, the main control parameter is the external capacitance of the circuit. If the capacitance is kept small, the breakdown process will be halted very early and will not be allowed to thermalize, Figure 5.

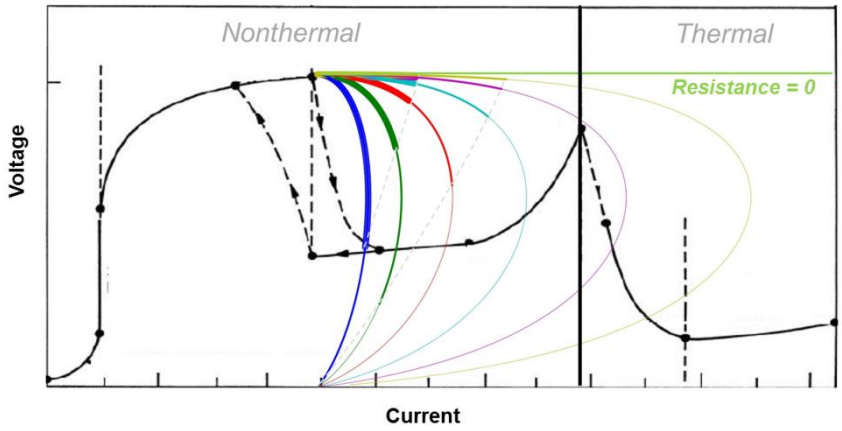

Figure 5 Voltage versus current characteristic showing the transient behavior of a capacitive discharge for increasing values of capacitance

It is expected that for high density mediums the plasma resistance will be very high, therefore thermalization can occur rapidly. This can be observed for example by analyzing the characteristic voltage-current curve as shown in Figure 5, for high values of *pd* (38). To prevent thermalization a very small capacitance is required. For constant dielectric strength, φ, the capacitance is related to the energy density as shown in Equation 4. From this and the previous equations it can be seen how controlling the energy density will also control the non-equilibrium nature of the plasma.

$$\rho = \frac{{}^{1}/_{2}\, CV_o{}^{2}}{\pi r^2 d} = \frac{\varphi C V_o}{2\pi r^2} \qquad 4$$

It is very common to limit the current of gas phase plasmas to create unique non-equilibrium chemistry for gas phase process, this can lead to glow discharges for example at low pressures or small gaps; but as the gas density becomes larger these unique steady state, non-thermal and non-equilibrium plasma regimes becomes

unobtainable. However, the key concept of controlling current, or more accurately energy density, can still lead to non-equilibrium transient discharges. This idea is easier to understand in the gas phase since electrical breakdown in the gas phase is well known, yet it is more difficult to understand this for liquid breakdown, where the breakdown process remains unknown. Experiments using very short breakdown pulses, nanosecond timescales, are expected to shed some light on the matter since it is the expected timescale for the breakdown process. These experiments will also be briefly reviewed.

Gas phase plasma initiation

The description of plasma initiation requires first understanding the movement of electrons through a gaseous medium when an electric field is applied. This has been a topic of investigations for nearly 110 years starting with J. S. Townsend in the early 1900s. There have been many techniques developed for make fundamental measurements of electron transport which typically fall into the title of electron swarm studies. These techniques have been valuable in the development of understanding fundamental breakdown processes and their description can be found in several books (39; 40; 41). The measurements made by such experiments can be related back to the Boltzmann Transport Equation to give parameters such as the mean electron energy and collisional cross sections. In swarm studies and calculations ionization and electron attachment are not considered and are therefore only valid at low values of reduced electric field (E/n) and gases with low electronegativity. When inelastic collisions

become important the rate coefficients of the processes must also be provided. Inelastic collisions leading to the production of more charged species are what lead to plasma formation.

It has been said that electron avalanching is a requirement for any breakdown mechanism; the exact quote from Raizer (6) is that, “An individual avalanche is a primary and inescapable element of any breakdown mechanism.” It is for this reason that the study of electron avalanching is very important for describing the plasma initiation process. A rather complete study of electron avalanching is provided in the very good book by H. Raether entitled, “Electron Avalanches and Breakdown in Gases” (42) and should be referenced for a more complete analysis of the process. Electron avalanching is an exponential process that is initiated by one or more free electrons, Equation 5.

$$n_e(x) = n_o e^{\alpha x} \qquad 5$$

The coefficient, α, is the mean number of ionizing collisions per electron over some distance and is often referred to as Townsend’s first coefficient. From Cloud Chamber experiments, the avalanches are known to have a wedge shape with a parabolic profile at the head of the avalanche; this is shape is described using Equation 6.

$$y = \left(\sqrt{\frac{8\alpha U_{th}}{3E_o}}\right)x \qquad 6$$

Here U_{th} is the thermal energy of the electrons in volts and E_o is the applied electric field. The width of the avalanche is proportional to the square root of the thermal energy of the electrons as would be expected by diffusion.

With an accurate discretion of the electron multiplication rate and the spatial distribution the electrical current that can be measured in the external circuit can be modeled. For a detailed derivation, the reader should reference Raether (42). Such a model can be used to extract some fundamental parameters from current measurements. For example, the broadening of the measured current pulse is directly related to the lateral diffusion of the electrons created by the avalanche; the growth rate of the current pulse is related to the first Townsend coefficient; the width of the current pulse is related to the mobility of the electrons. Analysis and modeling of the experimental current pulses are arguably underused as a plasma diagnostic. Further information is available when for the case when multiple avalanches occur.

A single avalanche is typically not sufficient to lead to breakdown; instead there are usually several successor avalanches that occur after a primary one or at the same time as others depending on the initial seed electron source. An example of a current measurement for a single avalanche followed by several successors is shown in Figure 6 for three different conditions based on the self-sustaining criteria, Equation 7.

$$\mu = \gamma_i[e^{\alpha d} - 1] \qquad 7$$

The parameter γ_i represents the secondary electron emission from photon emission, ion emission, or some other mechanism and *d* is the electrode gap.

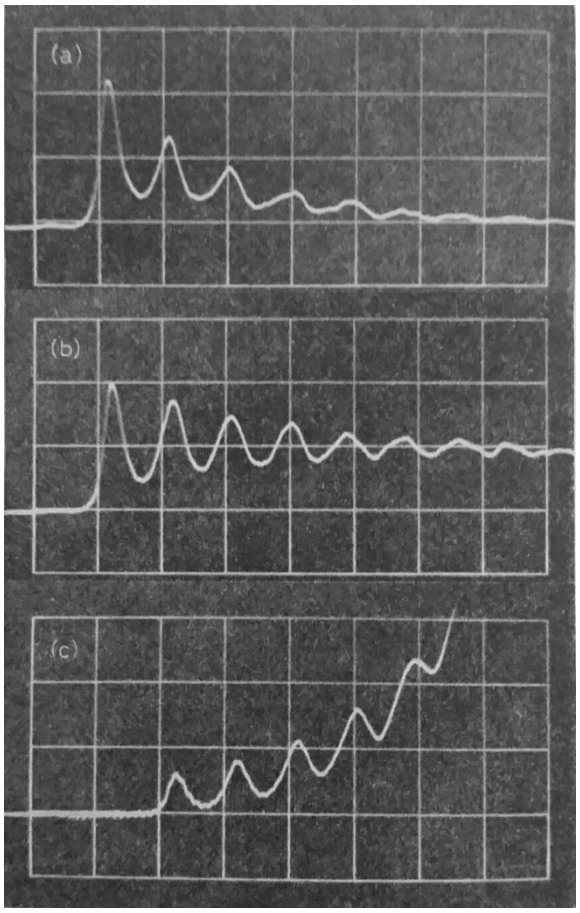

Figure 6 Current measurement for avalanches with photosuccesors for a) μ < 1, b) μ = 1, c) μ > 1 (42)

In this case, the subsequent avalanches are caused by photoemission when the electrons enter the anode, therefore the time difference between the current peaks are equivalent to the transit time of the electrons across the gap. Photoemission can occur at larger pressures and/or short gap lengths. If the criterion for a self-sustaining discharge is met, the current will increase exponentially and this was modeled by Raether (42). However, this model does not consider the effect of the external circuit. Conceptually there can be the situation that the applied voltage is sufficiently large to meet the self-sustaining criterion, yet the capacitance of the external circuit is so low that the current does not run

away. Instead, the current will begin to grow exponentially but will quick decay as according to Equation 3. This transient behavior is exactly the desired effect that is sought to maintain a non-equilibrium plasma in dense mediums.

Solid phase initiation

The electrical breakdown process of liquids is thought to be more like that of solids due to the similar densities; however, the mechanisms of plasma initiation in a solid are still not completely known. In gaseous plasma initiation, the electrical conduction was completely described by the electron and ion production and transport, however in solid polarization effects can also contribute to the current. Just as swarm experiments in gaseous were fundamental in understanding the prebreakdown process, simple electrical conduction is an important idea for solid breakdowns. Electrical conduction in solids for small electric fields are typically related empirically to temperature using Equation 8, where *A* and *u* are the empirical constants for the given material.

$$\sigma = A\mathrm{e}^{-\frac{u}{kT}} \qquad 8$$

Several models have been proposed to explain this relationship (43). Experimentally measuring these values accurately has proven complicated. The actual conduction of electrons in dielectrics is difficult to explain absolutely for several reasons. There are many processes that can occur simultaneously which contribute to the

conduction current. Impurities are difficult to avoid and can have a large effect on the conduction, for example by creating so called ‘traps’ which are more accessible for electrons. Material preparation can also lead to structural differences leading to grain boundaries which can affect the conduction mechanisms. Even with the experimental complications, the theoretical descriptions of the process of electrical conduction in such disordered material have been described (44).

The fundamental difference between conductive metals and insulating materials is the energy of the Fermi level relative to the energy of localized zones of free electrons. If the Fermi energy is within these localized free electron zones than the material is said to be conductive and electrons can be treated with normal transport theory if the mean free path is large compared to the electron wavelength. When the Fermi energy is far removed from these free electron zones, the material is an insulator or semiconductor. In this case, conduction is only possible by excitation to the free electron region or by electron hopping, whereby an electron hops between free electron zones (36).

It also known that the conductivity is largely dependent on the applied electric field when the electric field becomes large, therefore the parameter *u* from Equation 8 is actually a function of the applied field. The higher currents that are observed with these high fields are thought to be caused by charge injection from the electrodes or electron multiplication in the bulk of the material or both (36).

Eventually the field will be high enough to lead to a breakdown event. Electrical breakdown of solids is divided into three categories: 1) Intrinsic, 2) Thermal, and 3) Erosion electrochemical (36). The thermal and erosion electrochemical mechanisms are

not of interest within the scope of this dissertation since they occur at longer timescales. Intrinsic breakdown can occur within a few nanoseconds. Two different mechanisms of intrinsic breakdown were presented by Frohilich (45); a low temperature mechanism and a high temperature mechanism. The low temperature mechanisms considered interaction with the lattice and avalanching like the gas phase breakdown process (46). This kind of avalanching in solids was also seen to be consistent with laser-induced breakdowns (47), which is important since it eliminated that possibility of interfacial mechanisms. The low temperature model ignores electron-electron interactions however at higher temperatures collective behavior can become important (45). Furthermore, streamers mechanisms have also been proposed which are like gaseous streamers (48).

Many of the ideas that have been used to explain gaseous breakdown have been applied to describe the breakdown process of solids with some success. The ability for electrons to find conduction bands within the solid lattices are a critical aspect of the intrinsic solid breakdown mechanisms. The electron-lattice interactions are much different than the way electrons interact with molecules in the gas phase; furthermore, it has also been seen that collective behavior can also play a more important role in solids. However, it is important to note that these ideas are still largely just speculation and conclusive experimental evidence has remained elusive due to many of the complications described previously.

Liquid phase initiation

For small times scales, liquid breakdown can be conceptualized like solid breakdown. The two are fundamentally differences between liquids and solids from the point of view of electrical conduction; the liquid is constantly changing due to slightly weaker interaction forces compared to solids which are static due to strong interaction forces and liquids do not have well defined conduction bands. Therefore, it is expected that measured conduction and breakdown values may vary significantly for liquids from one instance to the next. To further complicate things, liquids have all the same complications as solids but also can have additional impurities such as gaseous bubbles and small particles which can become charged and conduct electrically or simply provide a low-density region to make breakdown easier.

In the paper of Sharbaugh (8), it is clearly stated that there are two principal schools of thought related to the underlying mechanism of electrical breakdown in liquids. The first school believes that it should be possible to have an electron multiplication much like Townsend theory of breakdown in gases. The second school of thought is referred to as the bubble mechanisms, whereby the breakdown process requires the formation of a bubble. Impurities and carbon formation are important and can cause difficulties in reproducibility of breakdown voltage measurements.

There are many reviews of liquid breakdown available from before the 1980's (49; 50; 51; 52; 53; 54; 55). Some authors have also attempted to consolidate these reviews in their books (36; 56). However, these authors have clearly pointed out that

there is still great uncertainty in the underlying mechanisms associated with liquid breakdown. Since the 1980, some of the more promising work tends to involve pulsed techniques.

Pulsing techniques have many advantages but were not used very often before the 1980s due to the experimental difficulties inherent in making reliable production and measurements of currents under very short pulse conditions, which are on the nanosecond timescale. In lieu of these capabilities laser induced breakdown of liquids seemed to be an effective method of generating electric fields that are high enough to cause breakdown yet short enough in duration to allow for more careful study of the breakdown process. A great review of laser induced breakdown was published in 1997 (57). While this review only considered aqueous media, it still provides a nice review of the proposed mechanisms. Laser breakdown has some advantages and disadvantages for studying the breakdown process. The obvious advantage is that pulse durations can be incredible short, on the femtosecond and picosecond time scale. This can allow for very find resolution. A disadvantage is that the laser must be focused and accurately controlled; multi-photon breakdown can result and careful analysis is required; furthermore, different absorption mechanisms must be accounted for. A careful energy balance can be carried out to quantify these effects quite accurately and provide further insight on the process (58). The models developed for laser-induced breakdown typically involve a cascading effect initiated by what is referred to as a “lucky electron”. There has also been some work on studying the non-equilibrium effects of laser-induced breakdown (59). Optical breakdown in dielectric liquids is a little more difficult to come

by, however there have been some important advances in this area as well (60; 61). In these studies threshold fields could be determined and related to molecular properties such as hydrocarbon chain length. This type of peculiar behavior seems to imply a photo-molecular absorption mechanism is taking place in this case, rather than an electron cascading type mechanism. Much more work needs to be carried out in this area.

There have been many interesting studies after the 1980s attempting to explain breakdown in dielectric liquids due to high electric field produced by electrodes. Optical techniques have been used to study streamer formation (62), however these studies are on relatively long, microsecond, time scales. Streamer breakdown in dielectric liquid has been investigated by other authors in the 1980s as well using microsecond pulses (63). While a lot of valuable information can be learned from these very good studies (64), they do not allow for very good resolution of the prebreakdown process, which can occur very rapidly on the nanosecond timescale (65). Recent advances in semiconductor devices have led to an increase capability for producing high voltage nanosecond pulses. With these technological advancements has come some very interesting work in the field of liquid breakdown (66; 67; 68; 69; 70; 71). Some work suggests that it is possible to create a liquid plasma without creating a low-density region at all (72). Other work suggests that cavitation is a critical part of the prebreakdown processes, while others seem to like the idea of an electrostrictive mechanism; however, the difference between these mechanisms is not clear. This is still a topic of debate; however, a careful comparison should be made between solid and liquid breakdowns. Solid breakdowns are

thought to occur with avalanching-like mechanisms since mean-free paths can be defined (7), and electron-lattice interactions can be accounted for. The situation is quite similar for liquids, however conductive channels will simply vary on the timescales of molecular motion. If cavitation is a fundamentally important and unavoidable precursor to liquid breakdown in dielectric media, then it may very well be an important aspect of solid breakdown in dielectrics. The yield strength of a liquid can be used to estimate cavitation, or cracking, of a liquid just as it can for solids; this will be carried out in the theory section. Regardless of what the actual initiation mechanism is, it is still possible to explore the generation of non-equilibrium plasma generation in liquids simply by controlling the energy density of the plasma.

Thesis objectives

There is much controversy in the field of plasma physics in the area of liquid phase plasma generation. Many professionals in the field are wondering if it is possible to generate liquid phase plasma; that is a high density ionized phase using external electrical fields. Furthermore, if such a phase is possible what might be its application? This thesis aims to add to the discussion of this issue by describing phase variations and field interactions from a more fundamental perspective. The applications of such phases are explored both theoretically and experimentally.

THEORY AND MODELING

To generate a non-equilibrium plasma in a liquid, phase the energy input must be controlled. To do this a new technique of generating plasma in liquids was created call the Electrodynamic Ball Discharge (EBD). The overall aim of an EBD is to convert electrical energy into desirable chemical reactions with low thermal losses. Converting electrical energy to chemical energy is accomplished by creating a low energy plasma in the form of a microspark. A microspark is created when a charged particle approaches surface that is held at a different potential. As the particle approaches, such a surface the electric field between them becomes stronger and can eventually exceed the breakdown strength of the medium. If the available charge from the external circuit is minimized then the amount of current available can be insufficient to achieve breakdown. However, assuming enough charge is available to achieve breakdown then the amount of charge that will be conducted after breakdown occurs will be small. Minimizing available charge in this way allows for the creation of very low energy and incomplete discharges. This current is converted into thermal energy while also promoting chemical reactions. These low energy plasmas, or microsparks, will have less thermal energy losses because there is not sufficient time for thermalization. Microsparks can also be generated by simply applying a high voltage across a small gap, however to reduce the energy of the microspark the capacitance of the external circuit must be minimized. It is difficult to reduce this capacitance below the picofarad range for such a setup simply due to stray capacitance that exists from wires for example. The EBD concept overcomes this

difficulty by utilizing particles with well-defined capacitances that are proportional to their size.

Plasma initiation from the liquid phase

Energy input considerations

Phase change is an important aspect of plasma initiation in liquids. It can be rather challenging to try to avoid a phase change during the liquid phase plasma initiation process. The reason for this is an inherent phase instability that can occur, Figure 7. To initiate a breakdown process in a high-density medium a high reduced electric field is required. If there is a small decrease in the local density, then the reduced electric field is increased. A larger reduced electric field will lead to more energy being transferred to free electrons effectively increasing their temperature. A high electron temperature will increase the rate of electron-translational relaxation leading to a larger internal energy in the molecules. A high internal energy will lead to a further decrease in the density completing the feedback loop leading to instability.

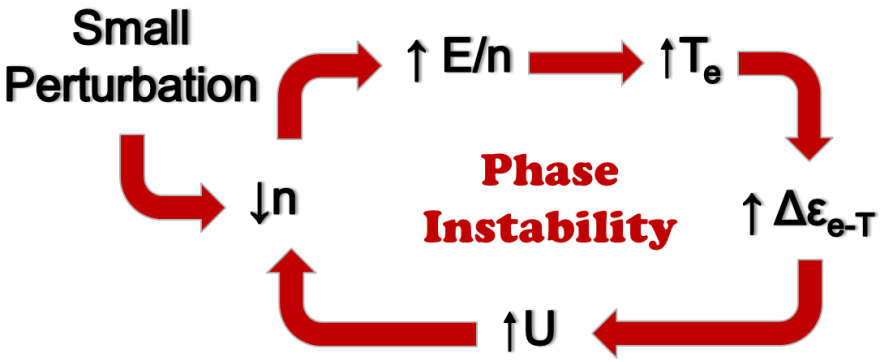

Figure 7 Phase instability that can occur during a high-density plasma initiation process

Due to the transient nature of the discharge it is crucial to try and analyze the total specific energy input; this also requires estimating the discharge size and duration. The energy density of a discharge is limited by the available energy of the external circuit. The energy provided by an external capacitor can be on the order of mJ to J; discharges can be on the order of 1e-13 m^3 to 1e-18 m^3 therefore specific energy inputs are expected to be around 1e9 kJ/m^3 to 1e12 kJ/m^3 which is about 1e6 kJ/kg to 1e9 kJ/kg for liquids with densities near water for the lower mJ discharges. If the intensity of the discharge can be considered an indication of its size then it appears size decreases with decreasing energy input; this will be tested experimentally in the experimental section. Because it is expected that the discharge size should scale with energy input, reducing the energy input can significantly decrease the specific energy input and for energies as low as 1 nJ the specific energy input can approach values down to 1 kJ/kg. Such low energy inputs may be difficult experimentally however by reducing the energy input for liquid plasma discharges it is expected to have increased selectivity and efficiency in chemical processing.

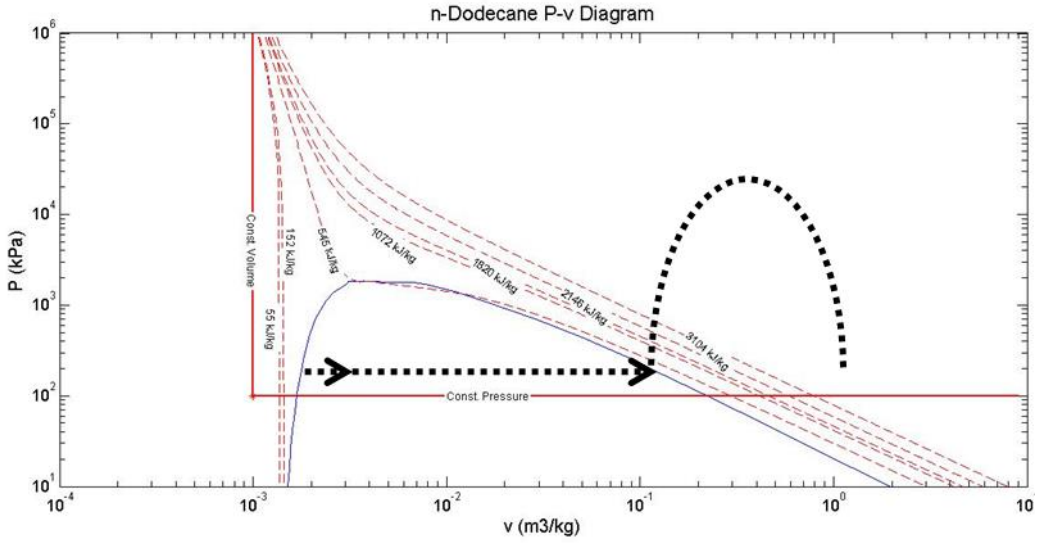

Figure 8 P-v diagram for n-Dodecane with lines (dashed) of constant energy

As an initial approximation, it can be assumed that all the energy is used to change the phase of the liquid. At extremely low energy inputs, less than about 100 kJ/kg, there is not enough energy available to change the phase of the liquid which may make it difficult for a plasma to occur, Figure 8. If the energy input is between 100 kJ/kg and 500 kJ/kg a vapor-liquid equilibrium would be expected however as vapor begins to form breakdown is likely; this can lead to a highly non-equilibrium state followed by rapid quenching. Through the process highly efficient chemistry can take place. If the specific energy input becomes too high, greater than 500 kJ/kg, thermal equilibrium is expected to occur followed by rapid quenching.

The energy input of the discharge does not have to completely go into changing the phase of the liquid, it is also used for chemistry and heating; the way that energy is distributed depends on the method by which the discharge is initiated. It may be possible that the discharge is initiated without a phase change, however for this to occur the

energy input must be carefully controlled; to try and gain more insight to the phase change process the time constants for phase changes can be considered. Then if the energy input for the discharge occurs at a rate faster than the phase change processes than it would be expected that no phase change occurs.

Time constant analysis

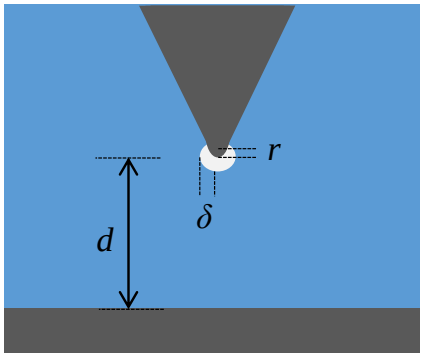

Figure 9 Electrode geometry used for the analysis of time constants

In general, when a voltage is applied across a solid-liquid interface several processes can occur. Three possible processes include electrolysis, local heating, and cavitation. For the case of a short transient pulse voltage the relative importance of these processes depends largely on how rapidly the voltage is applied; therefore, the characteristic times of these processes are important. Estimates for these characteristic times will be considered. The general setup is as shown in Figure 9, where a pointed electrode with tip radius r, is some distance, d, away from the other electrode and a small bubble is forming having a radius δ which will be the free variable for this

analysis. It will be approximated that the bubble growth away from the electrode grows with a cylindrical geometry having a constant cross sectional area.

The aim here is to approximate the time it takes for the bubble to grow to some length δ as predicted by the different mechanisms; these estimations will be made by considering an energy balance for each mechanism. Using these energy balances provides a boundary for the fastest possible rate at which these mechanisms can occur. As will be seen these estimations will take on a general form described by Equation 9, where C_i is some constant for the specified conditions that is to be determined for each associated mechanism.

$$\tau_i = C_i \delta \qquad 9$$

To determine these constants of proportionality for each mechanism the variables in table Table 2 will be used.

Table 2 Legend of variables used for estimating proportionality constants

Property	Variable	Units
Density	ρ	$\left[\frac{kg}{m^3}\right]$
Electric Field	E	$\left[\frac{V}{m}\right]$
Enthalpy of Vaporization	h_v	$\left[\frac{kJ}{kg}\right]$
Mobility	μ_i , $(i \stackrel{def}{=} species)$	$\left[\frac{m^2}{V * s}\right]$
Number Density	n_i , $(i \stackrel{def}{=} species)$	$[m^{-3}]$
Specific Heat	$c_{p,i}$, $(i \stackrel{def}{=} species)$	$\left[\frac{kJ}{kg * K}\right]$
Voltage	V	$[V]$
Yield Strength	Y	$\left[\frac{N}{m^2}\right]$

Electrolysis

Electrolysis requires the presence of mobile ions in the liquid to transfer charge; therefore, if there is no ion concentration in the liquid electrolysis will not occur. The electrolysis reaction that is of interest here is the half reaction at the cathode, Equation 10. This reaction has a reaction enthalpy of about h_r = 299,990 J/mol, which is simply the formation enthalpy of anion OH^-.

$$H_2O + e^- \rightarrow \frac{1}{2}H_2 + OH^- \qquad 10$$

The maximum rate of hydrogen production will be limited by the energy input at the electrode. Therefore, it will be assumed that all the electrical input energy is used to generate hydrogen in this way. These assumptions lead to the energy balance equation, Equation 11.

$$h_r \frac{dN_{H2}}{dt} = VI \qquad 11$$

For the specified geometry, the area through which current flows is a constant given by Equation 12.

$$A = \pi r^2 \qquad 12$$

Furthermore, the moles of hydrogen produced is only a function of the characteristic length as given by Equation 13, where everything in the parenthesis is assumed constant.

$$N_{H2} = \left(\frac{\rho_{H2}}{M_{H2}}\pi r^2\right)\delta \qquad 13$$

The current for a specific charged species (i) can be expressed in terms of the mobility, charge, and electric field as in Equation 14.

$$I_i = en_i\mu_i EA \quad (14)$$

It will be assumed that the geometry shown in Figure 9 can be approximated as a parabolic tip above a plane for the purposes of calculating the electric field. Furthermore, it will be the maximum electric field will be used to calculate the current flow; this is reasonable since it is the area of the highest stress. The maximum electric field is approximated using Equation 15.

$$E = \frac{2V}{r \ln {}^{2d}/_{r}} \quad (15)$$

Using Equations 11 through 14, plugging into Equation 15 and integrating provides an equation for the characteristic time as a function of characteristic bubble length, Equation 16.

$$\tau_e = \left[\frac{h_r \left({}^{\rho_{H2}}/_{M_{H2}}\right)}{\left({}^{E^2}/_{2}\right) r \ln\left({}^{2d}/_{r}\right) en_e\mu_e}\right]\delta \quad (16)$$

Boiling

A characteristic timescale can be estimated for boiling by considering a simple energy balance at the solid-liquid interface, Equation 17.

$$m\left(c_{p,H2}\Delta T + h_v\right) = VI\tau_b \quad (17)$$

Again, the current as described in Equation 14 is inserted into Equation 17 and then solved for time to obtain Equation 18.

$$\tau_b = \left[\frac{\rho_{H2}\left(c_{p,H2}\Delta T + h_v\right)}{\left(E^2/_2\right) r \ln\left(2d/_r\right) e n_e \mu_e}\right]\delta \quad (18)$$

Cavitation

For cavitation to occur the voltage must be strong enough to overcome the yield strength of the liquid; this is equivalent to pushing the interface apart leading to the creation of a low-density region. To estimate the characteristic time for this process the Yield strength of the liquid is balanced with the applied power, Equation 19.

$$Y\pi r^2\delta = VI\tau_c \quad (19)$$

Just as before the electric field will be related to the voltage using Equation 15 and the current will be given by Equation 14 and when combined with Equation 19 can be solved for time, Equation 20.

$$\tau_c = \left[\frac{Y}{\left(E^2/_2\right) r \ln\left(2d/_r\right) e n_e \mu_e}\right]\delta \quad (20)$$

The proportionality constants for the three different mechanisms have been obtained and can now be compared by plugging in actual numbers and plotting. To create this plot the number used are shown in Table 3.

Table 3 Values used for comparing the relative rates for each mechanism

Variable	Value	Unit
ρ_{H2}	89.9	g/m^3
n_{H2}	2.71e025	m^{-3}
$c_{p,H2O}$	1670	J/kg*K
$h_{v,H2O}$	42400	J/kg*K
n_{Na}	1.06e22	m^{-3}
μ_{Na}	5.19e-8	$m^2/(V*s)$
E	6.68e8	V/m
r	5e-6	M
d	1e-3	M
μ_e	1.80e-4	$m^2/(V*s)$
Y	45e5	N/m^2

Discussion and comparison of the three mechanisms

One of the most important parameters for this analysis is the electron density. This is illustrated in Figure 10 which plots the three different mechanisms each for two different electron density values. The electron density describes how many electrons are available to do work. Figure 10 illustrates that when there are more electrons available the characteristic times for all mechanisms can be much faster, as is to be expected.

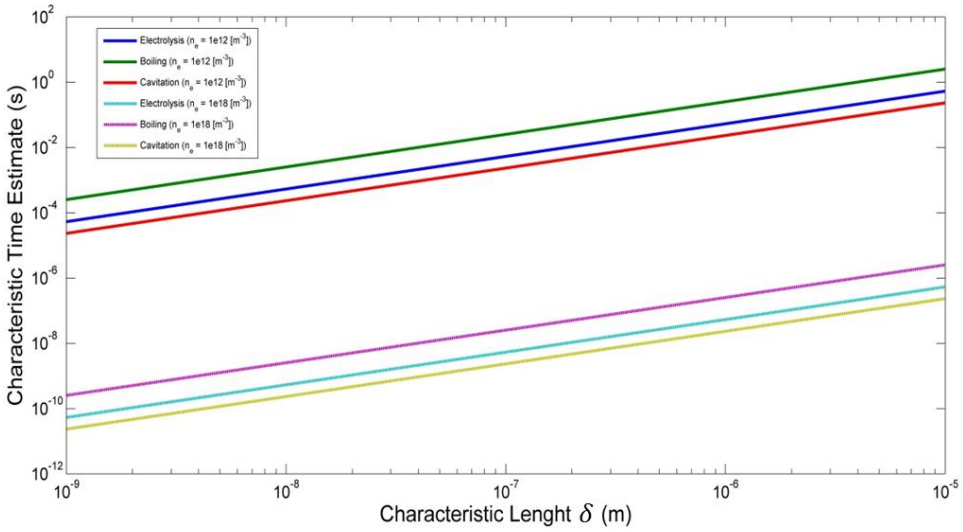

Figure 10 Time constants for low density bubble formation verses bubble size

Instead of varying the characteristic length, the electron density can be varied and the characteristic length can be held constant. This is useful if the bubble size is known for certain plasma initiation conditions in which case this model can be tested. For example, it can be asked how long it might take to form a 1 micron size bubble with these mechanisms. This has been plotted as shown in Figure 11. From experiments, it is known that a 1 micron bubble can be generated in about 1 microsecond for these conditions. This means that an electron density of about 1e16 m^{-3} would be required for cavitation, about 7e16 m^{-3} for electrolysis, and 1e18 m^{-3} for boiling to provide sufficient energy to generate a 1 micron bubble in 1 microsecond.

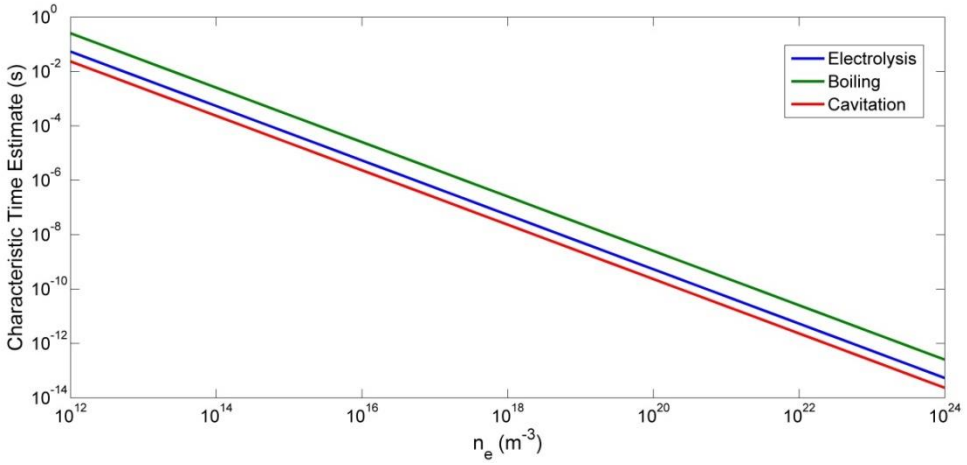

Figure 11 Characteristic times as a function of electron density for a constant characteristic length of 1 micron.

Lastly, it is useful to inspect the determined coefficients a bit closer. For each mechanism, the denominator is simply the power flux due to the electron current coming from the electrode, P_e, and the numerator is the energy density for bubble generation, $E_{b,i}$. Therefore, the coefficient can be written more generally as Equation 21.

$$C_i = \frac{E_{b,i}}{P_e} \qquad 21$$

Holding the power flux constant, the energy density for each mechanism can be compared which illustrates that in general the follow is true:

$$E_{b,boiling} > E_{b,electrolysis} > E_{b,cavitation}$$

This suggests that the energy required for cavitation is always less than the energy required by the other mechanisms and should have a faster characteristic time. This also suggests that if the energy density is controlled, then the mechanism of breakdown can be influenced.

It is obvious that this analysis does not consider a lot of the complex physics that can be taking place at the electrode liquid interface, however this analysis is not meant to provide an explanation of the initiation mechanism that takes place in liquid phase plasma formation, rather it is meant to provide a boundary to the time scales of initiation. If there are any reports that claim to see plasma or bubble formation that occurs faster than these characteristic times than there must be a mechanism other than those mentioned here that is occurring.

Electrodynamic ball discharge

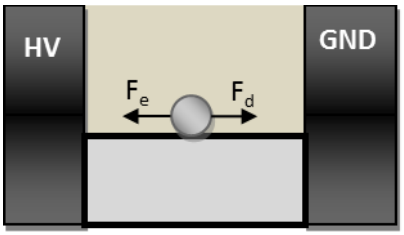

Figure 12 General configuration for an EBD

The most general configuration to generate an Electrodynamic Ball Discharge (EBD) is shown in Figure 12. The setup consists on a single metal ball and two electrodes. When a voltage is applied to the electrodes it can cause the ball to move from one electrode to the other once a certain voltage is achieved. This happens because the metal ball, when in contact with the electrode, will acquire a charge that is determined by the capacitance and the applied electric field. When the ball is charged, it will experience a Lorentz force due to the presence of the electric field. As the ball moves

through the medium, which could be either gas or liquid, it may lose some charge depending on the conductivity of the medium and how quickly the ball is moving; typically, the charge lost is very small. As the ball approaches the opposite electrode there will be a critical gap at which the local electric field, between the ball and the approaching electrode, become large enough to breakdown the medium. When breakdown occurs, charge will be transferred through the conductive plasma that is generated between the ball and the electrode. Within the plasma energy is released in the form of heat and chemical energy and the chemical change that occurs in the medium is goal of the EBD. The duration of the plasma is determined by the amount charge available on the ball which will determine the degree to which the plasma can thermalize. As it is desired to maintain a non-thermal plasma, small charges and lower energies are of most interest for the EBD.

Particle charging at a planar electrode in a uniform field

The method by which a particle becomes initially charged in this system is by directly contacting the electrode. It is also possible however for a particle to slowly accumulate charge without contacting an electrode from leakage current through the dielectric medium. Only the former charging mechanism will be considered here although it should be noted that the latter mechanism may be useful, along with polarization effects, to initiate particle motion when it is initially stationary within the gap of the electrodes. When the particle encounters an electrode, the once uniform electric field becomes modified as depicted in Figure 13 and described by Liu (73).

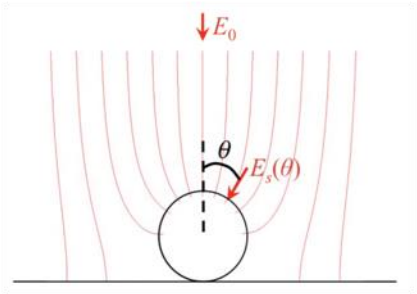

Figure 13 Modified electric field of a sphere near a flat electrode (73)

The charging of the particle will therefore be affected by the modified field. Without considering the modified field one would expect a simple relationship between the charge on the particle and the voltage applied to the particle according to Gauss's law, Equation 22.

$$Q = CV = \oiint \varepsilon \mathrm{E} \cdot dA \qquad 22$$

The proportionality constant relating charge and voltage is the capacitance of the system, which for an isolated sphere is determined by solving equation 1 for that case resulting in Equation 23.

$$C = 2\pi\varepsilon D \qquad 23$$

Therefore, the amount of charge on a particle for a given applied voltage is expected to depend only on the diameter of that particle.

When the modified field is considered an enhancement factor, β, is defined to account for the changes in the resulting capacitance of the system, Equation 24.

$$\beta \equiv \frac{E_s(\theta)}{E_0} \qquad 24$$

With reference to Figure 13, the enhancement factor is determined by integrating around the particle as described by Equation 22. An integrated field enhancement factor is defined using Equation 25, which can be considered a constant for this specified geometry of a particle in contact with a wall.

$$B \equiv \int_0^{\pi} \beta(\theta) \sin\theta \, d\theta \qquad 25$$

The integrated field enhancement factor can be used to redefine the capacitance of the system and provide a more accurate relation between the charge and applied voltage, Equation 26, where L is the gap of the electrodes producing the uniform electric field.

$$C_m = \frac{\pi}{2} \frac{B\varepsilon D^2}{L} \qquad 26$$

The value of the integrated field enhancement factor has been determined to be about $B \approx \pi^2/3$ (74). It can be useful to compare the modified capacitance of the system to the self-capacitance of an isolated sphere as it illustrates that the charge on the ball will always be smaller than the isolated sphere case, Equation 27.

$$C_m = \frac{\pi^2}{12} \frac{1}{(L/D)} C \qquad 27$$

Therefore, estimating the charge on a ball by assuming an isolated sphere capacitance will be inaccurate. As the electrode gap approaches the particle diameter the capacitance approaches approximately 0.82C and is the closest value to the isolated sphere

capacitance. However, for these very small gaps the field will become modified further by the presence of the second electrode and the actual value would be smaller than this equation implies. For larger gaps the modified capacitance of the system will be reduced in proportion to the number of ball diameters (L/D).

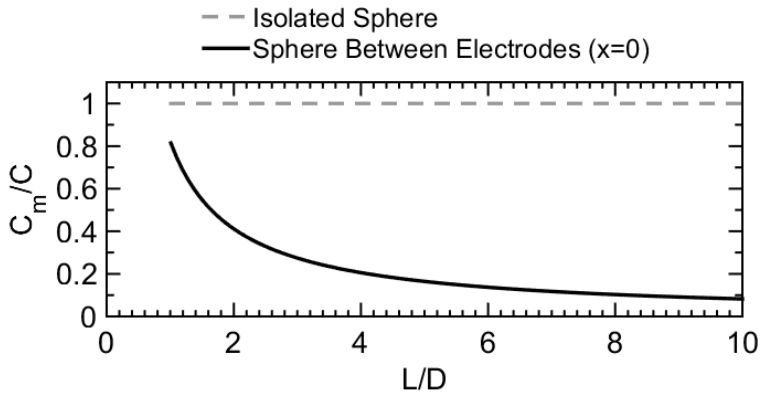

Figure 14 The modified capacitance of a sphere relative to an isolated sphere capacitance (x=0) versus L/D

It is apparent that when charging a particle through contact with an electrode that the actual charge on the particle will be a function of both the ball diameter and the electrode gap for a specified voltage, Equation 28.

$$Q_0 = \frac{\pi}{2}\frac{B\varepsilon D^2}{L}V \qquad 28$$

The ability to regulate the charge of the particle for this system can be quite important. For the particle to move within a given medium it must overcome static and dynamic forces such has surface friction and fluid viscosity. If the charge on the particle is too small the electric force may not be strong enough to move the particle and very high voltages may be required; of course, an upper limit to the voltage exists, whereby

electric breakdown of the material can occur. It may also be desirable for certain applications to transfer very small amounts of charge discretely to generate small energy pulses. In this case, the charge can be reduced greatly by using smaller particle diameters and operating with minimum electric fields. These conditions will be explored in the Design Parameters and Optimization section.

Lastly, the integrated enhancement factor is a theoretical value and a useful method for experimental verification can be made by measuring the vertical lift-off voltage which is simply the voltage required to overcome the gravitational force, Equation 29. Then solving for the enhancement factor in Equation 25, an expression for the integrated enhancement factor can be obtained, Equation 30.

$$Q_0 = \frac{mg}{E_0} \tag{29}$$

$$B = \frac{2mg}{V^2 \pi \varepsilon} \left(\frac{D}{d}\right)^2 \tag{30}$$

Dynamic capacitance and voltage

As the ball is moving between the electrodes the capacitance of the system changes, this should be known to determine the voltage between the ball and the wall as it approaches the wall. This in turn is determined by the geometry of the three electrodes, with reference to Figure 15, and is given by the dynamic capacitance values of the system.

Figure 15 Schematic for modeling the capacitance of the sphere between two planar electrodes

To determine theses voltages and capacitance a simplified geometry is used. This geometry assumes a sphere between two infinite planes and a uniform axial background electric field. In general, the capacitance is related to the charge as described using a capacitance matrix, Equation 31. The most important quantity from this matrix is Q_2 the charge of the ball therefore Equation 31 can be simplified to Equation 32.

$$\begin{bmatrix} Q_1 \\ Q_2 \\ Q_3 \end{bmatrix} = \begin{bmatrix} C_{11} & C_{12} & C_{13} \\ C_{21} & C_{22} & C_{23} \\ C_{31} & C_{32} & C_{33} \end{bmatrix} \begin{bmatrix} V_1 \\ V_2 \\ V_3 \end{bmatrix} \quad 31$$

$$Q_2 = V_1 C_{21} + V_2 C_{22} + V_3 C_{23} \quad 32$$

In Equation 32 three values of capacitance need to be determined, the capacitance between the sphere and the anode C_{21}, the capacitance between the ball and the cathode C_{23}, and the self-capacitance of the ball C_{22}, however V_1 is zero and therefore C_{21} will not influence the value of Q_2. To derive the charge of the sphere at any point between the electrodes using the method of images we can sum over all the image charges, as was done with the forces, to obtain the total charge as a function of V_2 and V_3 for any α, Equation 33. The limit as *h*, the sphere position from its center, approaches *R* results in

Equation 34 which is the same results as was determined in Equation 28 for the case when $B = \pi^2/3$.

$$Q = 4\pi\varepsilon R^2 \left(\frac{V_2}{h} \sinh\alpha \cosh\alpha \sum_{n=1}^{\infty} \frac{1}{\sinh n\alpha} + \frac{V_3}{d} \sinh^2\alpha \sum_{n=1}^{\infty} \frac{\cosh n\alpha}{\sinh^2 n\alpha} \right) \quad (33)$$

$$Q_2 = \left(\frac{2\pi^3}{3} \right) \varepsilon R^2 E_o \quad (34)$$

Equation 33 also allows for the determination of the voltage between the ball and the electrode at any point on its path for the case when the charge is known. As the ball moves away from the cathode and travels through the liquid medium towards the anode the charge remains constant, that is ignoring charge relaxation. Because the charge is considered constant and capacitance is changing (due to geometry changes with the ball moving) the voltage on the ball will also change. By combining Equation 32 and Equation 33 and setting V_2=0 and V_3=1 it is possible to derive an equation for C_{23}, Equation 35, and then by setting V_3=0 and V_2=1 it is possible to derive an equation for C_{22}, Equation 36.

$$-C_{23} = 4\pi\varepsilon \frac{R^2}{d} \sinh^2\alpha \sum_{n=1}^{\infty} \frac{\cosh n\alpha}{\sinh^2 n\alpha} \quad (35)$$

$$C_{22} = 4\pi\varepsilon \frac{R^2}{h} \sinh\alpha \cosh\alpha \sum_{n=1}^{\infty} \frac{1}{\sinh n\alpha} \quad (36)$$

With the capacitance of the system and the charge of the sphere both known it is possible to determine the voltage from the ball to the anode, Equation 37.

$$V_2 = \frac{Q_2 + C_{23}V_3}{C_{22}} \quad 37$$

Equation 37 is used to determine the position when the ball achieves the critical breakdown voltage. This critical position also provides the breakdown gap size.

Force balance on a charged particle

The dynamics of charged particle in dielectric, or leaky media has been described by several authors (75) (76). Electrodynamic particle motion in these heterogeneous fluids, where the particles can be gas, liquid, or solid, can be explained by either electrophoretic, forces on charged particles due to a uniform electric field, or dielectrophoretic, forces on dielectric particles due to a nonuniform field. A charged particle placed between two electrodes within a fluid will move from one electrode to the other and back again when the forces due to electrophoretic phenomena are large enough to overcome any buoyant forces, drag forces or other forces that may exist; this arrangement is illustrated in Figure 12.

Forces such as rolling or surface friction may be present but will be assumed negligible for this analysis. With these assumptions, the overall general equation is as shown in Equation 38.

$$m_e \frac{du(t)}{dt} = F_g + F_e + F_d \quad 38$$

where F_g is the gravitation force, F_e is the force due to the electric field and F_d is the drag force on the particle, and m_e is the effective mass given by Equation 39.

$$m_e = \left(\rho_1 + \frac{1}{2}\rho_2\right)\frac{4}{3}\pi R^3 \qquad 39$$

The force due to the electric field is determined using the Lorentz equation neglecting the magnetic field, Equation 40.

$$F_e = QE \qquad 40$$

It is often safe to simplify using $E = E_o$ (where E_o=V/L is the applied field) however this is invalid when the sphere is close to the electrode because the charged sphere sufficiently modifies the field, as noted with the analysis of the system capacitance and charge on the ball.

The drag on the ball can be approximated as Equation 41,

$$F_d = \frac{\rho_2(4\pi R^2)C_d}{2}u(t)^2 \qquad 41$$

where C_d is the drag coefficient. The drag coefficient can be determined using stokes law for low Reynolds numbers or the Oseen equation for slightly higher Reynolds numbers however these equations are inaccurate at much high Reynolds numbers. It is expected that typical Reynolds numbers for the EBR will be large and therefore the

approximations are best avoided. To avoid such errors experimental data was fitted using a piecewise cubic Hermite interpolation polynomial method and the fit was incorporated into the model, Figure 16.

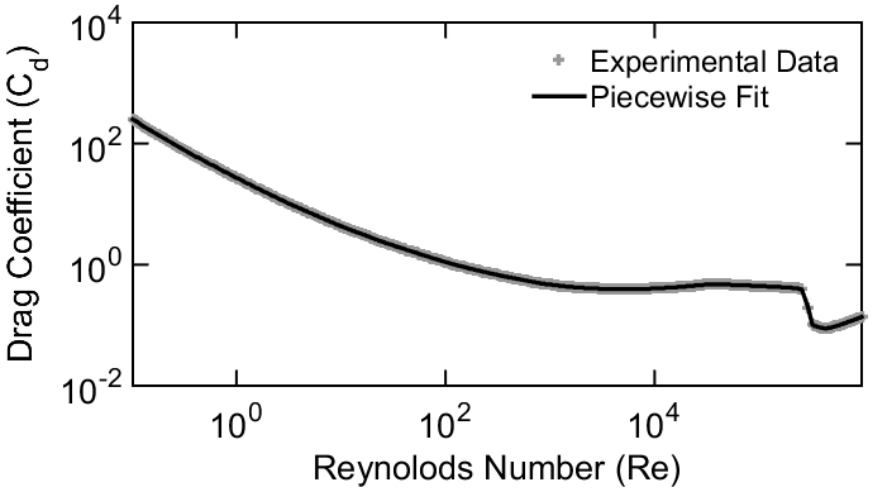

Figure 16 Experimental data for the drag coefficient as a function of Reynolds number and the piecewise fit that was incorporated within the model

The balance of these forces provides the complete equations for the position and velocity of the particle, Equations 42 and 43, where ρ_1 and ρ_2 are the density of the charge carrier and the fluid respectively, Q_s is the surface charge of the charge carrier (C/m^2), E is the electric field, θ is the angle at which the charge carrier is moving relative to the direction of gravity, d is the diameter of the charge carrier, and u is the velocity.

$$\frac{dx}{dt} = u(t) \qquad 42$$

$$\left(\rho_1 + \frac{1}{2}\rho_2\right)\frac{du(t)}{dt} = (\rho_2 - \rho_1)gcos\theta + \frac{6Q_sE}{D} - \frac{3\rho_2 C_d}{D}u(t)^2 \quad (43)$$

Ideally the charge on the particle should not change if the fluid is a perfect electrical insulator however typically some leakage is expected. The characteristic relaxation time for a fluid can be determined using Equation 44, where ε is the permittivity of the fluid and σ is the conductivity of the fluid. Typical values for the characteristic time of for dielectric mediums are on the order of 10-200 seconds and is therefore often negligible for the applications discuss here. However, if it becomes important the charge can be estimated using Equation 45.

$$\tau_e = \frac{\varepsilon}{\sigma} \quad (44)$$

$$Q_s(t) = Q_o e^{-t/\tau_e} \quad (45)$$

To determine when charge relaxation is important the characteristic time of charge carrier transport is defined using Equation 46, where L is the distance between electrodes and U is the average velocity.

$$\tau = \frac{L}{U} \quad (46)$$

Combining Equations 44 and 46 we can define an Electric Reynolds, Equation 47. For cases where Re_e << 1 charge losses are small during the half cycle of the particle and therefore charge can be considered constant.

$$Re_e = \frac{\tau_e}{\tau} \qquad 47$$

For the case of a horizontal configuration where it is assumed that the velocity rapidly achieves steady state and is constant, the frequency can be estimated using Equation 48, where *V* is the applied voltage and *D* is the distance between the electrodes.

$$f = \sqrt{\frac{Q_o V}{2\rho_2 C_d D^3}} \qquad 48$$

Although the drag coefficient will depend on the velocity and diameter of the ball as well as the fluid properties a typical value for the drag coefficient on a spherical particle is about 0.47 which can be used to estimate the possible frequency range. The frequency can be altered by adjusting the applied voltage, V, the distance between the electrodes *l*, and the charge on ball Q_o. A more accurate model for the dynamics of a particle is provided in the Design Parameters and Optimization section.

Electrodynamic ball discharge energy

At low Electric Reynolds numbers the main mechanism for charge transfer is through microsparks that occur just prior to collisions, either with the electrode or with other charge carriers if they are present. As the particle approaches an electrode the local

electric field increases. At some critical distance the electric field will become higher than the dielectric strength of the medium and breakdown will occur which initiates the charge transfer process. For fluids with high dielectric strengths the distances at which this breakdown will occur is on the order of microns and therefore has no significant effect on the dynamics of the system.

For gases, the critical breakdown voltage is related to the product of the pressure and the gap (pd_c) according to the well-known Paschen law, Equation 49.

$$V_c = \frac{Bpd_c}{\ln(Apd_c) - \ln\left(\ln\left(1 + \frac{1}{\gamma}\right)\right)} \qquad 49$$

Paschen's law can be used to determine where the breakdown will occur as the particle approached the wall in a gaseous medium, and therefore provides the expected size of the discharge, d_c. The case for a liquid is expected to be simpler since liquids are often described with a constant dielectric strength. With this assumption, the breakdown strength is directly proportional to the critical gap, Equation 50.

$$V_c = \varphi d_c \qquad 50$$

The critical distance is important because it defines the volume that is chemically reacting. Since the treatment volume is significantly smaller than the total volume of the medium it can be assumed to be spherical. The maximum energy density of the plasma can now be defined as Equation 51, which assumes all the charge is transferred through the plasma.

$$E_{plasma} = \frac{3QV_c}{8\pi {d_c}^3} \qquad 51$$

The case for a liquid medium with a constant dielectric strength simplifies to Equation 52.

$$E_{plasma} = \frac{3B\varepsilon\varphi^2}{d_c}\left(\frac{D^2}{L}\right) \qquad 52$$

From Equation 52 to control the energy density of the plasma the particle diameter and the electrode gap are the two variables that can be changed for a given medium. The total energy input is an important parameter as well and can be defined using Equation 53.

$$E_{total} = \left(E_{plasma}\frac{4\pi {d_c}^3}{3}\right)\frac{ft}{v} \qquad 53$$

These equations, coupled with the dynamic capacitance and voltage equations, are used to determine the energy of the discharge.

Design and optimization

All the equations described compose the complete model and are solved numerically using an ODE23 solver in MATLAB providing details regarding average velocity, transit time, and total charge relaxation. This model can therefore be used to see the effect of varying parameters of interest such as viscosity, ball diameter, electrode spacing, and applied voltage. A complete energy analysis can then be carried out to determine the most efficient method of energy utilization for the system. A typical result of the model is shown in Figure 17.

Table 4 Values used in the EBD model example

Property	Value	Units
Permittivity (ε)	3	N/A
Dielectric Strength (φ)	1	[MV/m]
Viscosity (ν)	25e-6	[m^2/s]
Fluid Density (ρ_f)	800	[kg/m^3]
Conductivity (σ)	5e-11	[S/m]
Ball Density (ρ_b)	2700	[kg/m^3]
Ball Radius (r)	0.0016	[m]
Electrode Gap (L)	0.0063	[m]
Applied Voltage (V)	15,875	[V]
L/D	2	

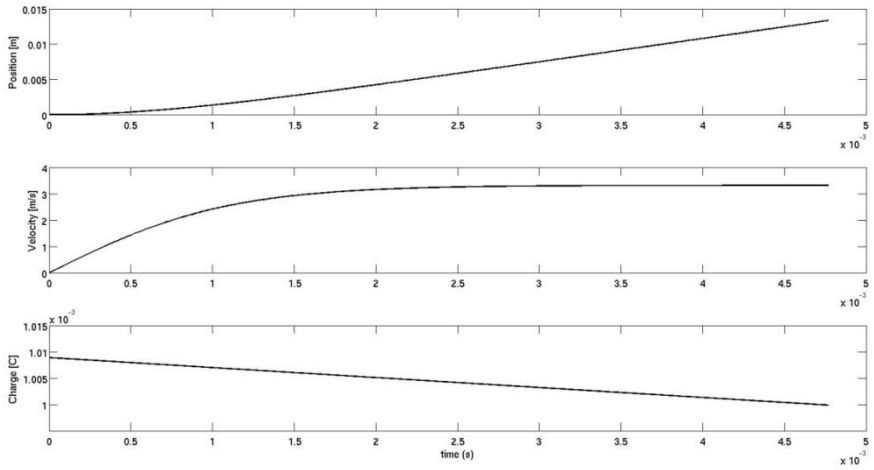

Figure 17 Example output of the model showing the ball position, velocity, and charge over time for the conditions provided in table

It is worth stating that for the actual EBR system multiple balls are used to process liquids faster. If the balls are isolated from one another this model applies for each ball within the reactor but ignores any effects that might exist between neighboring

balls; furthermore, it is assumed that parameters such as total power can be derived simply by multiplying the individual results by the number of balls in the reactor.

As mentioned previously, the goal of the EBR is to transfer all the energy supplied by the external circuit to the microspark where the actual chemical processing takes place therefore a more detailed energy analysis is required. Energy in this process can be consumed in several ways: 1) energy which flows through the liquid medium as a background current due to its conductivity (U_i), 2) energy which is transferred to the ball at the electrode (U_q), 3) frictional losses due to drag on the ball (U_f), 4) inelastic collisional losses when the ball hits the electrode (U_k). The energies are total energies for the EBR and can be defined in terms of specific energies, u_x, and total number of balls, n, as shown in Equation 54.

$$U_x = u_x n, \qquad x = p, q, f, k, i \tag{54}$$

It is desired to have as much energy transferred to the microplasma discharge (U_p) as possible, therefore anything else is considered a loss and will reduce the efficiency of the EBR. The plasma itself can also be considered to have its own efficiency, η_p, associated with the conversion of electrical discharge energy to desirable chemical conversions in the liquid. Using these terms, we can define an overall efficiency for the EBR, Equation 55. In the most ideal case all the energy stored in the ball will be used to create the plasma and Equation 55 simplifies to Equation 56.

$$\eta_{EBR} = \eta_p \frac{U_p}{U_i + U_q + U_f + U_k} \tag{55}$$

$$\eta_{EBR} = \eta_p \frac{U_p}{U_q} \quad (56)$$

To evaluate the EBR efficiency we must define expressions for the individual losses. We define 4 stages for the process, as shown in Figure 3, stage 1 where the ball is at the same potential as the cathode and is accelerated toward the anode, stage 2 just before the plasma discharge and charge transfer occurs where the ball has moved to very close to the anode. Stage 3 and 4 are similar for the oppositely charged ball. Ideally the system is symmetric and Stages 1&2 have the same characteristics as Stages 3&4.

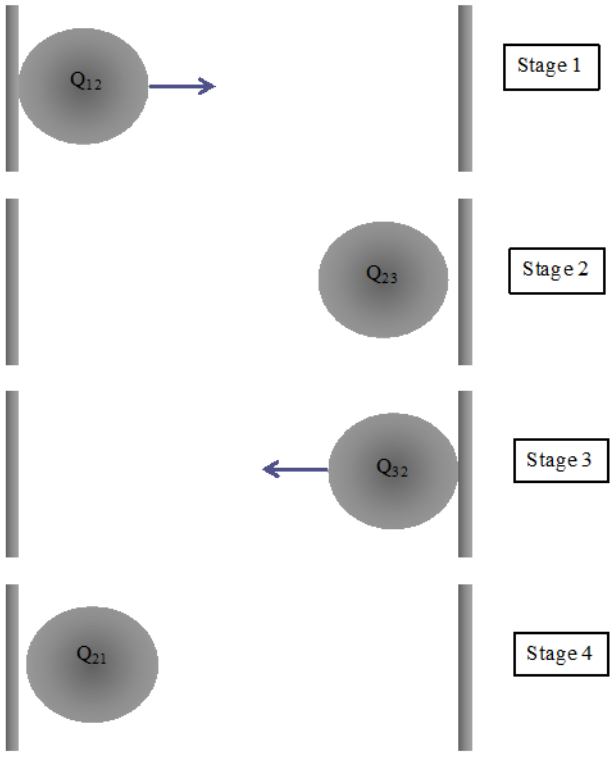

Figure 18 Stages of single particle motion 1) Ball in contact with anode 2) Ball at critical breakdown location near cathode 3) Ball in contact with cathode 4) Ball at critical breakdown location near anode

Fluid electrical losses

The cathode and anode are maintained at a constant applied potential during processing. Ideally the liquid would be a perfect dielectric however this is generally not an acceptable assumption, therefore when a potential difference is applied from the cathode to the anode a small background current will flow through the liquid. This background current can lead to joule heating of the liquid and if the liquid is too conductive it becomes difficult or even impossible to charge the ball due to fast charge relaxation to the liquid. The energy loss due to the background current during the balls motion is defined according to Equation 57, where V_{13} is the applied voltage, A_{el} is the area of the electrodes, σ is the conductivity of the liquid and T is the transit time of the ball from the cathode to the anode as defined by Equation 58, where L is the distance between the anode and the cathode, D is the diameter of the ball and v_{avg} is the average velocity of the ball from Stage 1 to 3. Within this paper, the transit time that is used will be directly extracted directly from the simulated ball motion.

$$U_i = \frac{A_{el} T \sigma {V_{13}}^2}{L} \tag{57}$$

$$T = \frac{L - D}{v_{avg}} \tag{58}$$

Typical values for the energy losses associated with background current can be determined by solving running the model for various L/D values and different conductivities; such a plot is shown in Figure 19.

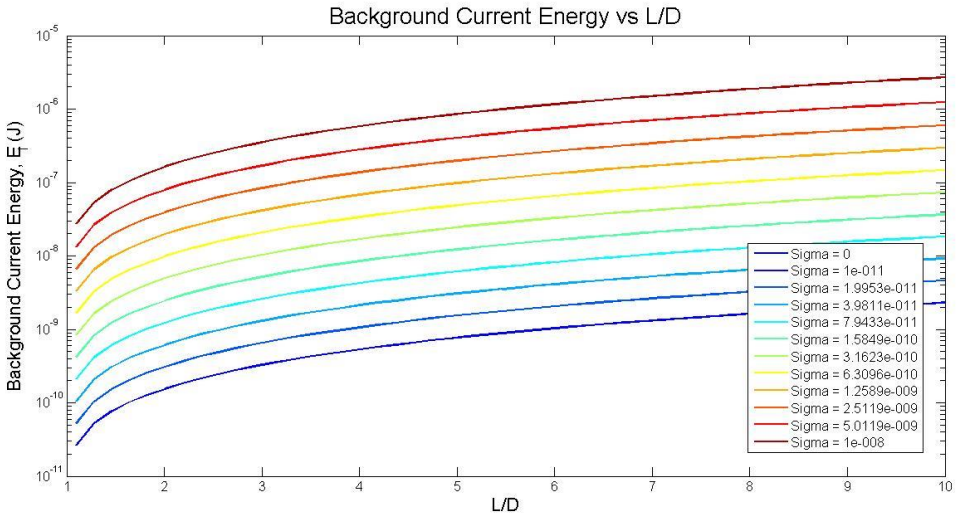

Figure 19 Background current energy losses verse L/D with ε=3, v=25e-6, ρ_1=2700, ρ_1= 800, and E=-5e-6 (half of the dielectric strength)

Energy transferred to ball

In Stage 1 the ball is charged at the cathode and achieves a charge Q_{12}. At this point the ball contains the total potential energy that we would like to use to for chemical processing. The ball travels to the other electrode, due to electrodynamic forces, and we define Stage 2 to be just before a microspark is generated. During the balls journey through the liquid from the cathode to the anode some charge relaxation occurs due the slight conductivity of the liquid. We define the energy on the ball as the work required to charge the ball at Stage 1 using Equation 59 where q_{final} is the charge on the ball after all charge is transferred and $q_{initial}$ is the charge on the ball prior to contacting the electrode; this equation was obtained by plugging in and integrating. The charge on a sphere in contact with an infinite plane in the presence of a uniform DC field, E_o, acquires a charge as given by Equation 34. The capacitances coefficients can be solved numerically and only depend on the parameter α and the distance between the electrodes.

$$U_q = \int_{q=q_{initial}}^{q=q_{final}} V(r)dq \tag{59}$$

$$= \frac{\frac{{q_{final}}^2}{2} - C_{23}V_3 q_{final}}{C_{22}}$$

$$- \frac{\frac{{q_{initial}}^2}{2} - C_{23}V_3 q_{initial}}{C_{22}}$$

Energy in the plasma discharge

As the ball moves through the fluid some of the charge will relax according to Equation 45. The total charge available when breakdown occurs can be determine using $Q_f = Q(T)$ where T is the transit time. The final charge, and therefore the energy of the plasma U_p, is determined using Equation 45 with the available charge at breakdown.

Energy lost to fluid friction

Due to the viscosity of the fluid, drag on the ball results in a loss of energy. The drag on a sphere is typically described using either stokes drag coefficient or a slightly modified version of stokes; however, this is only valid for low Reynolds numbers therefore empirical data is used. The losses due to drag are determined using Equation 60. This equation is a simplification of the fluid motion as a uniform free stream it is significantly more complicated particularly when the ball is near the wall and the fluid becomes trapped between the ball and wall.

$$U_f = \int_0^T F_d \cdot v(t)dt \tag{60}$$

Wall collision losses

When the ball hits the electrode some of the kinetic energy within the ball can transfer to the electrode, this in inelastic collision energy is defined using Equation 61.

$$E_k = KE_{23} - KE_{32} \quad (61)$$

Therefore, we have defined all the energy inputs which can be used to determine the overall efficiency of the EBR.

Overall efficiency

Using the previously defined efficiency, Equation 56, EBR efficiencies can be determined for various cases. For all the cases explored the kinetic losses are considered negligible and therefore are simply set to zero; the kinetic losses will have to be explored further later. The first case uses that constraint of a constant electric field, specifically E = -5e6 which is about half of the dielectric strength of an oil such as mineral oil. The EBR efficiency is plotted verse L/D for various conductivities in Figure 20. As L/D approaches 1 the efficiency approaches 1, however it can be seen that as that higher conductivities always reduce the efficiency due to background currents. For the case of a perfect dielectric, conductivity is zero, there are no background current losses and the only losses are due to viscous losses. As L/D gets bigger the viscous losses become more significant being responsible for nearly 60% of the losses at an L/D of 10. The losses due to the conductivity of the solution are more significant for smaller L/D. Furthermore, if the conductivity is too high it becomes impossible for the ball to collect enough charge

to move under electrophoretic forces; this can be seen in Figure 20 for the highest conductivity where the L/D of 9 is the largest gap possible and the ball will not move in a larger gap. For the constant electric field analysis, it appears that the highest efficiencies can be obtained at the smallest L/D. It should be noted however that this model is not entirely accurate for L/D <= 2 because image charges will appear on the second electrode and they must be considered which this model does not do.

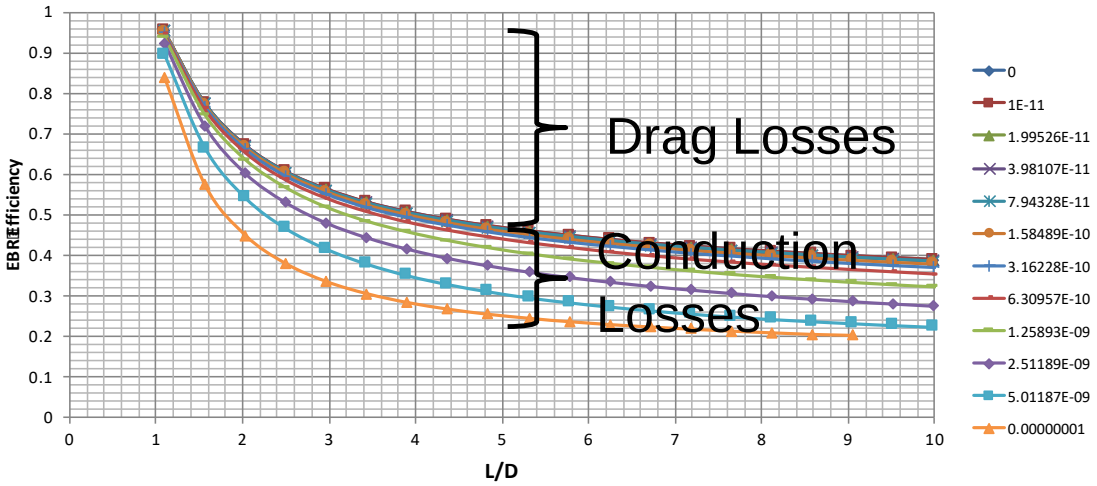

Figure 20 EBR efficiency verses L/D for various conductivities at constant electric field (ε=3, ν=25e-6, ρ_1=2700, ρ_1= 800, and E=-5e-6)

For the case of constant voltage, the analysis must be altered slightly to ensure that the voltage is not greater than the breakdown voltage. Therefore, the condition exists that if the voltage is greater than the breakdown voltage the model will be evaluated at the breakdown voltage instead of the constant voltage specified. This provides a more realistic picture since it is not possible to operate the EBR above the breakdown voltage. Due to the limitation of breakdown voltage a change in slope on the efficiency curve

occurs at the L/D where the specified constant voltage no longer exceeds the breakdown voltage. This occurs at L/D of 5 for the case shown in Figure 21.

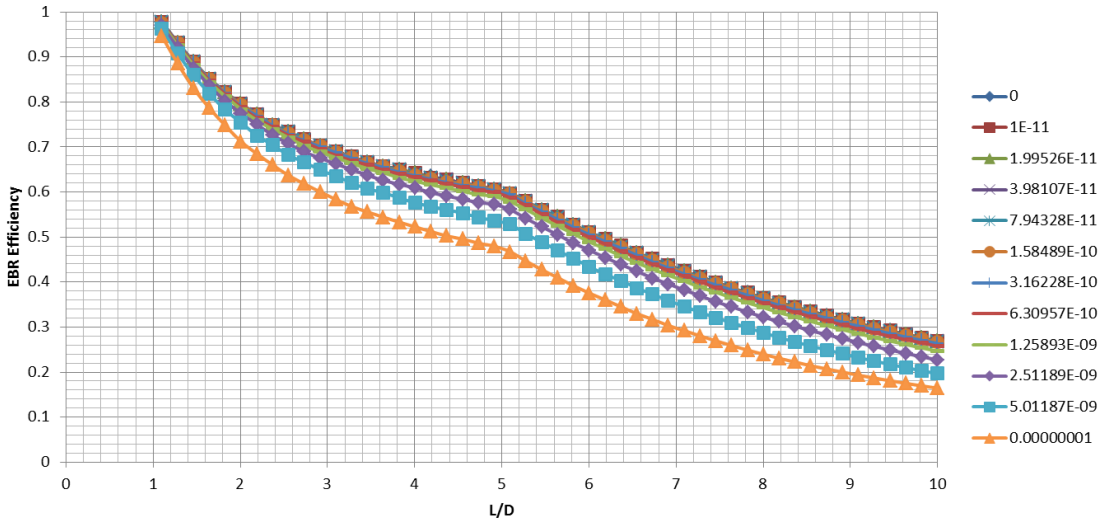

Figure 21 EBR efficiency verse L/D ε=3, ν=25e-6, ρ_1=2700, ρ_1= 800, and V_{const}= 20 kV

To carry out a further analysis of the operating parameters, the electric field was held constant to avoid the breakdown issue just mentioned. The case for varying the ball radius and the conductivity is shown in Figure 21. The frictional losses will be less for a smaller ball radius which is demonstrated by the results of the model. Furthermore, it is quite apparent that when the liquid is more conductive, the electrical losses can become very significant leading to a low EBR efficiency. This can be slightly alleviated by operating at smaller values of L/D. The operating power density is also seen two vary greatly with conductivity, Figure 23. There is no real optimum that can be extracted from these results. The optimum operating condition would be an L/D value of 1, however an L/D of 1 means that the ball is simply shorting the gap. Yet it might seem

that the engineer would want to operate with the smallest L/D possible. This would be true if they were only concerned with achieving the highest EBR efficiency. However, the situation is slightly more complicated than that. Once the plasma efficiency is considered, it might be important to operate at a specific energy density. In this case, the engineer would have to choose an L/D that provides the correct energy density; in other words, they must choose a desirable charge on the ball at the moment of discharge and work backwards to determine the best L/D for the given situation. This study of energy density and plasma efficiency is something that remains for future workers in the field and was not carried out by the current author.

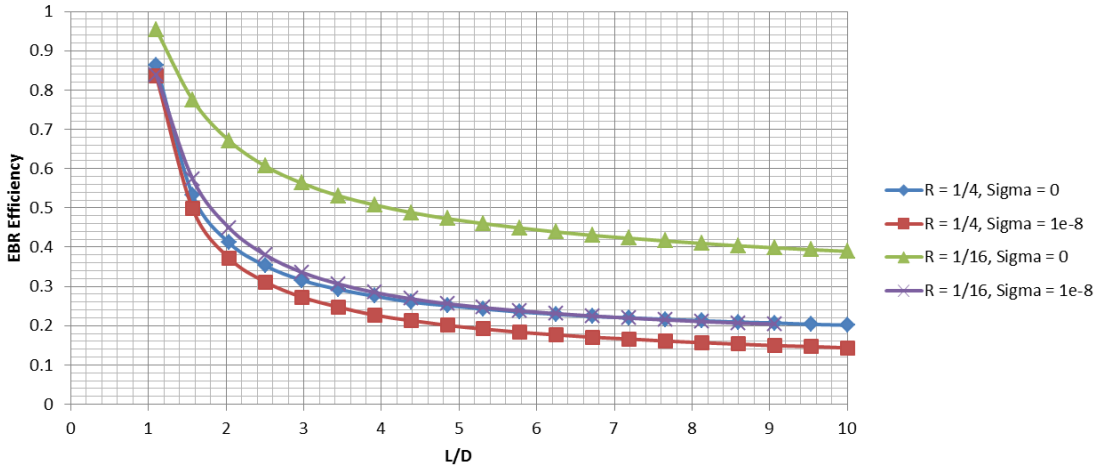

Figure 22 EBR Efficiency verse L/D (Effect of ball radius and conductivity)

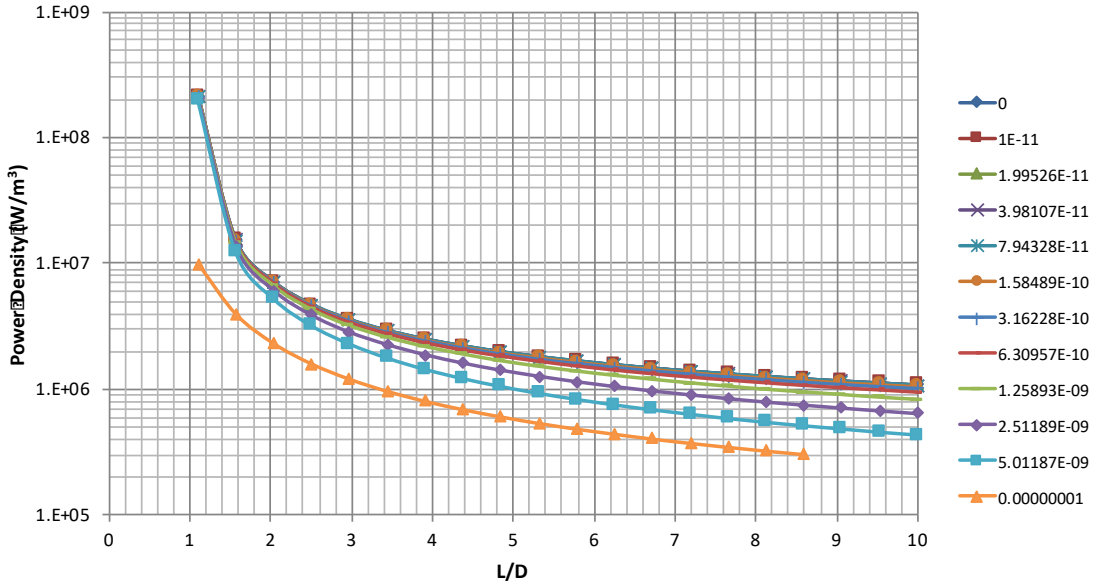

Figure 23 Operating power density as a function of L/D for various conductivity values

The efficiency of the EBR can approach 90% or higher, as shown in Figure 24. The ideal case for high efficiency is therefore a low viscosity and a low conductivity operating with a small L/D. It can also be seen from this plot that the model can

accurately predict when the ball will no longer move. This results from either too significant of a loss of energy from viscous drag forces or significant energy loss due to electrical conduction through the medium. This is an important aspect of the model, especially for engineering purposes, since it allows for determining the operating envelope. Therefore it can be seen that for the given conditions it will not be possible to operate above an L/D of 9.

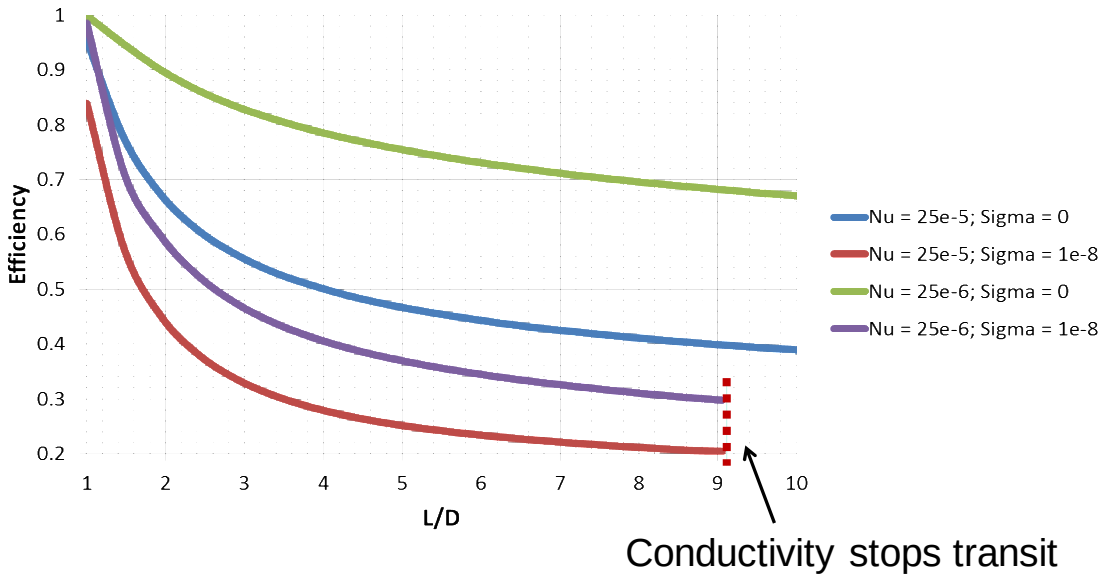

Figure 24 EBR efficiency as a function of L/D for different conductivity and viscosity values

EXPERIMENTAL RESULTS

Electrodynamic ball discharge

Breakdown voltage of mineral oil

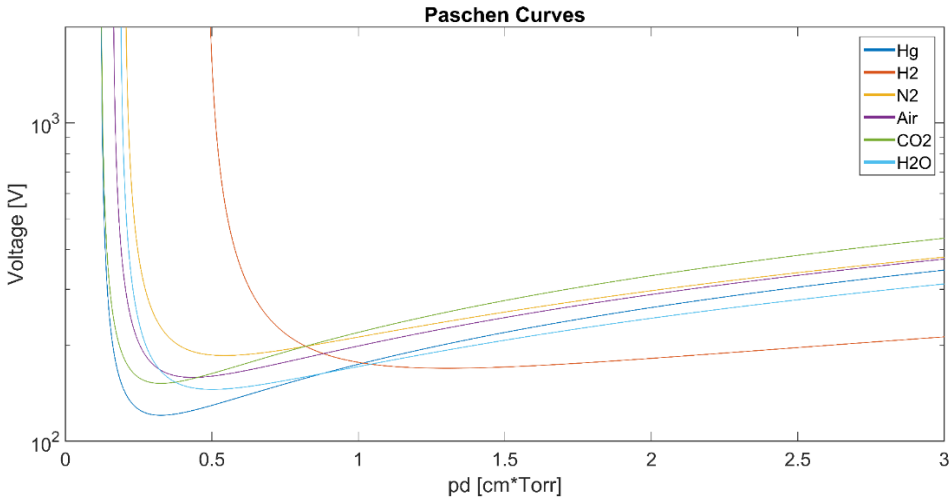

Figure 25 Paschen curve for various gases

The electrical breakdown of a fluid is often described using the dielectric strength; for mineral oil the dielectric strength is on average 12.5 kV/mm but can range between 10-15 kV/mm (77). The electrical breakdown properties of gases are known to follow the so called Paschen's Law. From this law, it was determined that the breakdown voltage of gases is a function of the product of the pressure with the gap distance, $V_{br} = f(pd)$. A typical Paschen curve is shown in Figure 25 for various gases. If the breakdown mechanism is initiated by electron avalanching it can explain the dependence of breakdown voltage on pd. The pressure is inversely proportional to the

mean free path (λ) and it is the ratio of d/ λ that is important. The Paschen law does not seem to work when the mean free path becomes very small as in the case of liquids.

For liquids, the molecules are held closely to one another by short range forces such as hydrogen bonding and London dispersion forces; although these bonds are relatively weak and are frequently broken and reestablished. The energy of these interaction forces is proportional to r^{-6} where r is the distance between the nuclei; this distance is on the order of 3-5 angstroms. Therefore, the concept of mean free path does not seem to apply for this liquid state; a rough estimation would be to consider the mean free path to be on the order of the distance at which these weak bonds break which would correspond to the minimum separation distance of the molecules and the maximum distance is not to be not too much larger as the bond would be reestablished quickly due to the density of the fluid. Since this mean free path is incredibly small the expected breakdown voltage according to Pachen's law would be very large.

$$V_{br,Townsend} = \frac{dE_i}{\lambda_e \ln \frac{d}{\lambda_e}}$$

A rough estimation assuming a Townsend type breakdown for a 1 mm gap in a long chain hydrocarbon such as n-octane with an ionization energy of about 11.7 eV and a mean free path of 5 angstroms would require a breakdown voltage of about 1.6 MV. This number is equivalent to 1600 kV/mm which is significantly larger than the dielectric strength of 12.5 kV/mm. Therefore, a different breakdown mechanism is most likely occurring. If we still maintain the Townsend breakdown assumption and consider the dielectric strength of mineral oil we can determine what mean free path is required.

In this case, it would be about 100 nm; this value corresponds with typical values for gaseous mean free paths such as air at standard temperature and pressure, ~96nm. Therefore, the dielectric strength of the mineral oil seems to correspond with a Townsend breakdown in the oil assuming the liquid has a similar mean free path of a gas. It is worth noting that this behavior is being observed at relatively long distances, $d/\lambda \sim 2e6$, where here the mean free path is still assumed to be on the order of 5 angstroms. The question remains if there is any Paschen-like behavior that exists as the distance between the gap decreases closer to the expected mean free path. If the gap is 1 μm then $d/\lambda \sim 2e3$ which is smaller than atmospheric air for a 1 mm gap, $d/\lambda \sim 1e4$; therefore, it may be possible to see some deviation from the constant dielectric strength and some dependency on d/λ.

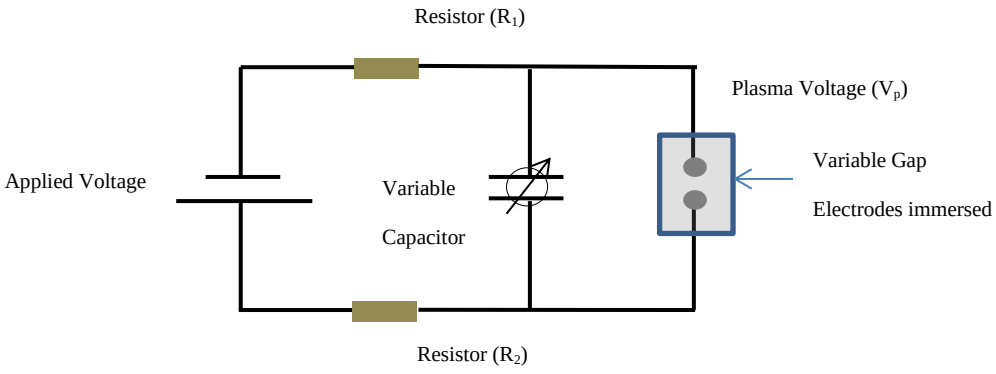

Figure 26 Experimental setup for measuring breakdown voltage

To study the breakdown in mineral oil at small gaps the setup illustrated in Figure 26 was used. The voltage source was a DC negative power supply capable of 100kV. The resistor R_1 acts as a ballast effectively eliminating the capacitance of the

power supply from the discharge gap. The length of the wires leading to the discharge gap were minimized to reduce stray capacitance and a variable capacitor, capable of 1-100pF, was connected parallel to the discharge gap to control the energy of the discharge however this is not necessary for determining breakdown voltage. The breakdown voltage is related to the applied voltage using the following equations.

$$V_o = V_{R_1} + V_{R_2} + V_p$$

$$V_{R_1} = IR_1$$

$$V_{R_2} = IR_2$$

If there is no current then the voltage at the gap is equal to the applied voltage. Therefore, to determine the breakdown voltage of the mineral oil the voltage was slowly increased while maintaining a constant gap until a breakdown occurred. It was assumed that the voltage on the gap was equal to the voltage being applied at the time of breakdown. The measurement was carried out for several gaps and is plotted in Figure 28. To measure the gap length a picture was taken of the electrodes using a microscope, Figure 27. Since the ball diameter of the electrode is known to be 3.175mm it was possible to convert pixels to distance and determine the distance of the gap based on the number of pixels. The results show that the breakdown voltages are consistently higher than that of the dielectric constant but seem to follow a similar trend as related to constant dielectric strength. It is possible that an error occurred due to the assumption that the gap voltage was the same as the applied voltage at the time of breakdown due to current leakage. This would cause a reduction in the experimental voltages. Therefore, these experiments should be repeated by measuring the voltage directly at the gap.

Breakdown voltage is an important parameter for the EBD is the for the oil. For air the breakdown voltage is a function of the pressure-gap distance product as well as the type of gas. This relationship is quite well defined according to the semi-emperical Paschen curve formula (78). For an EBD operating in a gas it would be expected that the distance at which breakdown will occur can be estimated using the pachen curve, however these breakdown gaps can be very small, on the order of microns. Recently it has been found that for very small gaps, less than 10 μm, there may be some deviations from the Paschen curve (79). According to the the Paschen law for air at atmospheric pressure the minimum breakdown potential should be 360 V at around 10 μm, however it seems that breakdown voltages at shorter gaps continue to decrease below the expected minimum (79). It should be noted that there is a little bit of ambiguity with respect to the proper value for the secondary electron emission coefficient but these values typically range from 0.01-0.1 (78). Therefore it might be expected that the breakdown voltages for an EBD will be lower than expected.

For the case of discharges in liquids things become more complicated and the exact mechanisms of electrical breakdown are still a topic of debate, but breakdown measurements seem to indicate that the dielectric strength of most liquids are relatively constant. For various dielectrics oils the breakdown strength is typically on the order of 100-300 kV/cm whereas air is about 30 kV/cm (78). Considering the density of the liquid is 1000 times more than the air that fact that the breakdown voltage is only about 10 times higher is curious. Since the EBD deals with small breakdown gaps the question arrises whether the small gaps will cause any deviation in the normal dielectric strength.

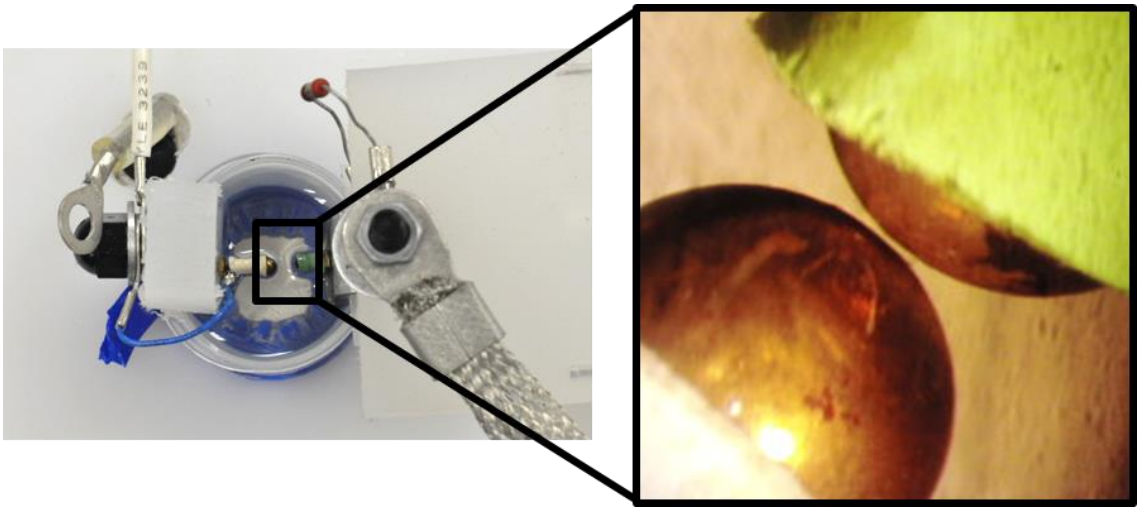

Figure 27 Experimental setup to measure small breakdown voltages in mineral oil

Figure 27 shows the experimental setup to study the breakdown voltage in mineral oil for very small gaps. This setup consisted of two spherical electrodes with a diameter of 1/16”. The smallest gap that was obtained with this configuration was 60 µm and the largest gap was 1.6 mm. The electrodes were placed within a plastic container that was fill with the testing oil, in this case it was light mineral oil. The voltage range investigated was from 0 to 25 kV.

The experimental procedure consisted of filling the container with the oil, setting the gap, taking a picture of the gap using a microscope as shown in Figure 27. The picture was used to determine the gap size by measuring the number of pixels in the gap and calibrating the pixels to the known diameter of the electrode. The breakdown voltages were obtained by slowly increasing the voltage until breakdown occurred. The mineral oil was changed after each breakdown to ensure there was no contamination.

The results of these experiments are shown in Figure 28, with comparison to transformer oil and submicron air measurements; the expected Paschen values for air are also shown.

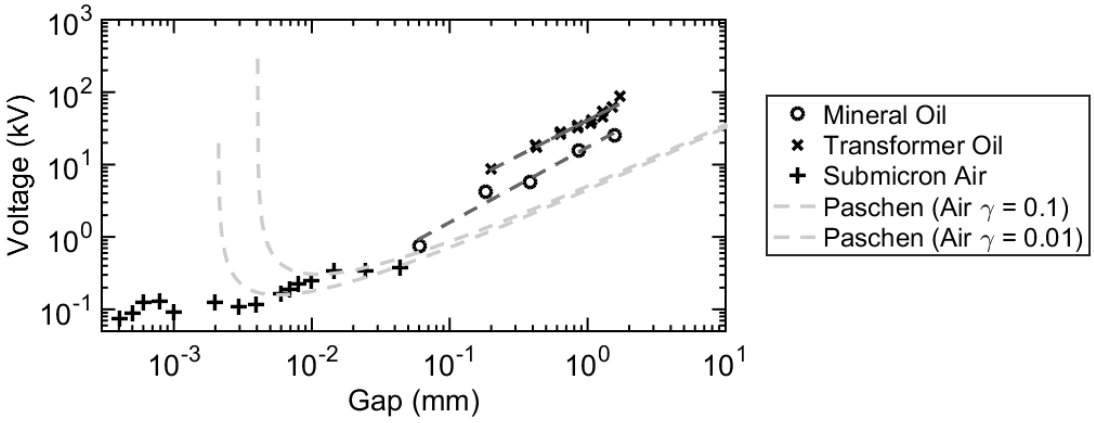

Figure 28 Breakdown voltages for 1) Mineral Oil, 2) Transformer Oil (80), and 3) Air (79)

The breakdown voltages for the oils at small gaps were fit with a log-log fit, Equation 62, to see if there was any significant deviation for linearity. The exponential factor, α, for the mineral and transformer oil were 1.04 and 0.98 respectively showing no significant deviation. The dielectric constant, given by the exp(β) was 174 kV/cm for the mineral oil and 408 kV/cm for the transformer oil.

$$\ln d = \alpha \ln V + \beta \qquad 62$$

It appears the calculated dielectric strength for mineral oil remains constant down to 60 µm. Measurements lower than this value become challenging and were not possible with the current setup. This analysis should be kept in mind when considering the EBD because the breakdown distances are generally smaller than 60 µm and might

still deviate from the expected values. Since smaller gaps were not yet measured any further analysis herein will assume that the constant dielectric strength will hold.

Current measurements and energy density analysis

Once breakdown is achieved charge will be transferred through the plasma causing a current to travel through the electrode. For small metal balls, 1/16”-1/8”, the values of these currents will be very and can therefore be challanging to measure accurately, however using a simple shunt can provide a measurement with a resonbile response time. The pulse of current that is generated by the charge transfer process can be integrated to determine how much charge was actually transferred through the plasma.

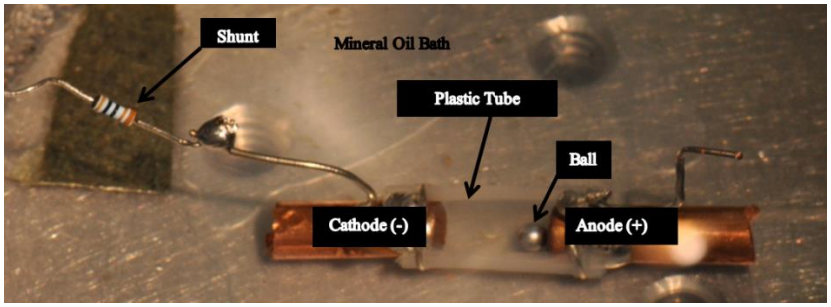

Figure 29 Experimental setup for measuring the current from an EBD with an 1/8” ball shown

A simplified setup was used to analyze the energy per pulse of the EBD, Figure 29. Two polished and rounded ¼ inch copper rods were used as the electrodes. These electrodes were connected to a polyethylene tube that was cut in half lengthwise. A 1/16” diameter aluminum ball was used for the current measurements and a ½ inch gap

was maintained between the electrodes. To the Cathode a resistor having a value of 1 kΩ was attached as a shunt to measure the current. Current and voltage measurements were made using a Lecroy WaveRunner 204MXi oscilloscope. The entire setup was submerged in a mineral oil bath, the same mineral oil used for the previously described breakdown voltage experiments. The measured current pulses are shown in Figure 30. It is interesting to note that the waveform of the current pulses looks remarkably like the current pulses measured by Raether, Figure 6. It is possible that the current measurements are showing the avalanches that initiated the plasma breakdown. The pulses seem to be at the correct timescale for the given breakdown gap and the successors seems to have the correct timescales for photoemission as well. The overall waveform resembles the case for a non-self-sustaining regime, however the voltage for the given gap is quite high. Therefore, it may be possible that while the self-sustaining criterion was met, the very low capacitance of the circuit inhibited the current and did not allow for exponential growth. If this speculation is accurate then it is a confirmation that the plasma being generated is indeed a non-equilibrium plasma and was inhibited from thermalization. These results are very interesting and should be repeated and investigated by future workers.

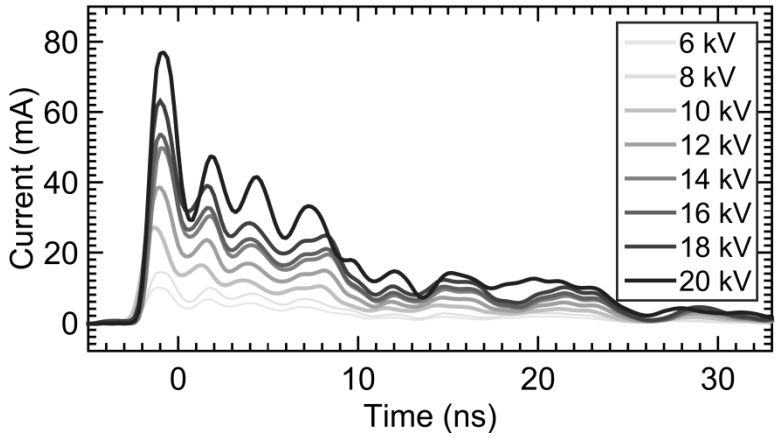

Figure 30 Current pulses measured for various voltages

The measured current values can be integrated according to Equation 63 to determine the amount of charge that was transferred during the discharge process.

$$Q = \int I(t)\, dt \tag{63}$$

Integrating the measured data resulted in charges that vary from about 100 pC to 600 pC for the voltage range of 6 kV to 20 kV. The amount of charge that is expected to be transferred to the ball can be estimated by calculating the capacitance using Equation 64.

$$C = \frac{\pi^3}{6}\frac{\varepsilon d^2}{D} \tag{64}$$

Here d, is the diameter of the ball, D is the gap between the electrodes, and ε is the permittivity of the medium. The calculated capacitance can be multiplied by the voltage to obtain the expected initial charge transfer to the ball at the electrode. These values are compared to the measured values in Figure 31.

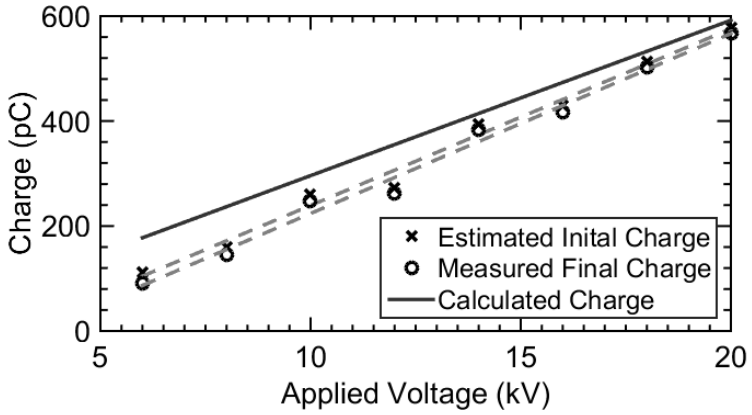

Figure 31 Measured and calculated charge as a function of applied voltage

The estimated initial charge shown in Figure 31 was determined with Equation 65.

$$Q_o = Q_f e^{2\sigma(D-d)/df\varepsilon} \quad 65$$

Here σ is the conductivity of mineral oil (5e-11 S/m), and f is the frequency of the ball traveling between electrodes. The frequency of the ball traveling between electrodes was measured for each voltage and is provided in Figure 32. These results show a slight difference between the expected charge and the measured charge. It is possible that this difference can be explained by considering that at the charge is being transferred through the plasma, and is being depleted from the ball, the decay of the local electrical field will eventually no longer be able to sustain the conductive channel. At that point, no more charge will transfer and some charge will remain on the ball until it moves closer. It is even likely that a second discharge even may occur. This however, was not observed in any of the experiments.

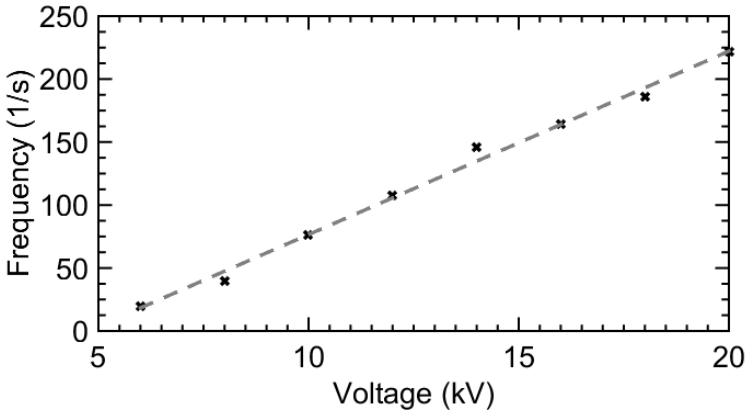

Figure 32 Frequency of ball as a function of applied voltage

The remaining question is how much energy this amount of charge correlates to, and to determine that, knowledge of either the voltage at breakdown or the capacitance at breakdown is required, Equation 66.

$$E = \frac{1}{2} Q V_b = \frac{1}{2} \frac{Q^2}{C_b} \qquad 66$$

Furthermore, to estimate either of these values the distance at which breakdown occurs is required as well. If the breakdown distance is known then the capacitance of the system could be estimated using the equations provided by Perez (81). Also, the breakdown voltage could be estimated by assuming the previously measured dielectric strength is still valid for the micron size gaps. If the capacitance value provided by Eq 3 is assumed valid, then the energy is approximation are as shown in Figure 33 and range from 137 nJ to 5.4 µJ.

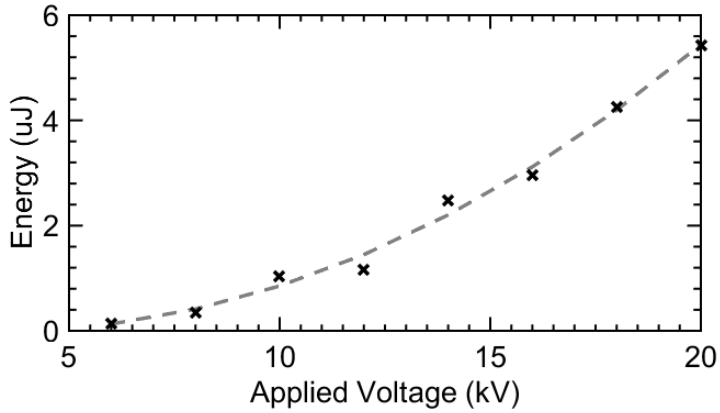

Figure 33 Energy input for EBD as a function of voltage (L/D = 4, Ball Diameter = 1/16")

If it is assumed that the calculated capacitance is correct, and the measure charge is also correct then the breakdown voltage can be obtained using Equation 64; these values are shown in Figure 34.

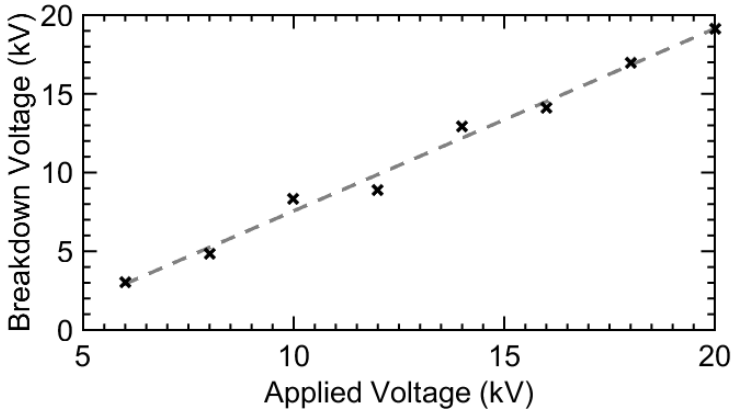

Figure 34 Breakdown voltage as a function of applied voltage

If it is assumed that the dielectric strength of 174 kV/cm is valid than these breakdown voltages would imply that the size of the plasma ranges from approximately 2 mm to 11

mm. However, it was determined from images captured of an EBD, Figure 35, that the discharge is only about 50 μm at the higher voltages of about 25 kV.

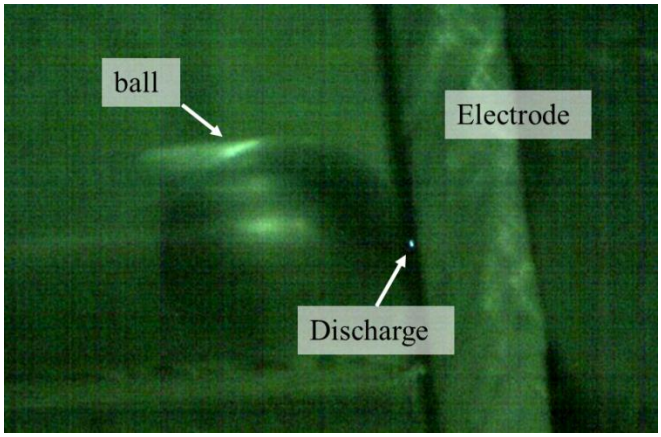

Figure 35 Picture of an EBD with an 1/8" ball

On one hand, if it is assumed that the breakdown voltage is correct, then the dielectric strength at submicron scales is about 3800 kV/cm. This might be explained by an increased pressure as the ball approaches the wall; however, it is difficult to imagine that would lead to an order of magnitude increase in the dielectric strength. On the other hand, if it is assumed that the dielectric strength should remain constant, then the breakdown voltage would be very low about 900V for a 50 μm gap; this would correspond to an energy value of about 500 nJ. However, does not seem to make much sense that the voltage between the ball and the wall is only 900V. Therefore, it seems most plausible that the dielectric strength of this system was somehow increased an order of magnitude in value.

Ball dynamics

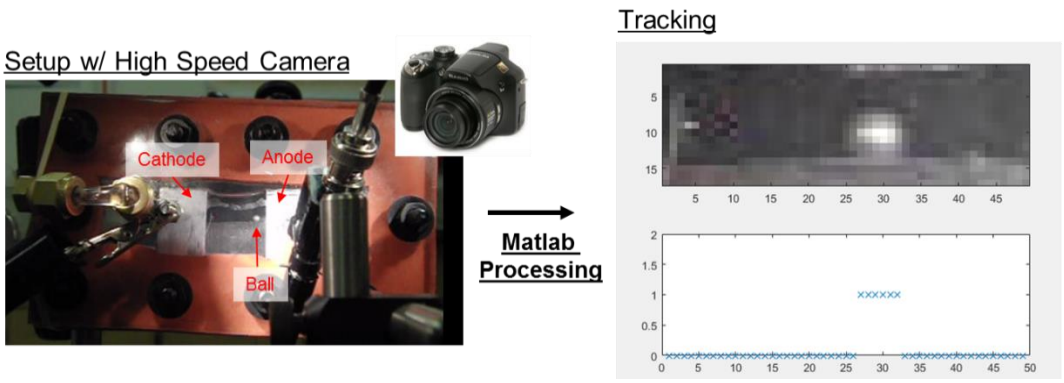

Figure 36 Setup for Ball tracking and example display of the ball tracking program that was created for tracking the ball

Several important parameters were obtained by capturing a high-speed video of the ball as it moves through the oil. The experimental setup consisted of two plastic plates bolted together with a thick gasket sandwiched between them. The gasket was cutaway in the middle where two electrodes were placed. Between the electrodes sat a plastic flow whereby a ball could be placed, Figure 36. This apparatus could be filled with any desirable fluid, but predominately mineral oil was used. Video was captured using a Casio Exilim EX0FH20.91 MP Digital Camera capable of recording up to 1000 fps. The video was then imported into MATLAB and a program was written to trace the position of the ball over time. Tracking the ball in this way provides the velocity as well as the acceleration and deceleration of the ball, Figure 37 .

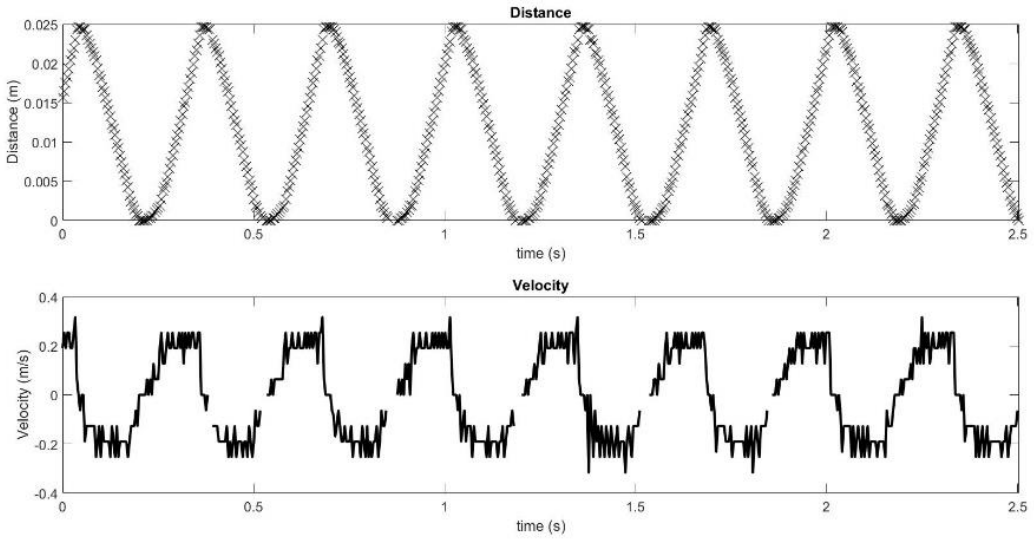

Figure 37 Example of particle position and velocity tracking for the case of 20 kV

The motion of the ball was a relatively smooth sinusoidal motion. The velocity can be seen to accelerate initially and then it flattens out at a constant velocity. When the ball approaches the electrode the velocity approaches zero and then begins to increase in the opposite direction. When the same conditions were plugged into the model, it was seen that the model could estimate the movement of the ball with reasonably good accuracy Figure 38.

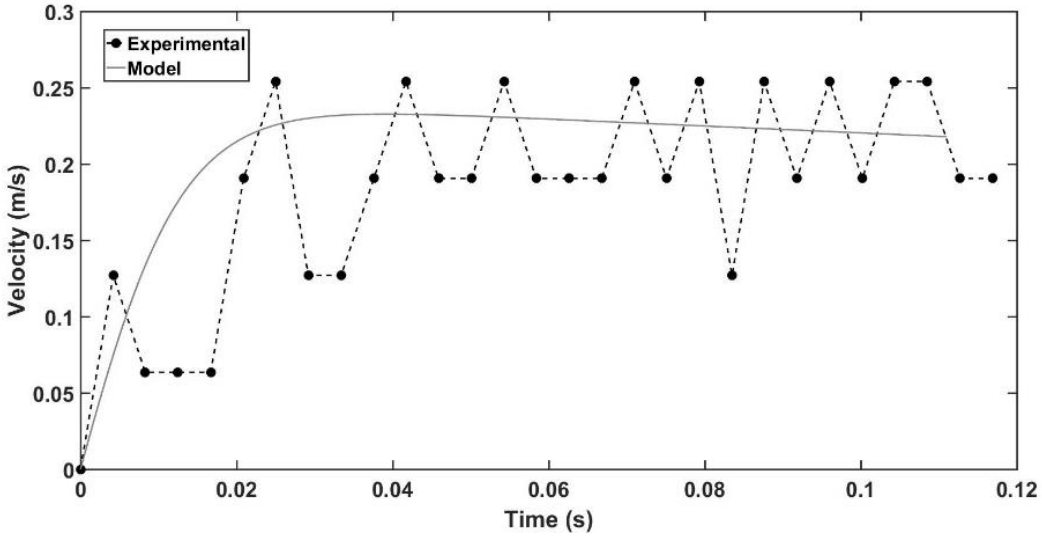

Figure 38 Comparison between experimental ball tracking experiments and model

This setup also allowed for a comparison of the model with the bounce frequency. The bounce frequency could be extracted from the video and the model estimated the bounce frequency simply by estimating the half cycle, since the model was used to calculate the ball motion in one direction; it should be noted however that the model can be used in either direction it just was not utilized for this work.

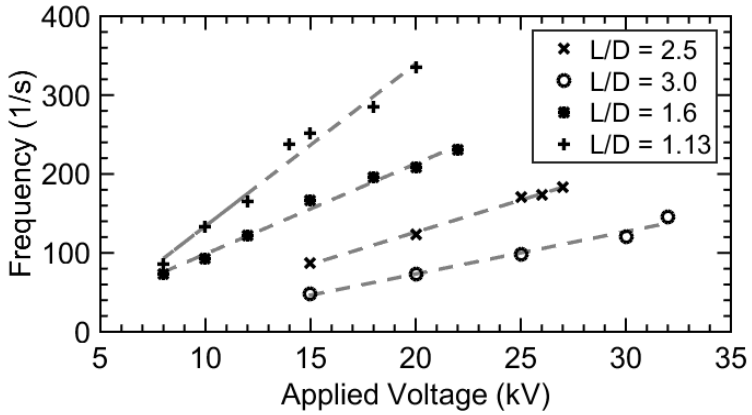

Figure 39 Frequency of ball as a function of applied voltage for several values of L/D

Several conditions were investigated and for some of those conditions the model did not work. An example of such a condition is shown in Figure 40. For this condition, the applied voltage was very near the breakdown voltage and therefore the ball was bouncing very fast. Due to the high velocity of the ball, the velocity was never actually seen to go to zero. Instead, the ball rapidly rebounds off the electrode and begins travelling in the opposite direction. This rebound effect is not considered within the model and therefore the model was unable to duplicate the results.

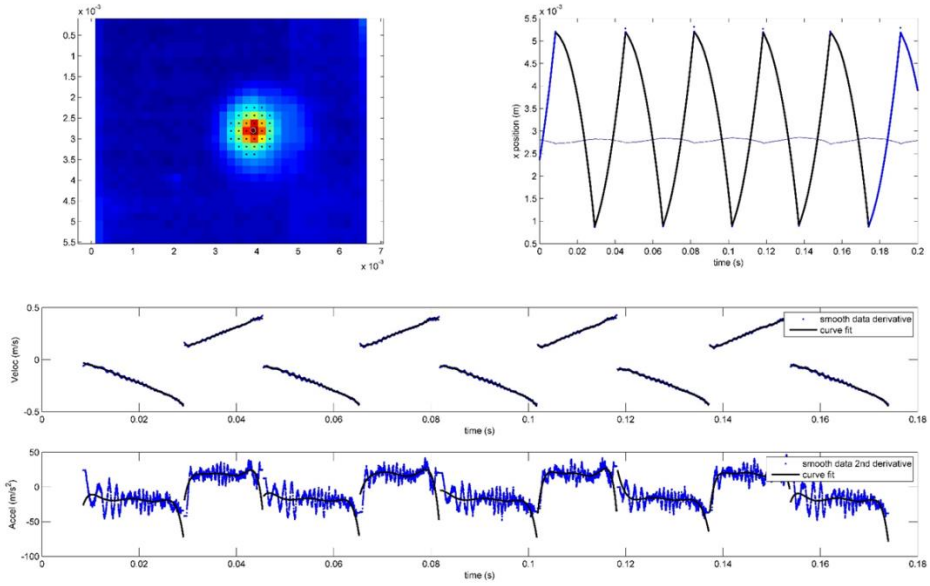

Figure 40 Ball tracking that was carried out at a higher voltage. The ball can be seen to rebound off the electrode due to the high velocity.

Lastly, by looking closely at the data it becomes apparent that the discharge event was actually captured by the tracking software, Figure 41. There was a single frame when the plasma becomes the brightest part of the image. Since the image

tracking software captured this even it allowed for the estimate of the breakdown gap size with reasonable accuracy.

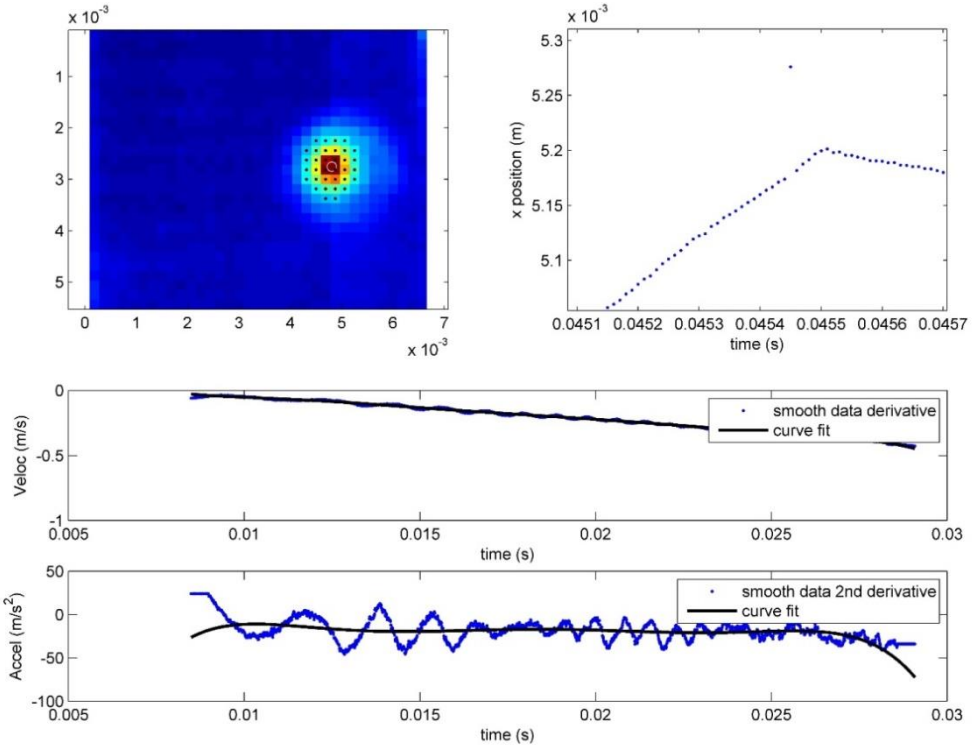

Figure 41 Ball tracking with good resolution was able to detect the instance when the plasma discharge occurred allowing for an estimation of gap size.

Optical emission intensity and spectroscopy

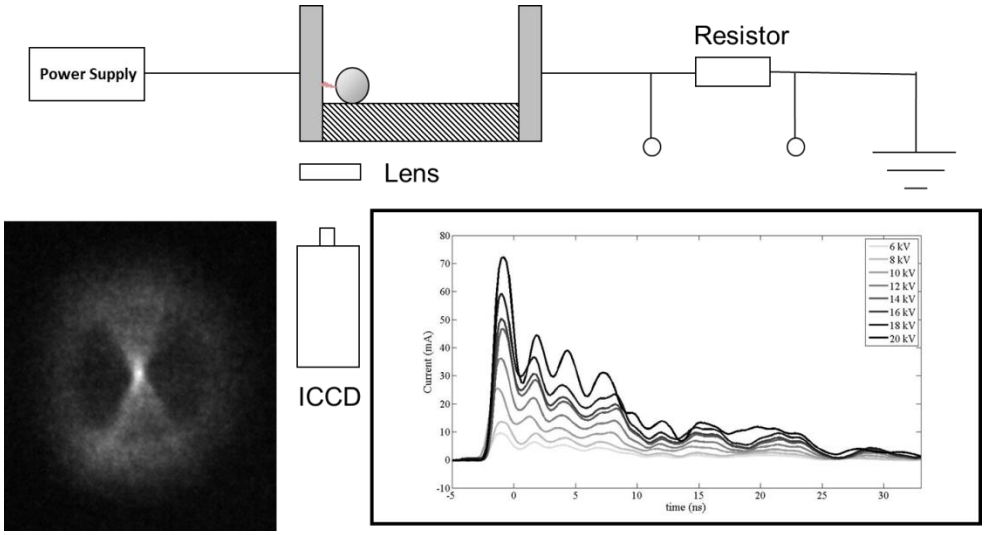

Figure 42 Schematic of experimental setup for correlating energy and light intensity. This configuration was also used for optical emission spectroscopy (OES), where the ICCD was replace with a spectrometer. A black and white example image of the discharge is shown.

The light emitted from an EBD can provide valuable information about the plasma. The light can be analyzed by measuring the intensity of the light using a 4 Picos ICCD Camera and the spectra of the emitted light can be analyzed as well using an TE Cooled CCD based spectrometer from Edmund. The current was used as a trigger. The intensity of the light emission is expected to be proportional to the energy. Using the relationship between applied voltage and energy, that was found previously, is used the intensity is seen to increase linearly with energy, Figure 43.

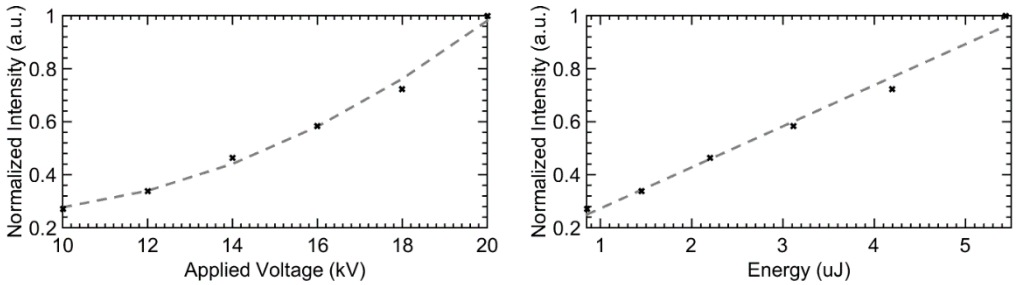

Figure 43 Plasma intensity of EBD (left) as a function of applied voltage and (right) as a function of discharge energy

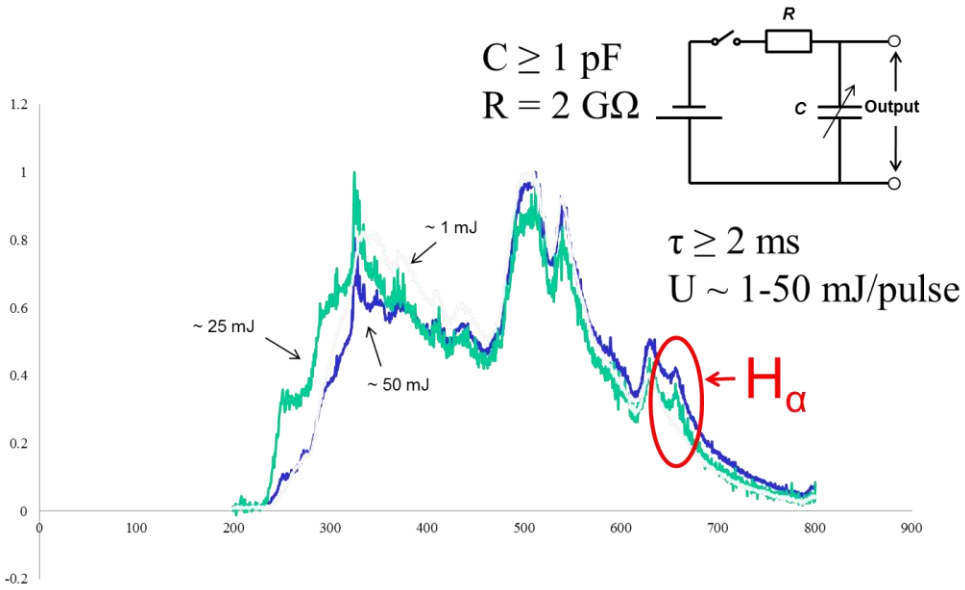

Figure 44 Optical emission for various energy inputs.

Optical emission spectroscopy was carried out for different energy inputs, Figure 44. The energy inputs that were explored are in the 1-50 mJ range, this is because for lower energies the light emission becomes very small and difficult to capture. While the emission spectra are quite broad, by varying the energy the hydrogen alpha line is seen to vary. For lower energies, the hydrogen alpha line is no longer visible. This is perhaps

an indication that the production of atomic hydrogen is being decreased for lower energies.

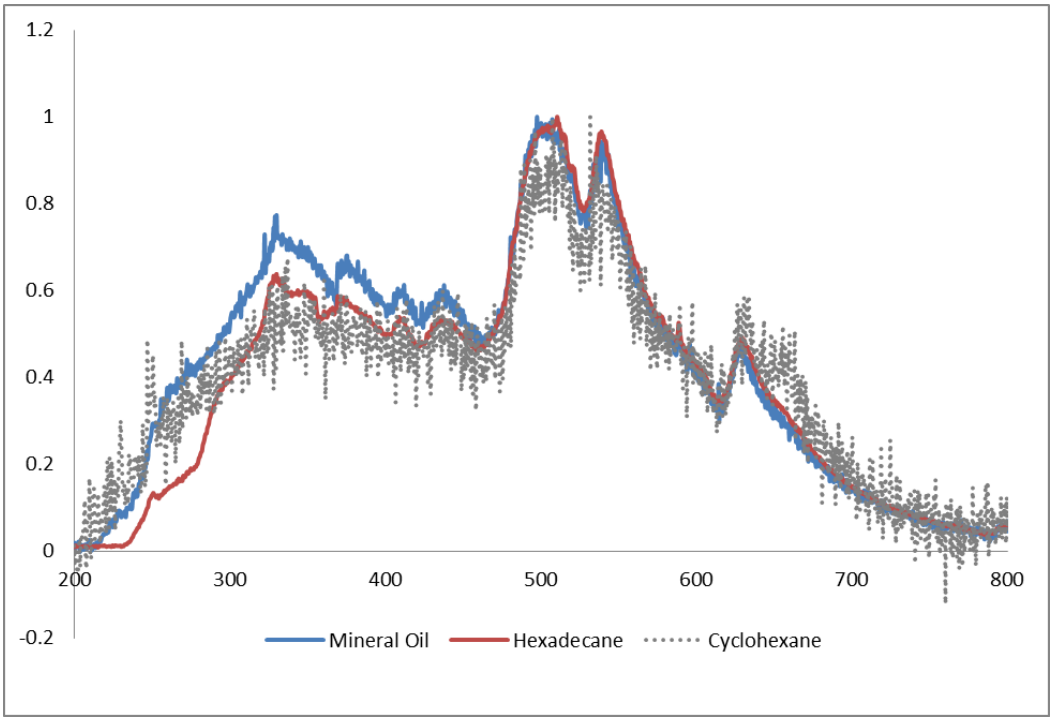

Figure 45 OES of mineral oil compared to hexadecane and cyclohexane (both normalized by max)

Optical emission spectroscopy was also carried out for different fluids. The similarity between the OES seems to indicate that what we are seeing as light emission is probably the result of similar species being generated. It is not too surprising that hexadecane and mineral oil look alike since they are both straight chain hydrocarbons with the only difference being that the mineral oil has a distribution of hydrocarbons. The cyclohexane on the other hand contain only aromatic hydrocarbons but still shows similar emission as the straight chain hydrocarbons. The emission is quite noisy, this is because of the difficulty in breaking down in cyclohexane; very high voltages are

required. This seems to suggest that the species that are causing emission are the same for these hydrocarbons. The species responsible for the emissions are likely H, H2, CH3, CH2, CH, C, C2, -[C-C]-, and -[C-H].

The controlled energy input for plasma generation in dielectric liquids may result provide a method of selective chemistry. At high energy inputs, it is likely that equilibrium will be achieved resulting in a thermal plasma. For the case of a thermal plasma the chemistry will be largely dictated by the rapid quenching that occurs at the boundary while the very hot plasma acts as a predominantly as a source of radicals. If the energy input is carefully controlled it may be possible to inhibit the initiation process of the plasma not allowing it to achieve equilibrium. In this case, the transient discharge can be considered a non-equilibrium plasma. This type of behavior has been observed for gaseous discharges but results in liquids have are difficult to find.

OES can provide information regarding equilibrium or non-equilibrium as well as if the chemistry that occurs during the transient process is different than the equilibrium chemistry. If the transient process can be described, hopefully in some simple way, it may lead to a very energy efficient chemical processing technique. Due to the complexity of the transient initiation process it is important to be able to understand the process before conclusion can be made.

Varying the energy input seems to only change the intensity of the emitted visible spectra. This could me that the duration of the plasma is decreasing, the plasma size is decreasing, or a combination of both effects is happening. Attempts to find an

absolute minimum energy input for planes generation is difficult and requires extremely low capacitance and so far, one could not be found.

Electrodynamic ball reactor (EBR)

One of the challenges of the EBR technique is that the treatment volume is very small and the energy input is also very small. Therefore, if a large volume of to be treated with a single particle it will likely take a very long time to treat the entire volume. To make the processing time faster the system can be scaled up using a multiple particle system. Doing so should reduce the processing time in proportion to the number of particles. When multiple particles are added to a liquid volume between two electrodes and an electric potential is applied, all the particle will begin to bounce around chaotically, Figure 46.

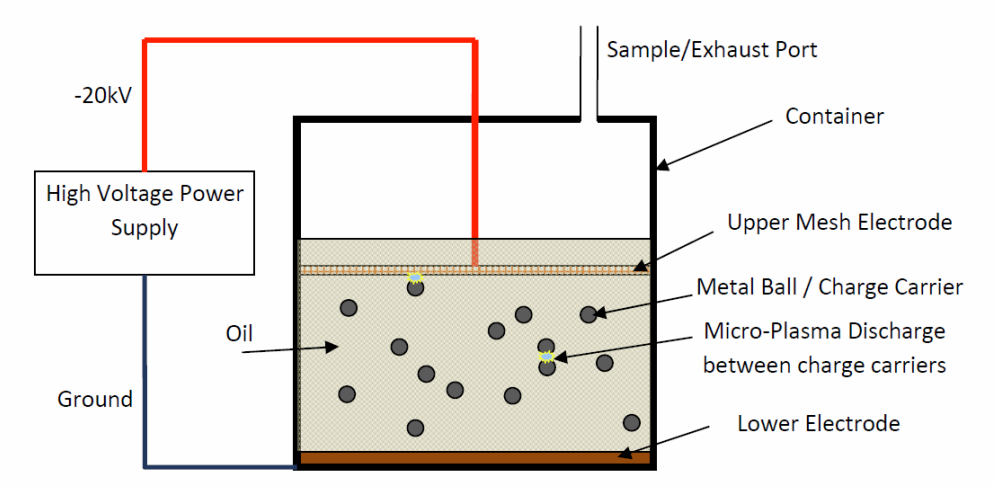

Figure 46 A simple configuration for a multiple particle EBR

From the simple configuration for a multiple particle EBR several observations can be made. Plasma discharges can be seen to occur not only at the electrode, but also between the charged particles, Figure 47.

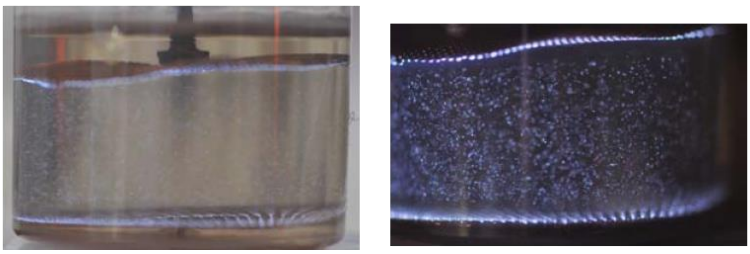

Figure 47 Simple multiple particle EBR (1 second exposure)

For the discharges that are occurring between the particles, the energy of the discharge can be some fraction of the energy of the discharge that occurs at the electrode. This is true if the particle loses some charge as it moves through the medium due to charge relaxation.

As the particles are bouncing around within the volume, they have a natural tendency to drift towards the electric field lines. As a result, the particles form particle chains that extend from one electrode to the other. Sometimes these chains can be relatively stable between the electrodes, rapidly bouncing against each other while maintaining a single column. However, this stable chain only exists when there is a sufficient gap between the particles. When there are no longer any gaps between the particles in the chain the particles effectively short the electrodes causing a large spark to initiate, Figure 48.

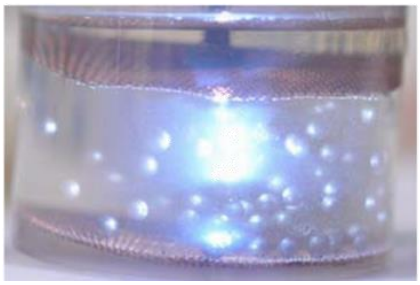

Figure 48 External circuit sparking due to particle chains

The energy of this spark will depend on the capacitance of the external circuit and it often quite large. Therefore, the spark can be quite intense. Once the spark is initiated it causes the particle chain to disperse and normal operation resumes shortly after. Since the goal of the EBR is to control the energy of the sparks that are occurring within the medium, these large sparking events are undesirable. To prevent these sparking events two approaches were tried. First a ballast resistor was placed in the external circuit to try and limit the current flowing into the particle chain. This has an interesting result of preventing sparking but allowing high energy arcs to be maintained between the particles, Figure 49.

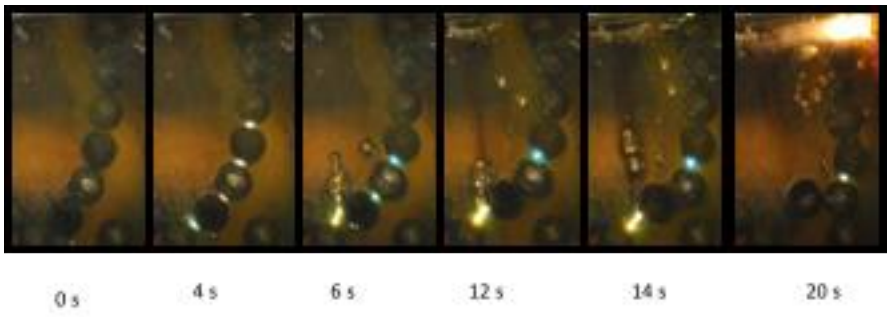

Figure 49 Particle chains shorting the external electrodes using an external ballast resistor

These arcs are quite hot and drive more and more current while maintaining the particle chain. During this process gas bubbles are produced between the particles. Eventually, the bubbles grow large enough to disrupt the particles chain causing them to fall apart again. While this method eliminates the sparking due to particle chains, it has yet another undesirable effect of producing high energy arcs. Therefore, a better solution to prevent sparking from particle chains is to restrain the particle motion to a single channel and ensure that there are not enough particles to short the gap. In fact, these channels can contain many or even just a single particle, Figure 50.

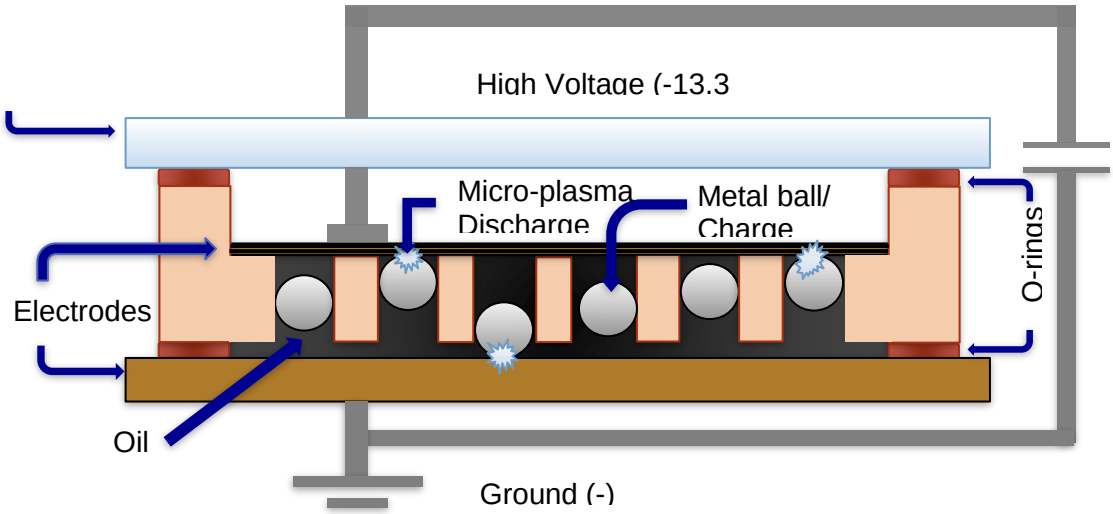

Figure 50 Multiple particle EBR reactor with single particle columns

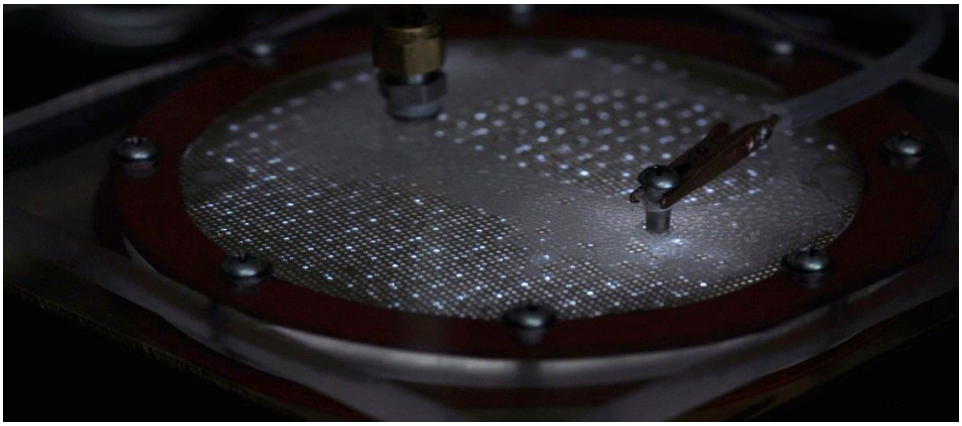

Figure 51 Picture of an EBR operating with a single ball in each column

Figure 50 illustrates the basic configuration for an Electrodynamic Ball Reactor (EBR) and Figure 51 shows the actual system in operation. The system consists of two main electrodes fully immersed in the oil to be processed and separated by some distance. Between the electrodes there are several metal balls within the oil. As voltage is applied to the electrodes a critical voltage will cause the balls to move from one electrode to the other. In this way, the balls are acting as charge carriers, transferring a certain quantity of charge from one electrode to the other. The characteristics of the voltage and current are dependent of the scale and can be accurately predicted, Figure 52.

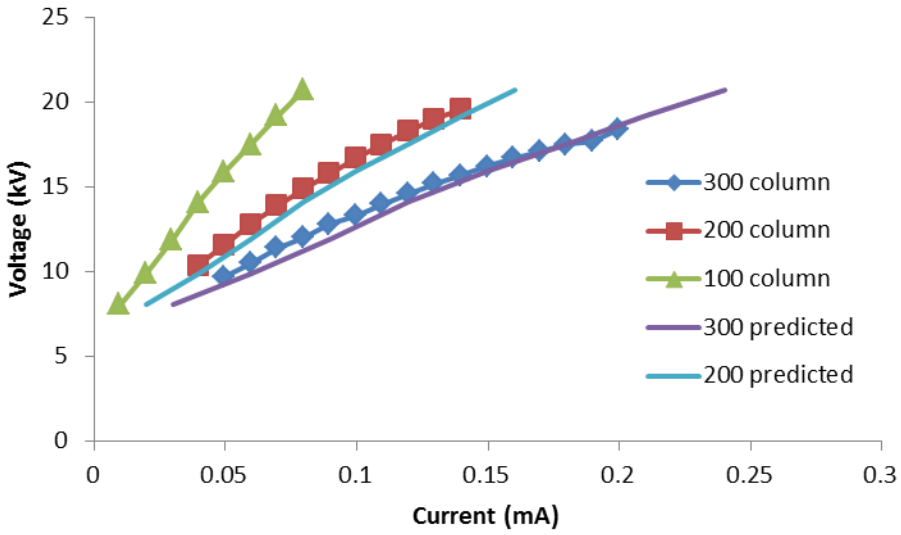

Figure 52 Voltage verse current characteristics for scaling of the EBRs

On some occasions the charge ball will encounter another charge ball of different charge; such a collision will result in a charge transfer between the two balls. All the charge transfer events that occur, whether they are between two balls or between a ball and an electrode, will occur by generating a plasma. These plasmas can be observed due to the light that is emitted Figure 53.

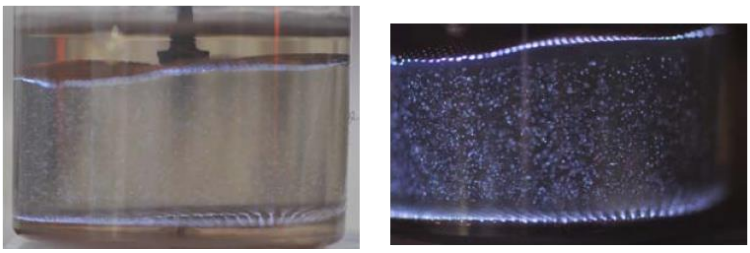

Figure 53 Electrodynamic Ball Reactor (EBR) processing mineral oil (exposure = 1 second)

The goal of the Electrodynamic Ball Reactor (EBR) is to crack the hydrocarbons in a controlled way to obtain more desirable small chain hydrocarbons. The main control

mechanism that is provided by an EBR is a control over the energy density of the sparks. It is expected that by controlling the energy density of the sparks it will be possible to control the chemistry and therefore the products that are produced.

Characterization of oil mixtures

Two fundamental properties of the oil are of primary interest for processing the oil with an EBR, namely the viscosity and the electrical conductivity. For oils that fall into the category of extra heavy crude the oil is often solid at standard temperature and pressure. To even begin processing these oils their viscosity must be at least temporarily reduced. This can be accomplished by either increasing their temperature or mixing them with lighter oil. Practically speaking, mixing heavy oil with lighter oil is uneconomical therefore increasing the oil temperature is typically a better option. However, from a research perspective it is useful to mix the heavy oil with lighter oil to carry out preliminary experiments with heavy hydrocarbon mixtures at room temperature. If the results from EBR experiments working with heavy/light mixtures seem promising than working with pure heavy crudes at temperature can be attempted. Therefore, preliminary results presented herein are with various mixtures and these mixtures must be characterized. Furthermore, the electrical conductivity is an important parameter for operating the EBR. If the medium is too conductive it will be very difficult to have electric fields that are high enough for electrophoretic forces to be effective.

Oil mixtures were made using mineral oil and a heavy crude oil. Five samples were prepared to determine how mixing affected the viscosity. The viscosity of these

mixtures was measured using a TA Instruments AR-G2 Rheometer. The technique involves sandwiching the oil sample between a temperature controlled base plate and a disc that can spin with minimal friction. For all measurements, the gap between the base plate and the disc was 1000 μm and the shear rate was held constant at 10 s^{-1}. The temperature was ramped at 15°C/min from 25°C to 80°C and the viscosity was recorded, Figure 54.

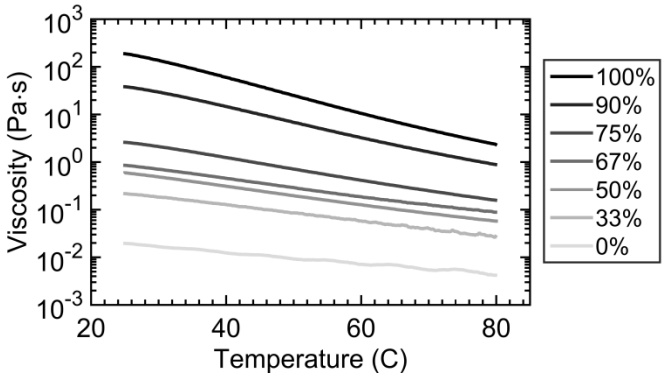

Figure 54 Viscosity versus temperature for heavy/light mixtures (mass fractions of heavy oil)

The electrical conductivity of both the heavy and light oil is not very high in general, which is desirable for the EBR; if the conductivity were too high too much energy will be lost to conduction and joule heating. The electrical conductivities of the mixtures however can be higher than the pure oils. This is because the heavy oil contains metals which can conduct easier when the viscosity is lowered either by increasing its temperature or by mixing with lights. Approximate values for the electrical conductivity were obtained by submerging two electrodes in pure heavy oil and applying a constant voltage of 15 kV while measuring the current. The oil was than heated using a standard

heating plate. Since the accuracy of the absolute conductivity value is typically not very good for this method, the values are normalized to the room temperature value to illustrate that the conductivity grows exponentially with temperature, Figure 55.

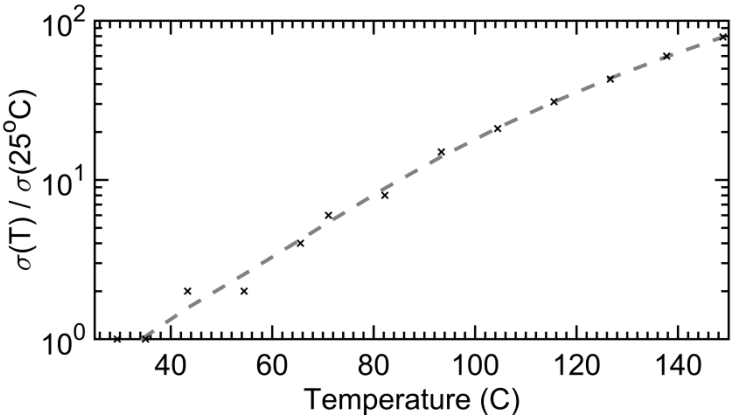

Figure 55 Normalized electrical conductivity versus temperature for heavy crude oil

The dependence of normalized electrical conductivity on the mass fraction of heavy oil for two temperatures is shown in Figure 56. As noted earlier the conductivity increases as the heavy oil is diluted with the lighter oil. The conductivity reaches a maximum value near about 20% and then starts to decrease once again. This maximum conductivity occurrence is a strong indication that the dominating conductivity is due to the metal particles in the heavy oil. It is likely the result of the increasing mobility of the metal particles along with the decreasing concentration of the metal particles as the viscosity is decreased.

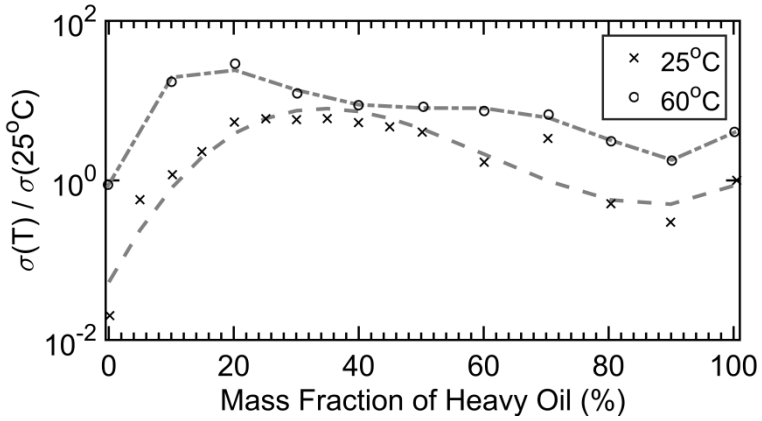

Figure 56 Normalized electrical conductivity versus mass fraction of heavy oil

This information was used to choose an appropriate mixture to obtain a reasonable viscosity and electrical conductivity to start experiments at room temperature. As will be seen in the experimental section, 70% (approx. 1 Pa*s) was chosen for most room temperature experiments. For this mixture, the electrical conductivity is low enough that only a small current leak, approximately less than 50 μA, will occur which is acceptable.

Viscosity reduction

A large batch of 70% heavy hydrocarbon mixture was prepared to run several experiments. First a small portion was put aside as a control. The rest was split into three even portions of about 24 grams each. The three samples were treated using the same EBR with the same applied voltage, however they were each treated for a different amount of time. The three samples were treated until 5 kJ, 10 kJ, and 20 kJ of energy was applied to the samples. The energy input was monitored through a Labview program

that monitored the current and voltage input. These energy input values were chosen to have a range of specific energy inputs from 0 to about 850 kJ/kg.

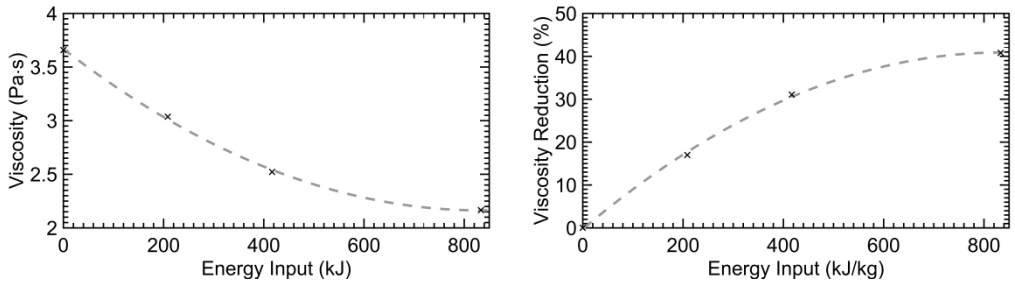

Figure 57 Viscosity change versus specific energy input for 70% heavy oil mixture

Figure 57 shows a decreasing viscosity with increasing specific energy input. With the high-energy input of about 833 kJ/kg a 40% viscosity reduction was achieved. Considering for a moment that the amount of specific energy input required to crack heavy hydrocarbons should be on the order of a 500 kJ/kg the efficiency of the system can be roughly gauged. To see even a 40% decrease in the viscosity it is required that only a very small fraction of the oil be cracked, perhaps about 1%. This leads to the conclusion that the reactor was approximately 0.6% efficient at cracking the heavy hydrocarbons.

To try and understand how the chemical composition of the oil changed during the treatment process the samples were sent out to be analyzed. Simulated distillation was carried out, whereby the samples were heated and the mass change was measured. These results are shown in Figure 58. It can be seen that a large portion of the heavy oil contains a significant amount of high boiling point hydrocarbons. Furthermore, the

treated sample shows an increase in the light fraction and a smaller increase in the heavy fraction. Therefore it would seem that while the plasma treatment process is not perfect, it can in some cases produce more light than heavy fractions. With even a very small increase in the lights, a significant viscosity reduction can be observed. Due to the complexity of the analysis of heavy crude oil experiments were carried out using pure hexadecane, Figure 59. The results from the hexadecane treatment more clearly show the cracking that is taking place.

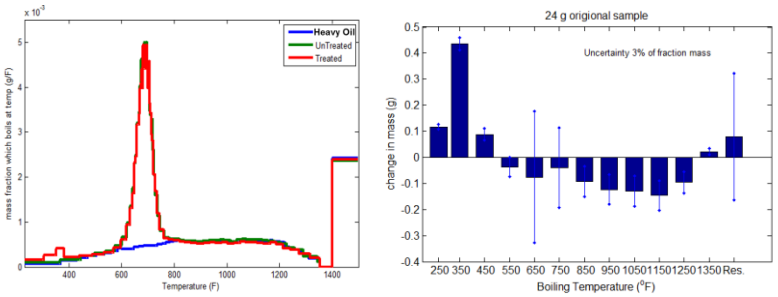

Figure 58 Simulated distillation of treated and untreated samples of heavy oil / mineral oil mixture (70/30) compared with pure heavy oil.

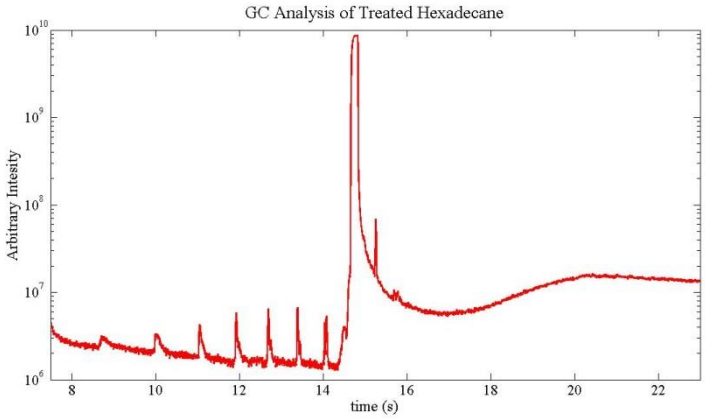

Figure 59 Composition of plasma treated pure hexadecane.

Gas production analysis

During EBR processing of the oil there is a certain amount of gas that is produced. The amount of gas coming out of the EBR was measured by attaching a syringe to the exhaust and running the reactor for a few minutes. This syringe was then injected into a SRI 8610C gas chromatograph (GC) equipped with a helium ionization detector (HID) and a thermal conductivity detector (TCD) to analyze the gases. In some cases, the amount of gas coming off was measured to be around 10 mg/s. This gas consisted of about 60% H_2 and 40% CH_4.

CONCLUSIONS AND FUTURE WORK

Summary

The exact mechanisms for explaining the plasma initiation in liquid are not yet satisfactorily explained, however within this dissertation the process was further explored with a focus on the energy input. The general thesis statement states, "Non-equilibrium plasma can be generated in a high density medium when the energy density is controlled." Even though the underlying mechanisms remain elusive, it is possible to make generalized statements about the state of the plasma that is generated. Specifically, the state of the plasma, whether it is in a state of equilibrium or non-equilibrium, will depend on the amount of energy that is provided to the process within a specific volume. Even when a breakdown condition is met, the plasma can be prevented from achieving equilibrium by limiting the available energy.

The experimental work presented in this dissertation illustrated that very low energy plasmas generated in liquids can provide unique chemistry. If highly thermal plasma, such as an arc, is produced in oil the production of carbon and hydrogen occur as would be expected in an equilibrium state at high temperatures. However, the low energy plasmas that were created using the Electrodynamic Ball Discharge technique could crack the large hydrocarbons into smaller hydrocarbons without a significant production of carbon; thus, suggesting that a more non-equilibrium process is taking place.

Work accomplished

To evaluate the thesis statement experimentally, a new technique of generating low energy plasma in liquids was engineered. The Electrodynamic Ball Discharge (EBD) provides a technique avoiding parasitic capacitance that naturally exists in external circuits, therefore allowing very small capacitance values (~ 0.05 - 0.5 pF) to be utilized in a controllable way. These small capacitance values can be used to produce plasma discharges of very low energy (~ 0.5 – 200 μJ). This technique was modeled numerically to determine the efficiency of the process. Energy losses were identified and quantified allowing for a complete characterization of the process. The model proved useful when designing and scaling the system. An optimum L/d value can be selected based on the properties of the liquid that is being processes. The model can also provide insight into the boundaries of the operating range; for example, the model can accurately determine the length at which the ball will stop moving due to significant conductive or frictional losses.

Experimental work with scaling the EBD to Electrodynamic Ball Reactors (EBR) was carried out and several important factors were identified. If the EBD technique is to be utilized to provide a significant chemical change in the liquid than it must be scaled, however it is very complicated to try and model a scaled-up version that contained many EBDs; therefore, this work was carried out experimentally only. The phenomena of chaining were identified, whereby the balls would line up along the electric field lines,

forming chains, which could bridge the gap between the electrodes leading to a short. If the external circuit contained a lot of energy it would create a large spark, which is exactly what the EBD is trying to avoid. To try and avoid the sparking, a ballast can be place in the external circuit, however this did not prevent the chaining. This time when the chaining occurs, the plasma would be a continuous arc rather than a rapid spark; this too was undesirable. The final solution was to isolate the balls into columns so that chaining could not happen at all. This scaling technique proved to work quite well and allowed for larger scale processing of oil which could demonstrate substantial viscosity reductions.

Suggested future work

Much of the work carried out in this dissertation required developing some new techniques for producing very small amounts of energy in a plasma produced in liquid. This technique offers a very interesting opportunity to explore high density, non-equilibrium plasma chemistry in a way that can scale. There is a lot more work that can be done in this area.

The author and his adviser explored using many different materials for the balls, including ceramics and plastics. Non-conductive material works as well but for very different reasons than the conductive balls. Even lower energy plasmas can be created in this way. Dielectrophoretic forces can becomes dominate in this case, which would require modification of the model created here. Furthermore, there are some benefits to

exploring AC fields. From some brief experiments, it was observed that AC fields can offer different ways of controlling the motion of the ball.

More work can be carried out for exploring the viscosity reduction. While some experiments were carried out on varying the ball radius and electrode gaps, more work is needed to completely characterize the effect of specific energy density on viscosity reduction.

The current measurements that were acquired showed some interesting characteristics which should be explored further. If the measured waveform is indeed capturing Townsend avalanching, then this can be modeled and more details can be determined about the breakdown process in liquids. Studying the current in this was can provide value information, however it must first be confirmed that these currents are indeed measuring avalanching.

The last recommendation for future work is to carry out more optical emission spectra. There is a lot to be learned from these measurements however they are very difficult to make, especially was the plasma is in a liquid. From some brief experiments, it was observed that the broadening of the spectra can be slightly alleviated by submerging a fiber optic probe in the liquid and positioning it as close to the light emission as possible. There were even attempts to use the metallic coating of the fiber optic probe as the electrode for the ball to discharge to. This proved difficult to control as EMI could not be sufficiently reduced.

REFERENCES

1. Slavens, Stephen Manson. *Microplasma Ball Reactor for Liquid Hydrocarbon Conversion.* s.l. : Texas A&M University, 2014.

2. The Richmond Institue. [Online] [Cited: 02 11, 2017.] http://www.richmondinstitute.com/article/endodontics/plasmadent-breakthrough-technology-dental-hygiene-dentistry.

3. *The Conductivity Produced in Gases by the Motion of Negatively Charged Ions.* Townsend, J S. 1606, s.l. : Nature, 1900, Vol. 62.

4. *The Diffusion of Ions into Gases.* Townsend, J S. s.l. : Philosophical Transactions of the Royal Society of London. Series A, Containing Papers of a Mathematical or Physical Character, 1900, Vol. 3.

5. *A Theory of Spark Discharges.* Meek, J M. s.l. : Physical Review, 1940, Vol. 57.

6. Raizer, Yu P. *Gas Discharge Physics.* s.l. : Springer, 1991.

7. *The mean free path of electrons in polar crystals.* Frohlich, H. and Mott, N. F. s.l. : The Royal Society of London. Series A, Mathematical and Physical Sciences, 1939.

8. *Progress in the Field of Electric Breakdown in Dielectric Liquids.* Sharbaugh, A. H., Devins, J. C. and Rzad, S. J. 4, s.l. : Trans. Electri. Insul., 1978, Vol. 13.

9. Fridman, Alex and Kennedy, L A. *Plasma Physics and Engineering. : CRC Press,* 2004.

10. Capitelli, M, et al. *Plasma Kinetics in Atmospheric Gases. : Springer,* 2000.

11. *Ozone synthesis from oxygen in dielectric barrier discharges.* Eliasson, B., Hirth, M. and Kogelschatz, U. s.l. : J. Phys. D: Appl. Phys., 1986, Vol. 20.

12. *On-board plasma-assisted conversion of heavy hydrocarbons into synthesis gas.* Gallagher, Michael J, et al. 6, s.l. : Fuel, 2010, Vol. 89.

13. *A comparative study of non-thermal plasma assisted reforming technologies.* Petitpas, G, et al. 14, s.l. : International Journal of Hydrogen Energ, 2007, Vol. 32.

14. *Nonthermal Plasma Processing for Air-Pollution Control: A Historical Review, Current Issues, and Future Prospects.* Kim, Hyun-Ha. 2, s.l. : Plasma Processes and Polymers, 2004, Vol. 1.

15. *Recent development of plasma pollution control technology: a critical review.* Chang, Jen-Shih. 3-4, s.l. : Science and Technology of Advanced Materials, 2001, Vol. 2.

16. *Ammonia Production From Solid Urea Using Nonthermal Plasma.* Iitsuka, Yoshihiro, et al. 3, s.l. : IEEE Transactions on Industry Applications, 2012, Vol. 48.

17. *Non-thermal plasma approaches in CO2 utilization.* Liu, Chang-jun, Xu, Gen-hui and Wang, Timing. 2-3, s.l. : Fuel Processing Technology, 1999, Vol. 58.

18. *Fabrication of vertically aligned single-walled carbon nanotubes in atmospheric pressure non-thermal plasma CVD.* Nozaki, Tomohiro, et al. 2, s.l. : Carbon, 2007, Vol. 45.

19. *Analysis of solid products formed in atmospheric non-thermal carbon monoxide plasma.* Geiger, Robert and Staack, David. 27, s.l. : Journal of Physics D: Applied Physics, 2011, Vol. 44.

20. Geiger, Robert. *Plasmachemical Synthesis of Carbon Suboxide. Master's thesis.* s.l. : Texas A&M University, 2012.

21. *Plasma assisted ignition and combustion.* Starikovskaia, S M. 16, s.l. : Journal of Physics D: Applied Physics, 2006, Vol. 39.

22. *Plasma display panels: physics, recent developments and key issues.* Boeuf, J P. 6, s.l. : Journal of Physics D: Applied Physics, 2003, Vol. 36.

23. *Non-thermal plasmas in and in contact with liquids.* Bruggeman, Peter and Leys, Christophe. 5, s.l. : Journal of Physics D: Applied Physics, 2009, Vol. 42.

24. *Bleaching and Degradation of Textile Dyes by Nonthermal Plasma Process at.* Abdelmalek, Fatiha, et al. 1, s.l. : Industrial & Engineering Chemistry Research, 2006, Vol. 45.

25. *Reforming of heavy oil using nonthermal plasma.* Prieto, G, et al. 5, s.l. : IEEE Transactions on Industry Applications, 2001, Vol. 37.

26. *Applied Plasma Medicine.* Fridman, G, et al. 6, s.l. : Plasma Processes and Polymers, 2005, Vol. 5.

27. *Electrohydraulic Discharge and Nonthermal Plasma for Water Treatment.* Locke, B R, et al. 3, s.l. : Industrial & Engineering Chemistry Research, 2006, Vol. 45.

28. *Nonthermal Plasma Inactivation of Food-Borne Pathogens.* Misra, N N, et al. 3, 2011, Vol. 3.

29. *Atmospheric-pressure, nonthermal plasma sterilization of microorganisms in liquids and on surfaces.* Akishev, Yuri, et al. 9, s.l. : Pure and Applied Chemistry, 2008, Vol. 80.

30. *Transportation of heavy and extra-heavy crude oil by pipeline: A review.* Martinez-Palou, Rafael, et al. s.l. : Journal of Petroleum Science and Engineering, 2011, Vol. 75.

31. *A review of recent advances on process technologies for upgrading of heavy oils and residua.* Rana, Mohan S., et al. s.l. : Fuel, 2007, Vol. 86.

32. *Liquid phase fuel reforming at room temperature using non-thermal plasma.* Matsui, Yoshihiko, et al. 1, s.l. : Prepr. Pap. Am. Chem. Soc. Dic. Fuel Chem., 2004, Vol. 49.

33. *Ozone Generation from Oxygen and Air: Discharge Physics and Reaction Mechanisms.* Kogelschatz, U, Eliasson, B and Hirth, M. 4, s.l. : Ozone: Science & Engineering: The Journal of the International Ozone Association, 1988, Vol. 10.

34. *High-energy-density Extended CO solid.* Lipp, M J, et al. s.l. : Nature Materials, 2005, Vol. 4.

35. *Physics and chemistry in high electric fields.* Kreuzer, H. J. s.l. : Surface Science, 1991, Vol. 246.

36. Kuffel, E., Zaengl, W. S. and Kuffel, J. *High Voltage Engineering Fundamentals.* s.l. : Butterworth-Heinemann, 2000.

37. Cobine, James Dillon. *Gaseous Conductors: Theory and Engineering Applications.* s.l. : Dover Publications, Inc, 1941.

38. *Microplasma Discharges in High Pressure Gases Scaling Towards the Sub-Micron Regime.* Chitre, Aditya Rajeev. s.l. : Texas A&M Thesis, 2010.

39. McDaniel, E. W. *Collision Phenomena in Ionized Gases.* New York : Wiley (Interscience), 1964.

40. Christophorou, L. G. *Atomic and Molecular Radiation Physics.* New York : Wiley (Interscience), 1971.

41. Huxley, L. G. H. and Crompton, R. W. *The Diffusion and Drift of Electrons in Gases.* New York : Wiley (Interscience), 1974.

42. Raether, H. R. *Electron Avalanches and Breakdown in Gases.* Washington DC : Butterworth & Co. (Publishers) Ltd., 1964.

43. *Electrical conduction in dielectrics at high fields.* Adamec, V and Calderwood, J. H. s.l. : J. Phys. D.: Appl. Phys., 1975, Vol. 8.

44. *Electrons in disordered structures.* Mott, N. F. 7, s.l. : Advances in Physics, 2001, Vol. 50.

45. *On the theory of dielectric breakdown in solids.* Frohlich, H. and Wills, H. H. s.l. : Proceedings of the Royal Society of London. Series A, Mathematical and Physical Sciences, 1946.

46. *Theory of Electrical Breakdown in Ionic Crystals.* Frohlich, H. 901, s.l. : Proc. of the Royal Society of London. Series A, Mathematical and Physical, 1937, Vol. 160.

47. *Laser-Induced Electric Breakdown in Solids.* Bloembergen, Nicolaas. 3, s.l. : IEEE Journal of Quantum Electronics, 1974, Vol. 10.

48. *On the theory of electron multiplication in crystals.* Seitz, Frederick. 9, s.l. : Physical Review, 1949, Vol. 76.

49. Lewis, T. J. *Progress in Dielectrics, Vol 1.* s.l. : Wiley, 1959.

50. *Progress in Dielectrics.* Sharbaugh, A. H. and Watson, P. K. 1962, Vol. 4.

51. *A review of recent investigations into electrical conduction and breakdown of dielectric liquids.* Swann, D. W. 5, s.l. : British Journal of Applied Physics, 1962, Vol. 13.

52. *Aspects of Electrical Breakdown of Liquid Insulating Material.* Kok, J. A. and Vroonhoven, C. Van. s.l. : Applied Science Research, 1961, Vol. 9.

53. *Breakdown of commercial liquid and liquid solid dielectrics.* Krasucki, Z. s.l. : High Voltage Technology, 1968.

54. *Conduction and Breakdown in Mineral Oils.* Zaky, A. A. and Hawley, R. s.l. : Pergamon Press, 1973.

55. *Simple Dielectric Liquids.* Gallagher, T. J. s.l. : Clarendon Press, 1975.

56. Christophorou, L. G. *Electron-Molecule Interactions and their Applications: Volume 2.* s.l. : Academic Press, 1984.

57. *Laser-induced Breakdown in Aqueous Media.* Kennedy, Paul K., Hammer, Daniel X. and Rockwell, Benjamin A. 3, s.l. : Prog. Quant. Electr., 1997, Vol. 21.

58. *Energy balance of optical breakdown in water at nanosecond to femtosecond time scales.* Vogel, A., et al. s.l. : Applied Physics B, 1999, Vol. 68.

59. *Non-equilibrium and equilibrium problems in laser-induced plasma.* Capitelli, Mario, Capitelli, Francesco and Eletskii, Alexander. s.l. : Spectrochimica Acta Part B, 2000, Vol. 55.

60. *Laser-induced breakdown in organic liquids.* Fujii, Haruhisa, Yoshino, Katsumi and Inuishi, Yoshio. s.l. : J. Phys. D: Appl. Phys., 1977, Vol. 10.

61. *Laser-induced breakdown in dielectric liquids.* Fujii, H., Yoshino, K. and Inuishi, Y. s.l. : Journal of Electrostatics, 1979, Vol. 7.

62. *Optical Study of Conduction and Breakdown in Dielectric Liquids.* Sakamoto, Saburo and Yamada, Hiroshi. 3, s.l. : Transactions on Electrical Insulation, 1980, Vol. 15.

63. *Breakdown and prebreakdown phenomena in liquids.* Devins, John C., Rzad, J. and Schwabe, J. s.l. : Lournal of Applied Phsyics , 1981, Vol. 52.

64. *Propagation and Structure of Streamers in Liquid Dielectrics.* Beroual, A., et al. 2, s.l. : IEEE Electrical Insulation, 1998, Vol. 14.

65. *Theoretical Study of the Initial Stage of Sub-nanosecond Pulsed Breakdown in Liquid Dielectrics.* Shneider, M. N., Pekker, M. and Fridman, A. 5, s.l. : IEEE Transactions on Dielectrics and Electrical Insulation, 2012, Vol. 19.

66. *Pulsed nanosecond discharge development in liquids with various dielectric permittivity constants.* Starikovskiy, Andrey. s.l. : Plasma Sources Science and Technology, 2013, Vol. 22.

67. *Non-equilibrium nanoscond-pulsed plasma generation in the liquid phase (water, PDMS) without bubbles: fast imaging, spectroscopy and leader-type model.* Dobrynin, Danil, et al. 10, s.l. : Journal of Physics D: Applied Physics , 2013, Vol. 46.

68. *Investigation of positive and negative modes of nanosecond pulsed discharge in water and electrostriction model of initiation.* Seepersad, Yohan, et al. 35, s.l. : Journal Physics D: Applied Physics, 2013, Vol. 46.

69. *Cavitation in the vicinity of the high-voltage electrode as a key step of nanosecond breakdown in liquids.* Marinov, I, et al. 4, s.l. : Plasma Sources Science and Technology, 2013, Vol. 22.

70. *On the electrostrictive mechanism of nanosecond-pulsed breakdown in liquid phase.* Seepersad, Yohan, et al. 16, s.l. : Journal of Physics D: Applied Physics, 2013, Vol. 46.

71. *Modes of underwater discharge propagation in a series of nanosecond successive pulses.* Marinov, I, et al. 46, s.l. : Journal of Physics D: Applied Physics, 2013, Vol. 46.

72. *Non-equilibrium plasma in liquid water: dynamics of generation and quenching.* Starikovskiy, Andrey, et al. 2, s.l. : Plasma Sources Science and Technology, 2011, Vol. 20.

73. Liu, Thomas Mu-Chang. *The Design Space of a Micro/Nano-Particle Electrostatic Propulsion System.* s.l. : University of Michigan, 2010.

74. *Forces et Charges de Petits Objets en Contact avec une Électrode Affectée d'un Champ Électrique.* Felici, J N. 1966, Revue Générale de l'Électricité, Vol. 75, pp. 1145-60.

75. Jones, Thomas B. *Electromechanics of Particles.* s.l. : Cambridge University Press, 1995.

76. Melcher, James R. *Continuum Electromechancs.* Cambridge : MIT Press, 1981.

77. Haynes, W. M. *CRC Handbook of Chemistry and Physics.* s.l. : CRC Press, 2019.

78. Fridman, Alexander. *Plasma Chemistry.* s.l. : Cambridge University Press, 2008.

79. *Submicron gap capacitor for measurement of breakdown voltage in air*. Hourdakis, Emmanouel, Simonds, Brian J. and Zimmerman, Neil M. s.l. : Review of Scientific Instruments, 2006, Vol. 77.

80. *Measurement of Transformer Oil Dielectric Strength.* Mohsin, M. M., et al. s.l. : IEEE TENCON 2004, 2004.

81. *Charge and force on a conducting sphere between two parallel electrodes.* Perez, Alberto T. 2, s.l. : Journal of Electrostatics, 2002, Vol. 56.

APPENDIX

EBD model

```
%Dynamics of a Charged Particle in a Uniform DC Field


solv=0
if solv
    clear
    set(0,'defaultfigureposition',[100 30 560 420]')

    %Fluid Properties
    epso        = 8.85e-12;     % [F/m]
    epsr        = 3;            % For oils, may range from 2 (Hexane)-5 (Castor Oil) also Glycerol (~50)
    ds          = 10e6;         % [V/m] Mineral oil range 10-15 MV/m
    nu          = 25e-6;        % [m^2/s] ~25e-6 (Measured Mineral Oil) - can also be varied
    rho2        = 800;          % fluid [kg/m^3] Mineral Oil ~ 800 kg/m^3
    eps         = epsr*epso;    % [F/m]

    %sigma      = 5e-11;        % [S/m] 5e-11(To be varied)
    sigma       = [0,logspace(-11,-8,11)];
    te          = eps./sigma;   % [s] charge decay time

    %Constants
    rho1        = 2700;         % aluminum ball charge carrier [kg/m^3]
    %rho1       = 800;          % neutral ball charge carrier [kg/m^3]

    %Vary L/D
    LD          = linspace(1.01,15,37);     % normalized inter-electrode spacing
    %LD          = 2
    R           = 1/8*25.4/2/1000;          % ball radius (1/8 inch diameter)(m)
    L           = LD.*2.*R;                 % Gap (m)
    Gap         = L-2.*R;                   % gap between ball and electrode
    vol         = Gap.*pi*R^2;              % approximate oil volume
    Eap         = 0.5*ds;                   % applied field = Half of the dielectric strength
    V           = Eap.*Gap;                 % applied voltage
    Eo          = V./L;                     % applied field w/o ball
    %V          = 10e3*ones(length(L));
    V_br        = ds.*Gap;                  % voltage which would cause breakdown

    h=waitbar(0,'Please Wait');

    %%Plot voltage condition compared to breakdown voltage % this is a check
    chkvlt=0;
    if chkvlt
        semilogy(LD,V./1000,'-x')
        hold on
        semilogy(LD,V_br,'-xr')
        xlabel('L/D')
        ylabel('Applied Voltage (kV)')
        title('Voltage vs L/D (Assuming Electric Field of 1/2 dielectric strength mineral oil)')
        legend('Applied voltage','Breakdown Voltage')
    end

    %Loops through the different conductivities
    for b=1:length(te)

        %Adjust calculation time according to characteristic time

        endtime = 2;
        t = linspace(0,endtime,2); %s

        %Loops through the different L/D
        for w = 1:length(L)

            %Initial Conditions
            x0      = 0;
            U0      = 0;
            Qs0     = V(w)/R*epso*epsr; %C/m^2 % this equation assumes the Capacitance of the ball is equal to that
for a isolated sphere in vacuum

            % check for spherical cap
            Cap1        = 4*pi*epso*epsr*R; % F
            Qtot1       = V(w)*Cap1;        % C
            SurfArea    = 4*pi*R^2;         % m^2
            Qs1         = Qtot1/SurfArea;   %check for spherical cap (should be same as Qs0)

            % ball near wall cap
            beta        = pi^3/6;    %Field modification factor due to nearby electrode
```

```
            Qtot2       = beta*epsr*epso*(2*R)^2*Eo(w); % C
            Cap2        = Qtot2/V(w);
            Qs2         = Qtot2/SurfArea;

            % sphere wall
            Cap3        = spherewallcap(epsr*epso,R,L(w));
            Qtot3       = Cap3*V(w);
            Qs3         = Qtot3/SurfArea;

            %        compare capacitance models

            [Qs0,Qs1,Qs2,Qs3]
            % pick one
            Qs = Qs2;
            Cap = Cap2;

            %Initial Conditions [position,velocity,chargedensity]
            y0 = [x0,U0,Qs];

            options             = odeset;
            options.Events      = @WallCheck;       % use event handler to stop ode solver
            options.MaxStep     = 1e-5;             % set max time step
            maxL                = 1.05*(L(w)-2*R);  % one event will be reaching 2nd electrode (1.05?)
            minQ                = Qs/1e3;           % the other will be minimum charge to continue calculating (1e3?)
            params              = [Eap,R,te(b),nu,rho1,rho2,maxL,minQ];

            %data.raw[:, (1) position, (2) velocity, (3) charge]
            %        [T,data(b,w).raw]  = ode23('MyODE',t,y0,options,params);
            solution            = ode23(@MyBallODE,t,y0,options,params);
            T                   = solution.x;
            data(b,w).raw       = solution.y';
            time(b,w).t         = T;

            validinds           = data(b,w).raw(:,1)<L(w)-2*R;
            hitswall            = data(b,w).raw(:,1)>L(w)-2*R;

            ind_2e              = max(find(validinds)); % index where ball strikes 2nd electrode or last ind
            tt                  = T(ind_2e);            %% same as prior calculation

            %Find the transit time
            [y1(w) y2(w)] = max(data(b,w).raw(data(b,w).raw(:,1)<L(w)-2*R));

            if ~isempty(find(hitswall))
                transit_t(b,w)  = T(y2(w));
                Qball(b,w)      = data(b,w).raw(y2(w),3); % charge density
            else
                transit_t(b,w)  = NaN;
                Qball(b,w) = 0;
            end

            solution_check = 1;
            if solution_check
                plot(T,data(b,w).raw(:,1),'.-',T(validinds),data(b,w).raw((validinds),1),'.-r')
                line(xlim,[L(w)-2*R,L(w)-2*R])
                text(mean(xlim),mean(ylim),['tt=',num2str(transit_t(b,w))])
                pause(0.01)
                xlabel('time (s)')
                ylabel('position (m)')
            end


            %Find charge density and energy at approach to other electrode
            Q_1e(b,w)       = Qs*SurfArea;                  % total charge at 2nd electrode
            Q_2e(b,w)       = Qball(b,w)*SurfArea;          % total charge at 2nd electrode
            V_2e(b,w)       = Q_2e(b,w)/Cap;                % voltage at other electrode (takes into account charge
loss), Capacitance is constant
            E(b,w)          = 0.5*V_2e(b,w)*(Q_2e(b,w));    % energy release in the discharge
            P(b,w)          = E(b,w)/transit_t(b,w);        % average power W
            P_den(b,w)      = P(b,w)/vol(w);                %W/m^3
            eta_Q(b,w)      = Q_2e(b,w)/Q_1e(b,w);          % charge efficiency

            waitbar(((b-1)*length(L) + w)/(length(te)*length(L)))
        end
        [Power(b) ind] = max(P_den(b,:));
        LD_opt(b) = LD(ind);

    end

    close(h)
end


%Make Plots
figure
```

```
plot(LD,Q_2e)
xlabel('L/D')
ylabel('Qball at 2nd electrode(C)')
lg = legend(num2str(sigma','%10.1e\n'))
lg.Location = 'bestoutside'

plt = Plot()
%plt.LineStyle   = {'--','none'}
plt.Colors      = {
    [0         0         0],
    [0.0714    0.0714    0.0714],
    [0.1429    0.1429    0.1429],
    [0.2143    0.2143    0.2143],
    [0.2857    0.2857    0.2857],
    [0.3571    0.3571    0.3571],
    [0.4286    0.4286    0.4286],
    [0.5000    0.5000    0.5000],
    [0.5714    0.5714    0.5714],
    [0.6429    0.6429    0.6429],
    [0.7143    0.7143    0.7143],
    [0.7857    0.7857    0.7857]};
plt.XLabel      = 'L/D';
plt.YLabel      = 'Charge at x=L (C)';
plt.XLim        = [1,15]
plt.XTick       = [1:2:15]
plt.export('Charge-xisL.png')


figure
plot(LD,transit_t.*1000)
lg = legend(num2str(sigma','%10.1e\n'))
lg.Location = 'bestoutside'

plt = Plot()
%plt.LineStyle   = {'--','none'}
plt.Colors      = {
    [0         0         0],
    [0.0714    0.0714    0.0714],
    [0.1429    0.1429    0.1429],
    [0.2143    0.2143    0.2143],
    [0.2857    0.2857    0.2857],
    [0.3571    0.3571    0.3571],
    [0.4286    0.4286    0.4286],
    [0.5000    0.5000    0.5000],
    [0.5714    0.5714    0.5714],
    [0.6429    0.6429    0.6429],
    [0.7143    0.7143    0.7143],
    [0.7857    0.7857    0.7857]};
plt.XLabel      = 'L/D';
plt.YLabel      = 'Transit Time (ms)';
plt.XLim        = [1,15]
plt.XTick       = [1:2:15]
plt.export('TransitTime.png')


figure
plot(LD,P_den)
lg = legend(num2str(sigma','%10.1e\n'))
lg.Location = 'bestoutside'

plt = Plot()
%plt.LineStyle   = {'--','none'}
plt.Colors      = {
    [0         0         0],
    [0.0714    0.0714    0.0714],
    [0.1429    0.1429    0.1429],
    [0.2143    0.2143    0.2143],
    [0.2857    0.2857    0.2857],
    [0.3571    0.3571    0.3571],
    [0.4286    0.4286    0.4286],
    [0.5000    0.5000    0.5000],
    [0.5714    0.5714    0.5714],
    [0.6429    0.6429    0.6429],
    [0.7143    0.7143    0.7143],
    [0.7857    0.7857    0.7857]};
plt.XLabel      = 'L/D';
plt.YLabel      = 'Power Density  (W/m^3)';
plt.XLim        = [1,15]
plt.XTick       = [1:2:15]
plt.export('PowerDensity.png')


figure
plot(LD,E)
lg = legend(num2str(sigma','%10.1e\n'))
lg.Location = 'bestoutside'
```

```
plt = Plot()
%plt.LineStyle   = {'--','none'}
plt.Colors      = {
    [0         0         0],
    [0.0714    0.0714    0.0714],
    [0.1429    0.1429    0.1429],
    [0.2143    0.2143    0.2143],
    [0.2857    0.2857    0.2857],
    [0.3571    0.3571    0.3571],
    [0.4286    0.4286    0.4286],
    [0.5000    0.5000    0.5000],
    [0.5714    0.5714    0.5714],
    [0.6429    0.6429    0.6429],
    [0.7143    0.7143    0.7143],
    [0.7857    0.7857    0.7857]};
plt.XLabel      = 'L/D';
plt.YLabel      = 'Discharge Energy (J)';
plt.XLim        = [1,15]
plt.XTick       = [1:2:15]
plt.export('Energy.png')

figure
plot(LD,eta_Q*100)
xlabel('L/D')
ylabel('Charge Efficiency(%)')
lg = legend(num2str(sigma','%10.1e\n'))
lg.Location = 'bestoutside'

plt = Plot()
%plt.LineStyle   = {'--','none'}
plt.Colors      = {
    [0         0         0],
    [0.0714    0.0714    0.0714],
    [0.1429    0.1429    0.1429],
    [0.2143    0.2143    0.2143],
    [0.2857    0.2857    0.2857],
    [0.3571    0.3571    0.3571],
    [0.4286    0.4286    0.4286],
    [0.5000    0.5000    0.5000],
    [0.5714    0.5714    0.5714],
    [0.6429    0.6429    0.6429],
    [0.7143    0.7143    0.7143],
    [0.7857    0.7857    0.7857]};
plt.XLabel      = 'L/D';
plt.YLabel      = 'Charge Efficiency (%)';
plt.XLim        = [1,15]
plt.XTick       = [1:2:15]
plt.export('ChargeEff.png')


figure
p = polyfit(sigma,LD_opt,20)
semilogx(sigma,LD_opt,'o')
hold('on')
semilogx(sigma,polyval(p,sigma))

plt = Plot()
plt.LineStyle = {'none','--'}
plt.Colors = {'black'}
plt.XLabel      = 'L/D';
plt.YLabel      = 'Conductivity (S)';
plt.export('OptLD.png')

cols = jet(length(data));
figure
for k = 1:length(data)
    subplot(3,1,1)
    p1=plot(time(1,k).t,data(1,k).raw(:,1));
    hold on
    ylabel('Position')

    subplot(3,1,2)
    p2=plot(time(1,k).t,data(1,k).raw(:,2));
    hold on
    ylabel('Velocity')

    subplot(3,1,3)
    p3=plot(time(1,k).t,data(1,k).raw(:,3));
    ylabel('Charge')

    hold on
    set([p1,p2,p3],'color',cols(k,:))
    xlabel('time (s)')
end
```

```
function yp = MyBallODE(t,y,params)

x   = y(1);
U   = y(2);
Qs  = y(3);

Eap     = params(1);
R       = params(2);
te      = params(3);
nu      = params(4);
rho1    = params(5);
rho2    = params(6);

g       = 9.81; %m/s^2
theta   = 0; %Incline
G       = (rho2-rho1)*g*sin(theta); %Gravity... units are not correct here?

a       = (G + 3*Qs*Eap/R - 9*rho2*nu*U/(2*R^2) - 27*rho2*U^2/(16*R))/(rho1+1/2*rho2);  %% the formula a function of
x,t,u

dx_dt   = U; %Position
dU_dt   = a; %Velocity
dQs_dt  = -Qs/te; %Charge
yp      = [dx_dt,dU_dt,dQs_dt]';



function [VALUE,ISTERMINAL,DIRECTION]=WallCheck(t,y,params)

xpos = y(1); %%
charge = y(3);
max_x = params(7);

ingap = xpos<max_x;
hascharge = charge>params(8);

%%if ball hits wall
VALUE = double(ingap&hascharge);
ISTERMINAL = 1;
DIRECTION = 0;




function Cap = spherewallcap(eps,R,L)
    D = L/R;
    nm = 4*pi*eps*R;
    dm = 0;

    for n = 1:1000
        dm = dm + sinh(log(D+sqrt(D^2-1)))/sinh(n*log(D+sqrt(D^2-1)));
    end
    Cap =nm/dm
```